REVISITING THE THEORY OF ALLOY THERMAL CONDUCTIVITY

A Dissertation

Presented to

The Academic Faculty

by

Hamid Reza Seyf

In Partial Fulfillment

of the Requirements for the Doctor of Philosophy in the

Mechanical Engineering

Georgia Institute of Technology

May 2019

REVISITING THE THEORY OF ALLOY THERMAL CONDUCTIVITY

Approved by:

Dr. Asegun Henry, Advisor
George W. Woodruff School of
Mechanical Engineering
Georgia Institute of Technology

Dr. Martin Maldovan
School of Physics
Georgia Institute of Technology

Dr. Ajeet Rohatgi
School of Electrical and
Computer Engineering
Georgia Institute of Technology

Dr. Samuel Graham
George W. Woodruff School of
Mechanical Engineering
Georgia Institute of Technology

Dr. Shannon Yee
George W. Woodruff School of
Mechanical Engineering
Georgia Institute of Technology

Dr. Peter J. Hesketh
George W. Woodruff School of
Mechanical Engineering
Georgia Institute of Technology

Date Approved: March 2019

ACKNOWLEDGEMENTS

This thesis and the work presented herein is a cumulative result of events in my life that were affected by certain individuals. Without the help, support and vision of these people the completion of this work would not have been possible. Most importantly, I would like to acknowledge my advisor and mentor Prof. Asegun Henry for giving me the opportunity to work with him. I couldn't have asked for a better advisor. I found him a deep thinker who can define important questions of the field. It was he who taught me to think about important questions of the field and not to be afraid of moving in directions that are orthogonal to the current research trends. His brilliant ideas, insightful comments, and constructive criticisms played a pivotal role in the shaping of my thesis. I must also particularly thank Prof. Henry for his advice toward several aspects of my personal life and professional development. I deeply indebted to him for having shared his knowledge and experience with me over the years, and invested his time and energy into my professional development. I learned a great deal of knowledge and life skills from him, have been always impressed by his passion towards science and deeply respect and admire him as a role model.

I also thank all of my committee members, Prof. Samuel Graham, Prof. Shannon Yee, Prof. Ajeet Rohatgi, Prof. Martin Maldovan, and Prof. Peter Hesketh for their insightful suggestions and advises on my thesis. I especially thank Prof. Yee and Prof. Rohatgi for great resourcefulness anytime I happened to drop by their offices. Prof. Yee has shared his insights on various aspect of research with me every time I spoke with him and I appreciate all his advice.

My sincere thanks also go to Luke Yates from Prof. Samuel Graham's group, Dr. Thomas Bougher from Prof. Baratunde Cola's group, as well as Jeomoh Kim, Mi-Hee Ji, and Dr.

Theeradetch Detchprohm from Prof. Dupuis's group who helped us in our efforts to synthesize thin film samples and measure their thermal conductivity.

I learned a lot by working and interacting with my colleagues in the Atomistic Simulation & Energy (ASE) Laboratory. I would like to thank Freddy DeAngelis, Drew Rohskopf, Dr. Kiarash Gordiz, and Dr. Wei Lv for our discussions on phonon transport. I also thank Dr. Diane England, Dr. Cansheng Yuan, Greg Wilk, Colby Jarrett, Malavika Bagepalli, Caleb Amy, and Daniel Budenstien for the stimulating discussions and all the fun we had during my PhD in the ASE lab.

Special thanks goes to my parents and siblings whom my happiness and well-being have been always of central interest to them. I owe so much to my parents that I could never repay, especially the guidance and direction they have both given me. No words of thanks could possibly measure up to their unyielding love and support.

This thesis is dedicated to my beloved wife, Sara, who accompanied me through much of my journey through graduate school. She has been my inspiration to reach for the stars and she should be acknowledged as a "co-author" for all her help. I am forever grateful to her for the many memorable years we spent together, and for all her love, help, support, and encouragement.

TABLE OF CONTENTS

LIST OF TABLES

LIST OF FIGURES

LIST OF SYMBOLS

Variables

C	volumetric specific heat J/m³K
$\hbar$	Planck constant divided by 2π, $1.054571800\times10^{-34}$ J.s
$\mathbf{p}$	momentum vector
$\mathbf{q}$	wavevector
$f^{(N)}$	probability density function
ν	polarization
k_B	Boltzmann constant, 1.38064852×10^{-23} J K^{-1}
$\mathbf{Q}$	heat flux vector, Wm^{-2}
J	thermal current density
S	normal mode amplitude
E	total energy of mode
E_P	potential energy of mode
E_K	kinetic energy of mode
V	volume of computational domain, m^3
T	Temperature, K
$\mathbf{v}$	group velocity, m/s
$\mathbf{u}$	atomic displacement vector, m
$\mathbf{r}$	distance between atoms, m
$\mathbf{e}$	eigenvector

$\mathbf{s}$	eigenvector of the fictitious mode
m	mass, kg
$\mathbf{x}$	atom position vector
$\dot{\mathbf{x}}$	atom velocity vector, m/s
$\mathbf{f}$	force vector, N
$\mathbf{D}$	dynamical matrix
X	normal mode position coordinate
$\dot{X}$	normal mode velocity coordinate
n	mode number
N	number of atoms
$f_{\mathbf{q},\nu}$	phonon distribution function
f_B	Bose–Einstein distribution function
f_Q	ratio of quantum to classical specific heat
F	mode force amplitude
D	thermal diffusivity $m^2 s^{-1}$
L	sample thickness
$\mathbf{G}$	reciprocal lattice vector

Greek symbols

Φ	potential energy
λ	wavelength, m
κ	thermal conductivity, $W m^{-1}K^{-1}$
ω	angular frequency, rad s^{-1}

τ	phonon relaxation time, s
Π	residual force
Υ	second order force constant
ψ	third order force constant
Ω	volume of unit cell
ω_c	cutoff frequency
ϕ	phase
Ψ	eigenvector periodicity function
γ	eigenvector periodicity parameter
α	ratio of the percentage of TC to the percentage of heat capacity

Subscripts

i,j,k	atom number
ij	from atom i to atom j
x, y, z	direction of coordinates
net	total heat flux
α, β, γ	directional components
b	boundary
$p-p$	phonon-phonon
m	mass disorder
min	minimum
max	maximum
o	equilibrium position

c	classical
q	quantum

LIST OF ABBREVIATIONS

2D	two-dimensional
3D	three-dimensional
PGM	phonon gas model
VCA	virtual crystal approximation
IPHC	infinitely large, pure, homogeneous crystal
RTA	relaxation time approximation
GK	Green-Kubo
GKMA	Green-Kubo modal analysis
TC	thermal conductivity
NMA	normal mode analysis
AF	Allen-Feldman
BTE	Boltzmann Transport Equation
EPA	eigenvector Periodicity Analysis
SF	structure Factor
MFP	mean Free Path
LD	lattice dynamics
a-Si	amorphous silicon
c-Si	crystalline silicon
a-SiO_2	amorphous silica
a-C	amorphous carbon
a-Ge	amorphous germanium
c-Ge	crystalline germanium

MD	molecular dynamics
SCLD	supercell lattice dynamics
PR	participation ratio
PQ	phase quotient
EPP	eigenvector periodicity parameter
DFT	density functional theory
EIP	empirical interatomic potential
IFC	interatomic force constant
IR	infrared

SUMMARY

Current understanding of phonons is based on the phonon gas model (PGM). According to the PGM, the vibrational modes in a material are assumed to be plane-waves, hence they can be modeled as a gas of particles that exchange energy through scattering events. During the last 100 years, the PGM has provided great insights into thermal transport in pure homogeneous crystals. However, when one attempts to apply the PGM to understand behavior in non-idealized materials that contain some level of disorder, however, there is growing evidence to suggest that the PGM fails. The problem is that conceptually, when any level of disorder is introduced, whether compositional or structural, the character of vibrational modes in solids changes, yet the PGM continues to assume phonons are still waves. For example, the phonon contributions to alloy thermal conductivity rely on this assumption and are most often computed from the virtual crystal approximation (VCA). In this dissertation, we show that the conventional theory and understanding of phonons requires revision, because the critical assumption that all phonons/normal modes resemble plane waves with well-defined group velocities is no longer valid when disorder is introduced.

Here, we first develop a new method for calculation of the degree of periodicity of individual vibrational modes in a generic solid, which is termed the eigenvector periodicity analysis (EPA). The EPA quantifies the extent to which a mode's character corresponds to a propagating mode, e.g., exhibits plane wave modulation. Using this method, one can quantify what fraction of the modes in a given structure are propagating as a function of the degree of disorder. We apply this method to $In_xGa_{1-x}As$ and show that the character of phonons changes dramatically within the first few percent of impurity concentration, beyond which phonons more closely

resemble the modes found in amorphous materials. We then devise two test cases to study and use a correlation-based theory, i.e., Green Kubo modal analysis (GKMA) to systematically examine the validity of the PGM/VCA in random alloys and investigate the fundamental reasons for failure of the PGM/VCA.

CHAPTER 1

INTRODUCTION:

THE THEORY OF PHONON TRANSPORT

1.1 Phonon transport in pure crystalline solids and random alloys

In crystalline dielectric solids, atoms located at lattice sites oscillate about their equilibrium positions. These atomic vibrations create a displacement field within the solid which comprises its thermal energy, which can be transported and also stored. In classical mechanics, this displacement field is described by a displacement vector obeying a homogeneous, linear, second order wave equation in time and space. The displacement field can be characterized as superpositions of sinusoidal plane waves, termed "normal modes", with wavelengths and frequencies obeying a nonlinear dispersion relationship. These normal modes can have different eigenvectors, depending on whether the displacement field is parallel (longitudinal) or perpendicular (transverse) to the wave vector. In fact, in the small wave vector (long wavelength) limit, the longitudinal modes become sound waves in a solid. From a quantum mechanical perspective, the atomic displacement field can be described by an infinite number of distinguishable quantized oscillators, termed phonons. The momentum of each phonon is proportional to its wave vector, i.e., $\hbar\mathbf{q}$, while the energy is a multiple of $\hbar\omega$, where $\hbar$ is the reduced Planck constant, ω is the angular frequency of the phonon, $\mathbf{q}$ is its wave vector, i.e., $2\pi/\lambda$, and λ is its wavelength. Furthermore, each phonon has a polarization vector field which describes the magnitude and direction of the vibration of atoms in a phonon. Phonons are bosons, which do not experience particle number conservation and have zero rest mass; the distribution of phonons in thermal equilibrium can therefore be described by Bose-Einstein [1,2].

In 3-dimensional materials, since each atom has 3 degrees of freedom (i.e., x, y, z), there exist $3N$ phonon or vibrational modes, where N is the total number of atoms. This includes the 3 translational modes, which are generally ignored. Constructive interference of a finite set of these phonons with different phases, amplitude and wave vectors generates a wave packet. The wave packet can be modeled as a particle or an envelope of a localized wave if its size is significantly smaller than the crystal size. According to this particle picture, the wave packets act as quasiparticles, propagating in solids and transporting heat at a group velocity $d\omega/d\mathbf{q}$. This particle description of phonons is useful in treating their interactions with impurities, defects, boundaries, and other particles such as electrons, photons, neutrons. Essentially, phonon can be treated as a "gas" of particles that interact with other particles including other phonons, and are responsible for heat transport. This physical picture for phonons is called phonon gas model (PGM), which is based on this special case of phonon behavior in an infinitely large, pure, homogenous, well-ordered crystal (IPHC).

According to the PGM, each phonon in the crystal with a frequency ω carries an energy of $\hbar\omega$ at a velocity $\mathbf{v}$. The thermal current density in a solid under a temperature gradient is caused by a deviation from an equilibrium distribution of phonons

$$J = \frac{1}{V}\sum_{\mathbf{q},\nu} \hbar\omega_{\mathbf{q},\nu}\left(f_{\mathbf{q},\nu} - f_B\left(\omega_{\mathbf{q},\nu}, T\right)\right)\mathbf{v}_{\mathbf{q},\nu} \tag{1.1}$$

where V is the volume of solid, T is the temperature, $f_{\mathbf{q},\nu}$ is the phonon distribution function, $\mathbf{v}_{\mathbf{q},\nu}$ is the group velocity of the phonon, and the indices $\mathbf{q}$ and ν refer to wave vector and polarization respectively. Equation (1.1) is the primary equation to describe the heat flux carried by phonons, according to the PGM, and is at the heart of virtually every expression for phonon transport,

because the derivation of almost all expressions begin with such a statement [1,2]. At thermal equilibrium, in the absence of a temperature gradient, phonons are distributed according to the Bose–Einstein distribution:

$$f_B\left(\omega_{\mathbf{q},\nu},T\right)=\frac{1}{\exp\left(\hbar\omega_{\mathbf{q},\nu}\Big/k_BT\right)-1} \tag{2.1}$$

In the presence of a temperature gradient, the distribution function deviates from f_B, and this deviation can be modeled using the Boltzmann Transport Equation (BTE)

$$\frac{\partial f_{\mathbf{q},\nu}}{\partial t}+\mathbf{v}_{\mathbf{q},\nu}\frac{\partial f_{\mathbf{q},\nu}}{\partial \mathbf{r}}=\left[\frac{\partial f_{\mathbf{q},\nu}}{\partial t}\right]_{collision} \tag{3.1}$$

where $\mathbf{r}$ and t are the position vector and time, respectively. At steady state, the rate of change in the distribution vanishes, i.e, $\frac{\partial f_{\mathbf{q},\nu}}{\partial t}=0$. Therefore,

$$\mathbf{v}_{\mathbf{k},\nu}\frac{\partial f_{\mathbf{q},\nu}}{\partial \mathbf{r}}=\left[\frac{\partial f_{\mathbf{q},\nu}}{\partial t}\right]_{collision} \tag{4.1}$$

The right-hand side of Eq. (4.1), i.e., the collision term, can be dealt with by the introduction of a relaxation time approximation (RTA). Within the RTA, the collision term is replaced by

$$\left[\frac{\partial f_{\mathbf{q},\nu}}{\partial t}\right]_{collision}=-\frac{f_{\mathbf{q},\nu}-f_B\left(\omega_{\mathbf{q},\nu},T\right)}{\tau_{\mathbf{q},\nu}} \tag{5.1}$$

where $\tau_{\mathbf{q},\nu}$ is the phonon relaxation time between two scattering events. In other words, it is the time that a phonon takes to return to equilibrium in a perturbed system.

Assuming local equilibrium, i.e., $f_{\mathbf{q},\nu} \approx f_B\left(\omega_{\mathbf{q},\nu}, T\right)$, the left hand side of the BTE can be written as

$$\mathbf{v}_{\mathbf{q},\nu} \frac{\partial f_{\mathbf{q},\nu}}{\partial \mathbf{r}} = \mathbf{v}_{\mathbf{q},\nu} \frac{\partial f_B\left(\omega_{\mathbf{q},\nu}, T\right)}{\partial T} \frac{\partial T}{\partial \mathbf{r}} \tag{6.1}$$

Substituting Eqs. (6.1) and (5.1) into Eq. (4.1) gives

$$f_{\mathbf{q},\nu} - f_B\left(\omega_{\mathbf{q},\nu}, T\right) = -\mathbf{v}_{\mathbf{q},\nu} \tau_{\mathbf{q},\nu} \frac{\partial f_B\left(\omega_{\mathbf{q},\nu}, T\right)}{\partial T} \frac{\partial T}{\partial \mathbf{r}} \tag{7.1}$$

Under the above assumption, the thermal current density, i.e., Eq (1.1) can be expressed as

$$J = \frac{1}{V} \sum_{\mathbf{q},\nu} \hbar \omega_{\mathbf{q},\nu} \left(-\mathbf{v}_{\mathbf{q},\nu} \tau_{\mathbf{q},\nu} \frac{\partial f_B\left(\omega_{\mathbf{q},\nu}, T\right)}{\partial T} \frac{\partial T}{\partial \mathbf{r}} \right) \mathbf{v}_{\mathbf{q},\nu} = -\kappa \frac{\partial T}{\partial \mathbf{r}} \tag{8.1}$$

According to Fourier's law $J = -\kappa \frac{\partial T}{\partial \mathbf{r}}$, hence the thermal conductivity (TC) can be given as

$$\kappa = \frac{1}{V} \sum_{\mathbf{q},\nu} C_{\mathbf{q},\nu} \mathbf{v}_{\mathbf{q},\nu}{}^2 \tau_{\mathbf{q},\nu} \tag{9.1}$$

where $C_{\mathbf{q},\nu}$ is the specific heat per phonon and is equal to $\hbar \omega_{\mathbf{q},\nu} \frac{\partial f_B\left(\omega_{\mathbf{q},\nu}, T\right)}{\partial T}$. Based on the Eq. (9.1), phonon TC depends on its group velocity ($\mathbf{v}_{\mathbf{q},\nu}$), heat capacity ($C_{\mathbf{q},\nu}$), and relaxation time ($\tau_{\mathbf{q},\nu}$). Since phonons can be scattered by different scattering mechanisms, an effective relaxation time can often [3] be used in Eq. (9.1), in lieu of solving the BTE with all of the scattering mechanisms coupled [3]. To calculate the effective relaxation time, Matthiessen's rule [1,2] is often used, which assumes scattering mechanisms are independent:

$$\frac{1}{\tau} = \frac{1}{\tau_{p-p}} + \frac{1}{\tau_{p-b}} + \frac{1}{\tau_{p-e}} + \ldots \tag{10.1}$$

where τ_{p-p}, τ_{p-b}, τ_{p-e}, τ_{p-d} are phonon-phonon, phonon-boundary, and phonon-electron relaxation times, respectively.

The relaxation time and specific heat are universal properties of all types of phonons. The former can be calculated using many methods proposed in the literature, including via analytical models with fitting parameters, time domain normal mode analysis (NMA), based on molecular dynamics (MD) simulations [3-5], third-order anharmonic lattice dynamics calculations [3,6,7], Fermi's golden rule, and iterative schemes to solve the linearized BTE [3,8,9]. In the case of the latter, the heat capacity can be obtained by calculating the phonons frequency using lattice dynamics (LD) [10]. In LD, by describing the chemical binding of atoms in the system using an interatomic potential, one can develop a formalism to obtain the phonon frequencies and consequently, heat capacity. One approximation which is usually made when calculating phonon frequencies and dispersion relations is the harmonic approximation. According to this approximation, to approximate the interatomic potential as harmonic, the crystal potential is taken as a Taylor expansion around the equilibrium atomic position, and only second order term is kept, while higher order terms are neglected. The motions of atoms in the solid then can be described by an eigen-system that can be solved to obtain the eigenvalues, which gives the phonon frequency at different wave vectors, as well as eigenvectors of each phonon mode.

Finally, group velocity is another important parameter in the PGM and it is necessary to calculate the contribution of each phonon to the thermal conductivity (TC). In well-ordered, homogenous, crystalline solids, due to the existence of structural and compositional periodicity,

all the phonon eigenvectors correspond to plane wave modulated vibrations (i.e., propagating waves). Therefore, one can define a wavelength/wave vector for phonons and consequently, a phonon dispersion relation, to describe the relationship between the frequency and wavelength. For such systems, the group velocity is can be calculated by taking the derivative of the phonon dispersion relation with respect to wave vector, i.e., $\frac{d\omega}{d\mathbf{q}}$.

For random alloys, the PGM can be extended using the virtual crystal approximation (VCA), a method introduced for the first time by Abeles in 1963 [11]. As will be explained in Chapter 2, under the VCA, one essentially replaces the disordered alloy with a perfect, single-species crystal with properties (e.g., dispersion, velocity, specific heat etc.) equivalent to a compositionally weighted average of the two starting materials (e.g., atomic mass and bond strength). However, the TC of crystalline alloys is not well described by a simple rule of mixtures for the base crystal phononic properties. To account for deviation from this simplified model, an additional mechanism for phonon scattering, namely alloy scattering must be superimposed. In other words, the VCA treats the presence of dissimilar elements in an alloy lattice as though they act as scattering centers for the phonon gas, and the expressions used to model this effect were derived by Tamura [12] in the context of modeling isotope scattering. This additional scattering mechanism ultimately yields much more frequent scattering, which reduces the TC, leading to much better agreement with experimental data [11,13-15], as compared to a simple rule of mixtures. Therefore, the impurity scattering term is what qualitatively causes the VCA to correctly predict the typical U-shaped curve observed in TC vs. composition in most alloys. For alloys, TC typically decreases by ~10x as the composition of a single impurity approaches ~10–25% at which point it remains approximately constant until ~75–90%, after which it quickly increases to the other pure crystal's TC.

Currently, the VCA is the most widely accepted/used theoretical framework for understanding phonon transport in random alloys, and this approximation has largely been justified in the literature, where good agreement between the VCA and experiments has been observed [13-18]. Given its success, it has become the sole theoretical approach for understanding of phonons in random alloys. However, there are instances where the VCA fails [19-23], even when adjustable parameters are used to fit the data to which it is compared. It is also important to note that these failures are not only quantitative [19-23], but also qualitative [19,20,22]; some alloys exhibit monotonically increasing TC or seemingly constant TC vs. temperature whereas the VCA always inherently yields the same qualitative temperature dependence as a pure crystal. This dependence consists of a low-temperature peak (typically dictated by the competition between phonon–phonon scattering and phonon–impurity scattering for > 10-20% alloy concentration) followed by monotonically decreasing TC due to anharmonic phonon–phonon scattering. Figure 1.1 (a, b) compares VCA predictions and experimental values of TC of some example random alloys at different temperatures and compositions. As seen from the figure, for these systems, VCA fails both quantitatively and qualitatively. Investigating the fundamental reason of failure of the PGM/VCA is the main focus of this thesis.

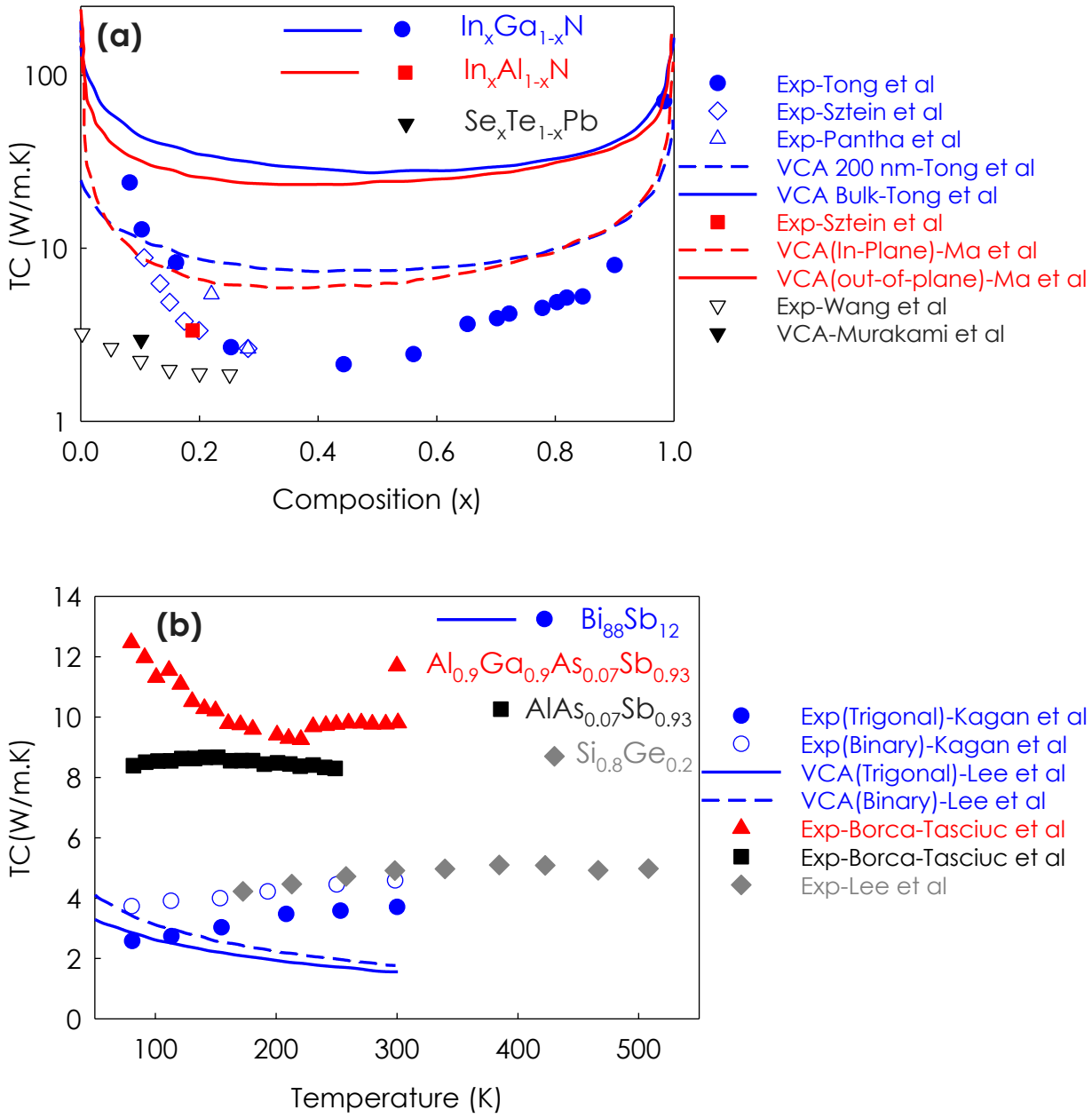

Figure 1.1 Some examples of alloys in which VCA fails to predict TC. (a) TC vs alloy composition, (b) TC vs temperature. The experimental data are collected from References [19,21,22,24-28] while the VCA prediction data are from Reference [16,19,29]. The VCA curves are calculated using *ab initio* calculations.

1.2 The fundamental problem

For more than half a century, all investigations of phonon transport in random alloys have been conducted using the VCA. Despite the prevalence of the VCA in the literature, there are several alloys in which the VCA fails to predict not only the value of TC, but also the trend of TC vs composition and/or temperature, as illustrated in Figure. 1.1. These failures suggest our understanding of the fundamental physics may need revision, and revisiting the underlying assumptions of the VCA is a logical starting point. There are two fundamental issues with the application of the PGM/VCA to random alloys:

- The assumption that all phonons/vibrational modes correspond to plane waves, thereby justifying invocation of expressions for TC that are based on the PGM.
- The derivation of the heat current in Eq. (1.1) by simple analogy to heat flow attributed to gas particles and was not rigorously derived from first principles.

With respect to the first point, in reality, adding a dissimilar atom or a defect/impurity into a previously pure homogenous crystal leads to the symmetry/periodicity of the system breaking. As a result, one obtains solutions to the equations of motion for the atoms that have a very different character than a plane wave modulated distribution of atom displacements/velocities. Due to the lack of plane wave characteristics of these solutions (phonons), one cannot define a wavelength or, consequently give a well-defined group velocity. Therefore, the application of the PGM/VCA to describe the transport of phonons in random alloys is questionable and inconsistent with the actual atomic vibrations in the alloy. This issue is critical, because almost all studies since 1963 are based on the assumption that phonons in random alloys have 100% plane wave character.

To observe the real vibrational modes in crystalline alloys, we conducted a supercell lattice dynamics calculation (SCLD) (see Figures 1.2-1.4) on an $In_{0.53}Ga_{0.47}As$ alloy as an example. As

seen in Figures 1.2-1.4, the eigenvectors for the normal modes of $In_{0.53}Ga_{0.47}As$ alloy fall into the same three categories identified by Allen and Feldman (AF) in 1999 for amorphous materials, namely propagons, diffusons and locons[30]. Propagons are typically low frequency modes that extended throughout the entire system and are delocalized, and generally exhibit some periodicity in their eigenvectors (i.e., a sinusoidal modulation to the displacement/velocity field). These modes are termed "propagons", largely because they resembled the traditional phonon in a crystal, which is a pure plane-wave that consequently propagates energy (Figure. 1.2) at a certain group velocity throughout the entire structure. The wavelength can be clearly recognized as the distance over which the wave's shape repeats. The average distance of propagation of a propagon would then be its mean free path (MFP).

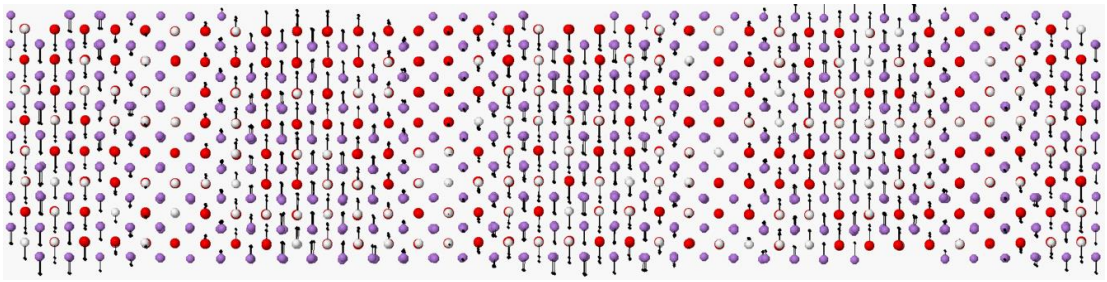

Figure 1.2. Eigenvectors of a propagon in $In_{0.53}Ga_{0.47}As$. The arrows represent eigenvector magnitude and direction.

The second category of phonons in $In_{0.53}Ga_{0.47}As$ is diffusons. They are delocalized modes that don't have any apparent propagating character and exhibit seemingly random eigenvectors. As can be seen in Figure 1.3, the vibration is of a random nature, hence one cannot define wavelength or group velocity for these types of phonons. The apparent randomness associated with these modes led to them being termed "diffusons", since there is no discernable periodicity, thus their displacement/velocity profiles are diffuse. It was furthermore hypothesized that diffusons

might contribute to heat conduction through a diffusive process, rather than propagation of energy from one location to another location. As will be discussed in the Chapter 4, the majority of phonons in the $In_{0.53}Ga_{0.47}As$ alloy studied herein are diffusons.

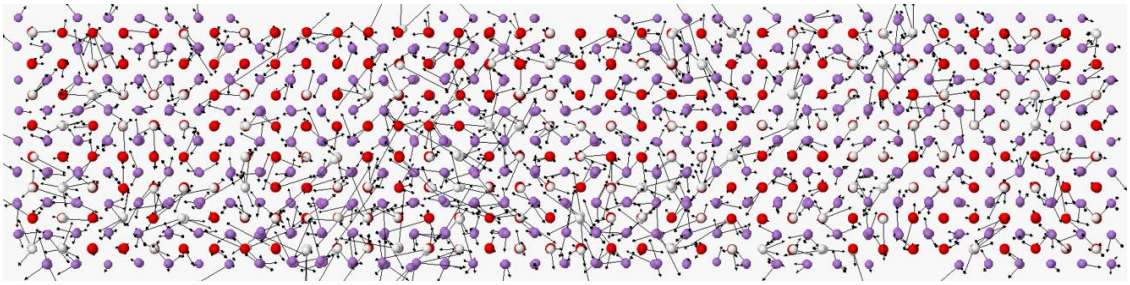

Figure 1.3. Eigenvectors of a diffuson in $In_{0.53}Ga_{0.47}As$. The arrows represent eigenvector magnitude and direction.

The third and last category of modes are high frequency modes that are spatially localized (Figure. 1.4), and subsequently termed “locons”. These modes do not involve the majority of the atoms in the system; instead only small groups or clusters of atoms in a small region participate in the mode.

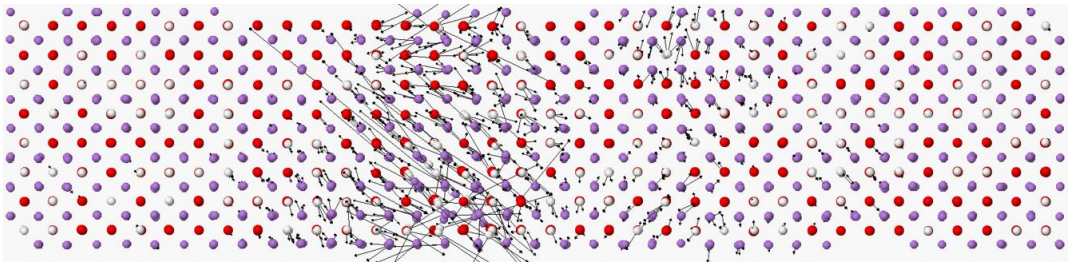

Figure 1.4. Eigenvectors of a locon in $In_{0.53}Ga_{0.47}As$. The arrows represent eigenvector magnitude and direction.

The existence of non-propagating vibrational modes, i.e., diffusons and locons clearly suggests the application of the PGM/VCA in random alloys would be problematic. The question

then arises is “What are the respective contributions that each category of modes (e.g., propagons, diffusons and locons) makes to TC?” Answering this question requires a different theory, because the existing PGM theory cannot be invoked for the diffusons and locons, because one cannot define their group velocities. For propagons, one can find an associated wavelength [30,31] and it is still conceivable that treating such modes via the PGM/VCA would therefore be valid. However, as will be shown in the following chapters, propagons only comprise a small fraction of the modes for 15–85% compositions, thus it is not clear *a priori* that all other modes can simply be neglected. For diffusons and locons, one must use alternative methods for describing their potentially significant TC contributions. Recently, Lv and Henry[32] have developed a general approach termed Green–Kubo modal analysis (GKMA), which combines SCLD with the fully anharmonic dynamics generated by MD simulations to solve this problem. The GKMA method can directly assess a mode’s TC contribution, without any invocation of the PGM, as one needs only to utilize the mode level contributions to each atom’s velocity to determine that mode’s contribution to the heat flux operator in an equilibrium MD simulation. In this sense, the key attribute of the GKMA approach is that it describes phonon transport in terms of correlation, rather than scattering, which is a major shift in perspective from the current understanding. As will be shown in the subsequent chapters, the main advantage of knowing the mode level contributions is that it allows one to look at trends in the behaviors with respect to the mode character. It would be useful to separate the contributions of propagons and diffusons to see if the trends in TC contribution or underlying mechanisms differ significantly, or if somehow, despite the differences in character, the PGM physical picture still holds.

1.3 Thesis questions

The overall aim of this study is to examine the validity of the PGM/VCA for predicting the TC of random alloys and understand the role of mode character on alloy TC. To reach this goal, this thesis will address the following primary research questions:

(1) As shown in Figures 1.2-1.4, compositional disorder gives rise to a change in mode character, yet due to the lack of alternatives, the PGM/VCA is still applied to alloys that likely consist of propagons, diffusons, and locons[30,31]. As a first step toward our main goal, it is critically important to develop a means of identifying each type of modes in random alloys in a quantitative/systematic way. As will be shown in Chapter 3, distinguishing locons from propagons and diffusons is straightforward, by using the participation ratio[31,33], which measures the extent to which a mode is localized. However, distinguishing between propagons and diffusons is challenging, as both are spatially delocalized. Therefore, the first question that arises is: how can one systematically and quantitatively discern the difference between propagons and diffusons? Developing a rigorous method of classification allows us to study the effect of disorder on the vibrational modes character and consequently identify the modes that cannot be studied by PGM/VCA. As will be shown in Chapter 3, the structure factor (SF) is one possible method to distinguish between propagons and diffusons, by testing the plane-wave character of vibrational modes at a particular polarization and wave vector[34,35]. The primary problem with the SF approach, however, is that SF quantifies the spatial and temporal frequency content of the collective motions of the eigenvectors. Therefore, it is not generally possible to assign a unique wave vector to individual modes. Furthermore, the SF is not normalized, and therefore yields different magnitudes of values for different

materials. Therefore, the magnitude of the SF alone cannot distinguish propagons or diffusons on a universal scale, and as a result, one must compare the relative magnitudes for different modes in the same structure. Therefore, it is important to have a universal scale by which a mode's character can be judged more generally, which would allow propagons and diffusons to be directly compared for different material systems. In Chapter 3, we introduce a new general method, termed "Eigenvector Periodicity Analysis (EPA)," for classifying vibrational modes and specifically distinguishing propagons from diffusons. EPA doesn't have the issue associated with the SF method, hence, one can compare individual modes in two different structures on a universal scale that is material agnostic. Using EPA, one can clearly quantify what fraction of modes in a given structure are propagons or diffusons as a function of the degree of disorder.

(2) Traditionally, the distinction between propagons and diffusons is often described by a transition/cut-off frequency, above which the modes are all diffusons and locons and below which the modes are all propagons[34]. Such a conclusion was solely made based on visual inspection of vibrational modes or the prediction based on the SF method. Therefore, the second question arises is: how does the transition between propagons and diffusons occur? Is there any sharp cutoff frequency between propagons and diffusons? In other words, is there any requirement that the mode character must change abruptly with respect to frequency? By applying EPA to various disordered solids in Chapter 3, we will address this question and show that that in general no strict set of rules that would require any abrupt shift in mode character.

(3) The third question arises is: "What is the fundamental reason for the failure of VCA in random alloys?" More specifically, what is the key fundamental information missing in the

PGM/VCA? Using GKMA and EPA to study the TC and vibrational modes in $In_xGa_{1-x}As$ as an example test case, we will systematically prove that the missing information in the PGM/VCA is knowledge of the vibrational mode character. As the second test case to examine the validity of PGM/VCA in random alloys, we will also show that the relaxation time is not a valid descriptor for non-propagating vibrational modes in random alloys. Other interesting questions that one can ask are: How does mode character change with composition in a random alloy?, what aspect of vibrational modes changes when the propagating character decreases? We will address these questions in detail in Chapter 4.

(4) As discussed above, due to the lack of periodicity in structurally/compositionally disordered materials, the majority of vibrational modes are non-propagating [23,30,31,34], so one cannot clearly define the phonon dispersion and group velocity. Therefore, one may not be able to extend insights about optical phonons in pure, homogeneous crystalline materials to disordered solids. However, as will be discussed in Chapter 3, for disordered solids, one can use phase quotient (PQ) to evaluate whether a mode shares more distinguishing properties with acoustic vibrations (PQ>0) or optical vibrations (PQ<0). The forth question will be answered in this thesis is: Do PQ<0 modes in structurally/compositionally disordered systems contribute significantly to heat conduction? Understanding the contributions to TC from PQ>0 and PQ<0 phonons is important, because once the dominant phonon types and their transport mechanism are understood, the means by which their contributions can be manipulated might then be explored. We will address this question in Chapter 5 and show that surprisingly the PQ<0 phonons can have a significant contribution to the TC of disordered solids.

This thesis first describes a new method for classifying vibrational modes in compositionally/structurally disordered solids such as amorphous materials and random alloys. Then, utilize GKMA, an entirely new paradigm to understand alloy TC that can treat modes with any character and experimentally confirm its new insights.

In Chapter 2, we discuss the correlation-based theory of alloy TC. We first review the Green-Kubo (GK) method, then we derive GKMA formalism, which utilizes MD and LD. Meanwhile, the existing theoretical framework for understanding of phonon transport in random alloys, namely PGM/VCA, will be briefly discussed.

In Chapter 3, we first review the existing methods for classifying vibrational modes in disordered solids, i.e., participation ratio and SF. Then, we introduce the EPA formalism and demonstrate its application to several crystalline and amorphous solids. Finally, we will explain the mathematical formalism of PQ, a useful quantity that can be used to evaluate whether a mode's properties are more similar to acoustic or optical vibrations.

In Chapter 4, we first study the effect of disorder on vibrational modes in $In_xGa_{1-x}As$ alloy. By applying EPA to $In_xGa_{1-x}As$ alloy at various compositions, we will show that how the vibrational mode change when alloy composition change. We will discuss the correlation between the trend of eigenvector periodicity parameter (will be introduced in Chapter 3) vs alloy composition and TC vs alloy composition. Afterwards, the TC of $In_{0.53}Ga_{0.47}As$ alloy is calculated using both the VCA and GKMA approaches. We first show the VCA fails to predict the TC, then discuss devise two test cases to more deeply examine the fundamental reason for the failure of the VCA.

In Chapter 5, we discuss the importance of PQ<0 phonons on TC of disordered solids. By calculating the PQ and phononic TC of various disordered solids, we will show the trend of PQ verses frequency and the role of PQ<0 mode to the TC of disordered solids. Finally, Chapter 6 lists potential future work and gives some concluding remarks.

CHAPTER 2

CORRELATION THEORY OF PHONON TRANSPORT

In this chapter we review the mathematical formulation of GKMA. As discussed in Chapter 1, GKMA is a general approach that can be used to investigate the mode TC of all class of solids ranging from well-ordered crystalline solids to fully disordered solids such as amorphous systems. GKMA is based on fluctuation-dissipation theory or GK formula, which is a general approach to calculate the TC of wide variety of materials including solids, fluids, and gases[1,36-38]. Although, GK has been used extensively to study TC various systems well-ordered and disordered including amorphous solids, it is not able to provide information about the contributions of individual vibrational modes to the TC. The extended version of GK, termed GKMA, combines GK formula and LD and allows one to study the contributions of individual modes to TC. In this chapter, we first review GKMA formalism. Then, we briefly review the existing analytical and computational approaches based on PGM/VCA for calculating the TC of random alloys. Finally, we will discuss fundamental differences between PGM/VCA and GKMA.

2.1 Green-Kubo formulation

GKMA is based on the GK formula which was derived from the linearized Liouville equation[1]. For a system with N arbitrary particles with momentum $\mathbf{p}$ and coordinate $\mathbf{r}$, one can define N particle distribution function $f^{(N)}$ representing the probability density of finding a state defined by N individual particle momenta $\mathbf{p}$ and locations $\mathbf{r}$. The response of such a system subjected to a thermal disturbance as a temperature perturbation, i.e., $\delta T(\mathbf{r},t) = \delta T \exp(i\omega t)$

with input frequency of ω, is heat flux ($\mathbf{Q}_{net}$) which can be determined by solving the linearized Liouville equation for the N particle distribution function [1,39,40]

$$\left\langle \mathbf{Q}_{net}(t) \right\rangle = -\frac{V}{k_B T^2} \int_{-\infty}^{t} \left\langle \mathbf{Q}(t) \cdot \mathbf{Q}(t-t') \right\rangle \cdot \vec{\nabla} \cdot \delta T \cdot dt' \tag{2.1}$$

Where $\mathbf{Q}_{net}$ is the net heat flux in the system, k_B is the Boltzmann constant, T is the system temperature, and V is the volume of the system. By extracting the temperature gradient from Eq. (2.1), an expression for the heat current, similar to heat current defined by Fourier's law $\mathbf{Q} = -\kappa \cdot \nabla T$ can be obtained. Substituting Fourier's heat current equation, we can derive an expression for the TC, using a Fourier transform to rewrite the integral to obtain:

$$\kappa_{\alpha\beta}(T,\omega) = \frac{V}{k_B T^2} \int_{0}^{\infty} \left\langle \mathbf{Q}_{\alpha}(0) \cdot \mathbf{Q}_{\beta}(\tau) \right\rangle \cdot \exp(-i\omega \cdot \tau) d\tau \tag{2.2}$$

Where $\kappa_{\alpha\beta}(T,\omega)$ is TC tensor, the $\alpha\beta$ subscripts denote the directional components. ω and T are the perturbation frequency and the temperature of the system, respectively. $\mathbf{Q}$ is the heat flux of the system and τ the correlation time, V is the volume of the system, and $\langle ... \rangle$ represents the autocorrelation function. For macroscale situations, the atomic scale fluctuations are orders of magnitude faster than the time scale of the system perturbations. Therefore, the zero frequency limit of Eq. (2.2)[41] is required

$$\kappa_{\alpha\beta}(T) = \frac{V}{k_B T^2} \int_{0}^{\infty} \left\langle \mathbf{Q}_{\alpha}(0) \cdot \mathbf{Q}_{\beta}(\tau) \right\rangle d\tau \tag{2.3}$$

However, if the input frequency of perturbation is similar to atomic fluctuations frequency, the frequency dependent TC can deviate from Eq. (2.3).

In Eq. (2.3), the heat current $\mathbf{Q}$ as a function of microscopic variables can be extracted from atomistic simulation. For the case of MD simulations in which empirical interatomic potentials (EIPs) describe the system energy and interaction forces, Hardy[37] derived a general heat current operator that can be applied to any EIP. Essentially, he first used a generic form for Hamiltonian operator to express the heat current operator in terms of microscopic quantities available in atomistic simulations. He then defined a spatial weighting function to describe the local energy density as a continuous function, then integrated to obtain the volume averaged heat current operator as,

$$\mathbf{Q}(t) = \frac{1}{V}\sum_i \left[E_i \dot{\mathbf{x}}_i + \sum_j \left(-\nabla_{\mathbf{r}_i} \Phi_j \cdot \dot{\mathbf{x}}_i \right) \mathbf{r}_{ij} \right] \tag{2.4}$$

Where E_i is the potential and kinetic energy of atom i, V is volume of the system, Φ_j denotes potential energy of atom j, $\mathbf{r}_{ij}$ is distance between atom i and j, and $\dot{\mathbf{x}}_i$ is the velocity of atom i. In Equation (2.4), there are two physically meaningful terms that correspond to two different mechanisms of heat transport in materials. The first term dominants in liquids and gasses because in fluids the heat and energy is transported through the kinetic energy of molecules. In solids, the second term dominates, because of larger interatomic forces and atoms are constrained to their local environment, which yields continuous interactions (i.e., not intermittent scattering events). For example, McGaughey *et al*. has shown that for solid crystalline argon, the total heat current due to the second term dominates[42].

GK is fundamentally a different approach to calculate the TC of materials compared to the PGM. GK is a general approach based on fluctuation-dissipation theory and describes the response of the system to small external disturbances from equilibrium, while the PGM treats phonons as particles and their interactions are considered as scattering events. In the PGM, the TC is function

of the frequency of scattering events, i.e., the higher the frequency of the scattering, the higher the thermal resistance and consequently the lower the TC. The GK formula on the other hand describes the TC as a function of the heat current autocorrelation, which can be calculated using Eq. (2.3). Based on the GK correlation paradigm, any form of correlated pattern in the system's trajectory can contribute to TC. Physically, the correlation of the heat current in Eq. (2.3) measures how similar the heat current is at some time t and another later time t'. The more similar the heat current fluctuations are, the longer the memory of the initial perturbations the system experienced, and as a result, the inner product between the two is larger. This leads to more correlation and consequently higher the TC. Thus, in low TC solids, the correlation is usually short-lived (i.e., a few picoseconds), while in high TC materials, the fluctuations remain correlated for longer times (i.e., tens to hundreds of picoseconds) as the memory of the earlier state dissipates more slowly.

Since the GK formula can be evaluated using MD simulations, all degrees of anharmonicity, i.e., 3-phonon, 4-phonon up to N-phonon interactions are naturally included in the heat current therefore TC. Furthermore, GK can be used to study defects, disorder, and finite size effect explicitly, as opposed to treating them as perturbations to some homogeneous and infinitely large system. In this way, on can evaluate the dynamics of an actual and specific configuration of atoms, rather than relying on effective medium and perturbation schemes. Instead one can evaluate effects like disorder by statistically sampling different configurations that have the same descriptor of interest, i.e. the same defect density or the same interface roughness etc. Finally, since the GK formula doesn't cast TC in terms of phonons directly, but instead in terms of atoms, there is no utilization of quantities such as group velocity to calculate the TC. In fact, it makes no assumptions about the phase of matter, and as a result, this approach can be used to predict TC of materials with

broken symmetry such as non-crystalline solids, random alloys, amorphous materials and even single molecules.

Although GK has several advantages it is not able to provide information on the contributions of individual vibrational modes to the TC. This is because it is formulated completely independent of the notion of a phonon, as it is equally valid for liquids and gasses, where phonons are not even a well-defined phenomenon and arguably do not exist. Nonetheless, for solids/rigid bodies, phonons exist, and in the next section, we explain GKMA in which one can calculate the contribution of each phonon to the TC. In the next section, we first review the general form of the LD formulation and then discuss GKMA approach.

2.2 Lattice dynamics formulation

Lattice dynamics is a generalized formulation that can provide a useful picture into the spectral characteristics of phonons. In well-ordered solids, the potential energy Φ of the solid can be expanded in a Taylor series in powers of the atomic displacements u

$$\Phi = \Phi_0 + \sum_{i\alpha} \left.\frac{\partial \Phi}{\partial u_{i,\alpha}}\right|_0 u_{i,\alpha} + \frac{1}{2}\sum_{i,j}\sum_{\alpha,\beta} \left.\frac{\partial^2 \Phi}{\partial u_{i,\alpha}\partial u_{j,\beta}}\right|_0 u_{i,\alpha}\, u_{j,\beta} + \frac{1}{3!}\sum_{i,j,k}\sum_{\alpha,\beta,\gamma} \left.\frac{\partial^3 \Phi}{\partial u_{i,\alpha}\partial u_{j,\beta}\partial u_{k,\gamma}}\right|_0 u_{i,\alpha}\, u_{j,\beta} u_{k,\gamma} + \ldots \tag{2.5}$$

The i and j sums over the atoms in the systems, and the α and β sums are over the $x-$, $y-$, and $z-$directions.

At equilibrium, the system is in a minimum energy configuration hence the first derivative of the potential energy with respect to atomic displacement is zero

$$\left.\frac{\partial \Phi}{\partial u_{i,\alpha}}\right|_0 = 0 \tag{2.6}$$

The second derivative of the energy with respect to atomic displacements yields the second-order force constants

$$\Upsilon_{ij,\alpha\beta} = \left.\frac{\partial^2 \Phi}{\partial u_{i,\alpha}\partial u_{j,\beta}}\right|_0 \tag{2.7}$$

and the third derivative of energy yields the third-order force constants

$$\psi_{ijk,\alpha\beta\gamma} = \left.\frac{\partial^3 \Phi}{\partial u_{i,\alpha}\partial u_{j,\beta}\partial u_{k,\gamma}}\right|_0 \tag{2.8}$$

Therefore, we can write the potential energy in terms of the force constants as

$$\Phi = \frac{1}{2}\sum_{i,j}\sum_{\alpha,\beta}\Upsilon_{\alpha\beta}u_{i,\alpha}u_{j,\beta} + \frac{1}{3!}\sum_{i,j,k}\sum_{\alpha,\beta,\gamma}\psi_{\alpha\beta\gamma}u_{i,\alpha}u_{j,\beta}u_{k,\gamma} + \ldots \tag{2.9}$$

By expanding the potential energy up to the second order with respect to atomic displacement, one can show that the displacements can be written in terms of vibration modes which are completely decoupled. For b th atom in the l th unit cell the equation of motion is

$$m_b\ddot{\mathbf{u}}\begin{pmatrix} l \\ b \end{pmatrix} = -\sum_{b'l'}\Upsilon\left(bl;b'l'\right)\cdot\mathbf{u}\begin{pmatrix} l' \\ b' \end{pmatrix} \tag{2.10}$$

Where m_b is the mass of atom b. $\Upsilon\left(bl;b'l'\right)$ is the 3×3 force constant matrix describing the interaction between atoms bl and $b'l'$, $\mathbf{u}\begin{pmatrix} l' \\ b' \end{pmatrix}$ is the displacement of atom bl from its equilibrium

position, and the summation is over every atom in the system. Now assume a plane wave (i.e., harmonic) solution to Eq. (2.10), which will be a sum over all the normal modes (i.e., over all wave vectors and polarizations), which have frequencies $\omega\begin{pmatrix}\mathbf{q}\\ \nu\end{pmatrix}$:

$$\mathbf{u}\begin{pmatrix}l\\ b\end{pmatrix}=\frac{1}{\sqrt{m_b N}}\sum_{\mathbf{q}}\mathbf{e}_b\begin{pmatrix}\mathbf{q}\\ \nu\end{pmatrix}\exp\left[i\left(\mathbf{q}\cdot\mathbf{r}_0\begin{pmatrix}l\\ b\end{pmatrix}-\omega\begin{pmatrix}\mathbf{q}\\ \nu\end{pmatrix}t\right)\right] \tag{2.11}$$

Where $\mathbf{r}_0\begin{pmatrix}l\\ b\end{pmatrix}$ is the equilibrium position of the lth unit cell, $\mathbf{e}_b\begin{pmatrix}\mathbf{q}\\ \nu\end{pmatrix}$ is the eigenvector, N is the total number of atoms, and $\mathbf{q}$ is the wave vector, and ν is dispersion branch.

Substitution of Eq. (2.11) in Eq. (2.10) leads to the following 3N simultaneous equations,

$$\omega\begin{pmatrix}\mathbf{q}\\ \nu\end{pmatrix}^2\cdot\mathbf{e}\begin{pmatrix}\mathbf{q}\\ \nu\end{pmatrix}=\mathbf{D}(\mathbf{q})\cdot\mathbf{e}\begin{pmatrix}\mathbf{q}\\ \nu\end{pmatrix} \tag{2.12}$$

Where $\mathbf{e}\begin{pmatrix}\mathbf{q}\\ \nu\end{pmatrix}$ is a complex eigenvector which depicts the direction of atomic displacement. $\mathbf{D}(\mathbf{q})$ is the dynamical matrix containing the mass and stiffness information as $\mathbf{D}(\mathbf{q})$ is projected onto a particular propagation direction. The $\mathbf{D}(\mathbf{q})$ matrix elements are given by[10]

$$D_{\alpha,\beta}(bb',\mathbf{q})=\frac{1}{\sqrt{m_b m_{b'}}}\sum_{l'}\Upsilon_{\alpha\beta}(b0,b'l')\cdot\exp\left(i\mathbf{q}\cdot\left[\mathbf{r}_0\begin{pmatrix}l'\\ 0\end{pmatrix}-\mathbf{r}_0\begin{pmatrix}l\\ 0\end{pmatrix}\right]\right) \tag{2.13}$$

The summation is over all unit cells and α or β equals 1 for x, 2 for y, and 3 for z. The dynamical matrix is symmetric and Hermitian, guaranteeing real eigenvalues that are all positive for stable structures. By solving the eigenvalue problem for all allowed wave vectors, the normal mode

frequencies and eigenvectors are obtained. From the frequencies, one can calculate mode specific heats using Bose-Einstein and build phonon dispersion curves and the density of states.

The above formalism can be extended to compositionally/structurally disordered solids. For such systems, the structure can be treated more generally in the sense that we do not attempt to describe the solutions in terms of plane waves and wave vectors. In this case, one can treat the entire simulation cell as if it is a single unit cell on a cubic lattice, such that all of the LD calculations are carried out at the gamma point ($\mathbf{q}=0$). Substituting $\mathbf{q}=0$ in Eq. (2.11)-(2.13), the dynamical matrix elements can be written as

$$D_{\alpha,\beta}\left(bb',\mathbf{q}=0\right)=\frac{1}{\sqrt{m_b m_{b'}}}\sum_{l'}\Upsilon_{\alpha\beta}\left(b0,b'l'\right) \tag{2.14}$$

In Eq (2.14), b and b' represent any atom in the simulation domain instead of only atoms in a unit cell. In this supercell LD (SCLD) approach, one effectively treats the entire super cell calculation domain as one unit cell. This approach then allows us to generalize the LD formalism to systems with any degree of order or disorder or lack of periodicity, such as crystals, random alloys, amorphous materials and individual molecules. Using SCLD, we can obtain the mode shape/eigenvectors of the phonons. The next step is to input the mode information into GK and heat current formula such that one can calculate mode level information from MD simulation that include anharmonicity.

2.3 Green-Kubo modal analysis method formulation

As discussed in section 2.2, for an arbitrary rigid structure with N atoms, using a SCLD calculation one can obtain 3N collective modes of vibration. With the 3N modes determined, one

can then use the individual polarization vectors for each atom in a mode as a basis set for projecting the anharmonic trajectory from MD. Towards this end, we first show transformation from individual atom coordinates to normal mode coordinates, where the normal mode coordinates of position $X_n(t)$ and velocity $\dot{X}_n(t)$ for mode n can be written as,

$$X_n(t) = \sum_j \sqrt{m_j}\mathbf{e}_{j,n}^{*} \cdot \mathbf{x}_j(t) \tag{2.15}$$

$$\dot{X}_n(t) = \sum_j \sqrt{m_j}\mathbf{e}_{j,n}^{*} \cdot \dot{\mathbf{x}}_j(t) \tag{2.16}$$

where $\mathbf{e}_{j,n}$ is the eigenvector that gives the magnitude and direction of motion for atom j in mode n , * represents the complex conjugate, m_j is the mass of atom j, while $\mathbf{x}_j$ and $\dot{\mathbf{x}}_j$ are the displacement and velocity vectors of atom j in the system, which can also be obtained from the reverse transformation that starts with known normal mode coordinates,

$$\mathbf{x}_j(t) = \sum_n \mathbf{x}_{j,n}(t) = \frac{1}{\sqrt{m_j}} \sum_n \mathbf{e}_{j,n} \cdot X_n(t) \tag{2.17}$$

$$\dot{\mathbf{x}}_j(t) = \sum_n \dot{\mathbf{x}}_{j,n}(t) = \frac{1}{\sqrt{m_j}} \sum_n \mathbf{e}_{j,n} \cdot \dot{X}_n(t) \tag{2.18}$$

Equations (2.17)-(2.18) essentially state that at every instant, every atom's position and velocity are a superposition of individual contributions from all normal modes of vibration in the system. These individual contributions are proportional to $X_n(t)$ and its time derivative $\dot{X}_n(t)$. Recognizing the meaning of this forward and backward transformation, one can then substitute the modal contributions to the velocity of each atom into the heat flux operator derived by Hardy[37],

to obtain each mode's contribution to the volume averaged heat flux at each time step in an EMD simulation,

$$\begin{aligned}\mathbf{Q} &= \sum_{n}^{3N}\mathbf{Q}_n(t) = \sum_{n}^{3N}\frac{1}{V}\sum_{i}\left[E_i\dot{\mathbf{x}}_{i,n}(t)+\sum_{j}\left(-\nabla_{\mathbf{r}_i}\Phi_j\cdot\dot{\mathbf{x}}_{i,n}(t)\right)\mathbf{r}_{ij}\right] \\ &= \sum_{n}^{3N}\frac{1}{V}\sum_{i}\left[E_i\left(\frac{1}{m_i^{1/2}}\mathbf{e}_{i,n}\dot{X}_n(t)\right)+\sum_{j}\left(-\nabla_{\mathbf{r}_i}\Phi_j\cdot\left(\frac{1}{m_i^{1/2}}\mathbf{e}_{i,n}\dot{X}_n(t)\right)\right)\mathbf{r}_{ij}\right]\end{aligned} \tag{2.19}$$

This then yields the individual modal contributions to heat flux as,

$$\mathbf{Q}_n(t) = \frac{1}{V}\sum_{i}\left[E_i\left(\frac{1}{m_i^{1/2}}\mathbf{e}_{i,n}\dot{X}_n(t)\right)+\sum_{j}\left(-\nabla_{\mathbf{r}_i}\Phi_j\cdot\left(\frac{1}{m_i^{1/2}}\mathbf{e}_{i,n}\dot{X}_n(t)\right)\right)\mathbf{r}_{ij}\right] \tag{2.20}$$

where $\mathbf{Q}(t)=\sum_{n}\mathbf{Q}_n(t)$. By substituting Eq. (2.20) into Eq. (2.3), one can obtain the contribution of mode n in total TC,

$$\kappa_{\alpha\beta,n} = \frac{V}{k_b T^2}\int\left\langle\mathbf{Q}_{\alpha,n}(t+t')\cdot\mathbf{Q}_{\beta}(t)\right\rangle dt' \tag{2.21}$$

If one sorts the vibrational modes (n) based on their frequencies, the modal contributions to TC can be represented in the form of the frequency-based TC accumulation function. It is important to emphasize here that having the full mode level detail is powerful because one can resort the contributions of the different modes according to any descriptor as desired. For example, one could compute the relaxation times or MFPs associated with different modes in a crystal, to then determine the accumulation as a function of MFPs[36]. Alternatively, one could sort the modal contributions by another descriptor, such as the PQ [43] or any other descriptor that can be well defined for all the modes in a given structure. Furthermore, one can also substitute the summation

of modal contributions to the heat flux in both places of the heat flux autocorrelation to obtain the TC as a double summation over individual mode–mode heat flux cross-correlation functions,

$$\kappa_{\alpha\beta} = \frac{V}{k_b T^2}\int\left\langle \sum_n \mathbf{Q}_{\alpha,n}\left(t+t'\right)\cdot\sum_{n'}\mathbf{Q}_{\beta,n'}\left(t\right)\right\rangle dt' = \frac{V}{k_b T^2}\sum_{n,n'}\int\left\langle \mathbf{Q}_{\alpha,n}\left(t+t'\right)\cdot\mathbf{Q}_{\beta,n'}\left(t\right)\right\rangle dt' \quad (2.22)$$

This allows the TC contribution due to correlation between pairs of modes can be calculated as

$$\kappa_{\alpha\beta,nn'} = \frac{V}{k_b T^2}\int\left\langle \mathbf{Q}_{\alpha,n}\left(t+t'\right)\cdot\mathbf{Q}_{\beta,n'}\left(t\right)\right\rangle dt' \quad (2.23)$$

Equation (2.21) allows one to obtain each mode's contribution to the total TC while equation (2.23) can be used to examine how the correlation between pairs of modes contributes to TC. Here, it should be noted that the correlation between mode n and n' contains all the levels of phonon-phonon interactions and should not be interpreted as two-phonon interactions. In the PGM paradigm, the scattering events create or annihilate phonons [1,2] at a short timescale (i.e., much shorter than the time of flight), but this physical picture is disjoint with what actually occurs in a MD simulation. In a MD simulation the phonon interactions occur continuously, as there is no sudden scattering event or discrete change in amplitude. If one were to for example generate wave packet, all the phonons participating in the wave packet oscillate continuously together to contribute to the heat flow. During these oscillations, the different modes are continually interacting, and the energy in the modes gradually couples to other modes which breaks up the collective oscillation over a time scale equivalent to the relaxation time. Thus, the MD perspective is that phonons continuously interact and wave packets made from groups of phonons gradually dissipate their energy via attenuation, which differs from the particle based physical picture consisting of discrete scattering events.

In concept, PGM based methods attempt to measure the time/distance between dephasing or the loss of correlation for wave packets, while on the other hand, GKMA measures the amount of time it remained correlation itself. In the GKMA paradigm, the correlation for a pair of modes n and n' does not translate to a two-phonon interaction, but instead it includes all 3-phonon, 4-phonon and higher order scattering related information. It has not yet been proven, but it should be noted that by representing the potential energy as a Taylor expansion, one might be able to extract two-phonon, three-phonon, and N-phonon scattering related information. This is because the heat flux and TC would become separable into 2nd order, 3rd order, and higher contributions. However, from the GKMA perspective, all that matters is how long two phonons (n and n') stay correlated, which is proportional to their corresponding contribution to TC. The longer they remain correlated, the more they contribute to the net heat flow.

2.3.2 Quantum correction

Since GKMA can provide frequency dependent TC, one can apply a quantum correction to the classical MD GKMA results at different temperatures to map classically predicted TC onto a corresponding quantum corrected value. The underlying assumption in doing so is that only the quantum effect on the specific heat must be accounted for. Turney and McGaughey [44] have shown that for crystalline materials there are two quantum effects, (i) quantum effects on the scattering rate due to incorrect mode–mode occupations, and (ii) quantum effects on the heat capacity. The first is important, as one could envision that in the limit that only a single mode is excited in the system, the time it takes for it to couple to other modes and relax towards equipartition is a strong function of the amplitudes of other modes. Thus, when other modes are simultaneously excited, it affects the rate at which mode–mode interactions occur. It has been shown that for crystalline solids this effect is critical [44], and because classical MD trajectories

do not yield the correct quantum mode amplitudes observed at low temperatures, MD incorrectly predicts higher scattering rates. However, even though this issue is important for crystalline solids, in situations where the phonon–phonon scattering processes are not the primary mechanism governing the low frequency mode TC contributions, one would imagine that the error associated with incorrect mode–mode occupations at low temperatures could become negligible. For instance, in low dimensional (e.g., nanoparticles and nanowires) systems where the majority of the low frequency phonon contributions are limited by scattering with the boundaries, the net relaxation time for most modes is dictated by the system dimensions and not the detailed mode–mode interactions, which require the mode occupations to be correct. This is especially the case for the low frequency modes which are the only modes that remain excited at low temperatures. As a result, in such a situation, one would imagine that application of a quantum heat capacity correction could still lead to good predictions/agreement with experimental data.

Using GKMA one can calculate the TC of individual modes. However a few temperature dependent corrections are needed to accurately predict the TC. Due to its classical nature, MD results in a constant heat capacity with respect to temperature, since every mode is equally excited at all temperatures. However, once each individual mode's TC is obtained, one can easily apply a quantum specific heat correction, which extends the MD based predictions to essentially any temperature. To obtain the an accurate temperature dependence TC, Lv and Henry[45] used following expression

$$\kappa(T) = \sum_{n} f_Q\left(\omega_n(T), T\right) \cdot f_{k,n}(T) \tag{2.24}$$

where index n denote the n^{th} vibrational mode in the system. Equation (2.24) includes three explicit functions of temperature, namely f_Q, f_k and ω. In this equation the function f_Q

represents the ratio of quantum to classical specific heat for mode n, which has frequency ω at temperature T and is unit-less. The function f_k represents the GKMA derived modal contributions to TC (e.g., it has the units of TC), obtained from MD simulations conducted at the simulation temperature of T. The function ω represents the phonon frequency of mode n, which itself might also exhibit some temperature dependence.

The quantum to classical specific heat ratio (f_Q) is the most important source of temperature dependence. It restricts the contributions of the high frequency modes at low temperatures and modulates the MD derived TC contributions determined from the GKMA method. The quantum expression of volumetric specific heat, based on Bose-Einstein statistics is given by,

$$C_q(\omega,T) = \frac{k_B x^2}{V} \frac{e^x}{\left(e^x - 1\right)^2} \; ; \; x = \frac{h\omega}{k_B T} \tag{2.25}$$

and the classical volumetric specific heat is given by $C_c = \frac{k_B}{V}$. Thus, the quantum heat capacity correction factor which is the ratio of C_q and C_c is

$$f_Q(\omega,T) = \frac{C_q(\omega,T)}{C_c} = \frac{x^2 e^x}{\left(e^x - 1\right)^2} \tag{2.26}$$

The second source of temperature dependence enters through the GKMA derived TC contributions (f_k). As temperature changes, the modal interactions change, and the contributions of different modes are inherently temperature dependent via the anharmonic nature of the interactions. However, unlike the quantum specific heat correction, which is a continuous function of temperature, MD simulations are run at discrete temperatures. To then generate a piece-wise continuous function for TC vs. temperature, one can interpolate the data for f_k at discrete values

of temperature. Here, one can use the data at a few initial temperatures and determine by inspection, what temperature ranges may require additional simulations to improve the resolution of the temperature dependence, e.g., in temperature ranges where the contributions change more rapidly. This is because it is advantageous to minimize the number of temperatures needed for f_k to minimize computational expense. Suppose for a given material, we calculated the frequency dependent TC at 3 temperatures, i.e., κ_{T_1}, κ_{T_2} and κ_{T_3}. Since in the classical MD simulations, all of the modes are excited, one can determine the mode diffusivity from the mode TC by dividing it by the classical specific heat, i.e., $D_T = \kappa_T / C_c$. For the intermediate temperatures, one can linearly interpolate the mode diffusivity using the two temperatures GKMA results for each individual mode diffusivity

$$D_T = \frac{D_{T_1}(T_2 - T) + D_{T_2}(T - T_1)}{(T_2 - T_1)} \tag{2.27}$$

After interpolation, one obtains the mode diffusivity and multiplies by the quantum corrected specific heat using Bose-Einstein statistics to yield the TC at a given temperature.

Finally, the phonon frequencies (ω) can slightly change with temperature, due to anharmonicity and thermal expansion[46]. If the GKMA simulations are performed at constant volume, thermal expansion does not play a role, but anharmonic effects can still cause the mode frequencies to change. The extent of the frequency shift as a function of temperature can be determined by interpolation of the data at discrete temperatures, using the peak frequency obtained from a Fourier transform of the mode amplitudes.

Using GKMA and temperature dependent corrections, one can accurately calculate the temperature dependent TC. It should be noted that in Eq. (2.24), the quantum effect is included

once for every individual mode. After calculating one mode correlations with all other modes, the specific heat is corrected for that mode. Using this method, we consider whether one mode is activated or not at a specific temperature based upon its specific heat ratio. However, Eq. (2.21) does not consider whether the other modes, which it correlates with, are excited from ground state or not at the specific temperature. However, this can be remedied by applying the quantum correction to both modes in each pair. The idea here is to use the square root of each mode's quantum correction so that when multiplied a combined correction with the correct units is obtained via,

$$\kappa_{\alpha\beta,nn'} = \frac{V}{k_b T^2}\int_0^\infty \left\langle \left(Q_{\alpha,n}(t)\sqrt{\frac{C_q(\omega_n,T)}{C_c}} \right)\cdot\left(Q_{\beta,n'}(0)\sqrt{\frac{C_q(\omega_{n'},T)}{C_c}} \right)\right\rangle dt \tag{2.28}$$

where n and n' represent two modes, Q is heat current for a mode, C_q is quantum specific heat from Bose Einstein statistics, and C_c is classical specific heat, and ω is frequency of the mode. It should be noted that the choice of using the product of square roots of each mode's heat capacity is not arbitrary, but instead motivated by a derivation given in prior work by Henry and Chen[36]. In their derivation, they represented the heat flux according to the PGM and merged it with the GK approach by substituting the phonon heat flow for the volume averaged heat flow derived by Hardy. The result of that derivation ultimately led to an expression that contained the square root of one phonon's quantum heat capacity multiplied by the square root of another phonon's quantum heat capacity. The remainder of the expression contained quantities that were related to the phonon-phonon interactions, but the main point of relevance here, is that a quantum version of the GK expression that expresses the TC of phonons, is proportional to the product of square roots of the two modes interacting. This is the motivation behind the form of Eq. (2.28), which can be applied to the 2D correlation maps. This second approach is not equivalent to the expression in

Eq. (2.24) and will yield different total TC values, but this approach is possibly better in the sense that it may, to some extent, account for the second quantum effect on the scattering rate due to incorrect mode–mode occupations.

2.4 GKMA Validation

In this section, we have introduced a correlation based modal analysis method, i.e., GKMA to understand and calculate the TC from atomistic level simulations. Importantly, the results using GKMA have produced good agreement with experiments for several amorphous materials and a random alloy, as shown in Figure. 2.1 [23,32,43,47,48]. What is noteworthy about the data in figure. 2.1 is the fact that all of the phonon contributions in all of the materials were computed with the exact same formalism, without any modification. This means that GKMA provides a unified formalism with which phonons can be understood in any material system where atoms vibrate around equilibrium positions, including individual molecules[49].

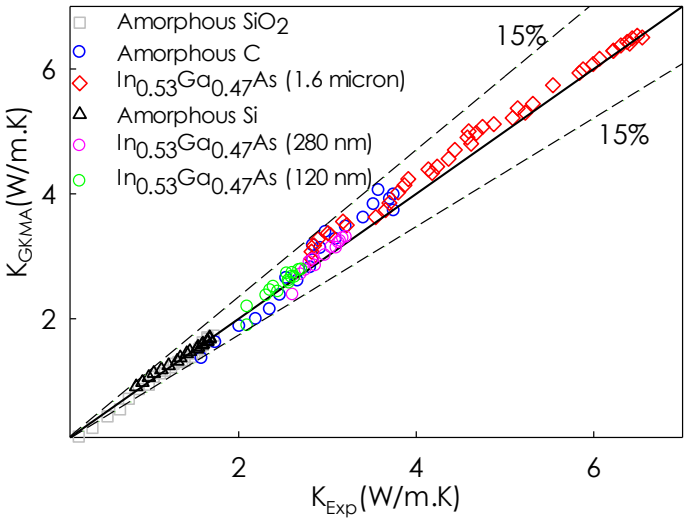

Figure 2.1. GKMA TC predictions for various solids

2.5 Virtual Crystal Approximation Method

In this section two widely used VCA[13,50] methods that have been used throughout this thesis are briefly reviewed. As discussed in chapter 1, the VCA is based on the PGM and is consistent with the predominant paradigm for interpreting all phonon contributions to TC in terms of the phonon MFPs. However, as a consequence, it requires that every normal mode/phonon have an associated velocity. In the VCA, one must first calculate each phonon's properties such as its specific heat and group velocity, both of which are derived from the model of the dispersion, as well as the phonon-phonon scattering rates. The base assumption in the VCA is then that all of the aforementioned phonon properties are appropriately weighted averages of same properties from base pure crystals. In this thesis, two primary VCA approaches will be used, termed VCA-1 which utilizes an analytical model with 5 fitting parameters developed by Wang and Mingo[50], and VCA-2 which is based on the use of Fermi golden rule for calculation of three phonon scatterings and Klemens theory for calculation of phonon-alloy scattering.

The Wang and Mingo model[50] uses analytical models for phonon dispersion, and phonon-phonon and phonon-alloy impurity relaxation times. These analytical models should empirically fit to experimental results, which limits the predictive capability of the Wang and Mingo model[50]. In this approach the TC of $A_x B_{1-x}$ alloy is given by

$$\kappa = \int_0^{\hbar\omega_c/k_B T} \frac{k_B^4 T^3}{2\pi^2 v \hbar^3} \tau(T,y) y^4 \frac{e^y}{\left[e^y - 1\right]^2} dy \tag{2.29}$$

Where k_B is Boltzmann's constant, T is temperature, $\hbar$ is Planck's constant divided by 2π, $y = \hbar\omega/k_B T$ is a dimensionless parameter, ω_c is the cut-off frequency and obtained using Debye

model. The average velocity v is calculated by $v=\left[(1-x)v_B^{-2}+xv_A^{-2}\right]^{-1/2}$, where x is element A concentration and v_A and v_B are the average speeds of sound in element A and B, respectively. The scattering time for a given frequency is related to individual processes via Mattheissen's rule

$$\tau=\left(\tau_{p-p}^{-1}+\tau_m^{-1}+\tau_b^{-1}\right)^{-1} \tag{2.30}$$

Where τ_{p-p}^{-1}, τ_m^{-1}, and τ_b^{-1} are the umklapp, mass disorder, and boundary scattering times, respectively. These are given by

$$\tau_{p-p}=\left[(1-x)\tau_B^{-1}+x\tau_A^{-1}\right]^{-1},\ \tau_m=\left[x(1-x)\zeta\omega^4\right]^{-1}\ ,\ \tau_b^{-1}=L/2v \tag{2.31}$$

Where

$$\tau_{B(A)}^{-1}=\vartheta_{B(A)}\omega^2\exp\left(-\chi_{B(A)}/T\right) \tag{2.32}$$

Where L is film thickness and constants ζ, ϑ, and χ are fitting parameters[50]. While this approach can calculate alloy TC and mode properties from the analytical models, it is not a predictive method.

The predictive version of VCA is based on the solution of phonon BTE for a virtual crystal with weighted average atomic mass, force constants, and lattice constant. In this approach, the harmonic and anharmonic IFCs are first calculated using direct displacement method [51-53] and then using Fermi's golden rule, the anharmonic phonon lifetimes will be calculated[51-53]. Afterwards, the total lattice TC can be determined under the RTA by summing up the modal contributions[51-53].

As discussed in section (2.2), the ground state energy of a crystal can be expressed in terms of IFCs by Taylor expanding about the equilibrium positions,

$$\Phi = \Phi_0 + \sum_{i\alpha} \Pi_\alpha u_{i,\alpha} + \frac{1}{2}\sum_{i,j}\sum_{\alpha,\beta} \Upsilon_{\alpha\beta} u_{i,\alpha} u_{j,\beta} + \frac{1}{3!}\sum_{i,j,k}\sum_{\alpha,\beta,\gamma} \psi_{\alpha\beta\gamma} u_{i,\alpha} u_{j,\beta} u_{k,\gamma} + \ldots \quad (2.33)$$

Where Υ and ψ are harmonic and cubic IFCs, respectively. Subscripts $\alpha, \beta,$ and γ indicate the direction of the Cartesian displacement u from the equilibrium position. The residual force Π is zero as potential is expanded around minimum energy configuration hence,

$$F_\alpha = -\Pi_\alpha - \sum_{i,j}\sum_{\alpha,\beta} \Upsilon_{\alpha\beta} u_{j,\beta} - \frac{1}{2!}\sum_{i,j,k}\sum_{\alpha,\beta,\gamma} \psi_{\alpha\beta\gamma} u_{j,\beta} u_{k,\gamma} + \ldots \quad (2.34)$$

The IFCs can be obtained by the real-space direct displacement method[51,53]. In this approach, various sets of force-displacement data are calculated by displacing atoms in the supercell. Then, the displacement-force data are fitted to Eq. (2.34), taking the translational and rotational invariances into account. Usually, considering the IFCs up to cubic terms can lead to accurate TC calculations. For harmonic IFCs a small magnitude of displacement, i.e., 0.005 Å should be used to suppress the anharmonic contributions while for anharmonic IFCs calculation larger displacements are necessary to increase the accuracy of sampling and reduce the error in anharmonic IFCs. To model the atomic interactions and calculate the forces one can use either EIP or forces directly calculated using DFT. After obtaining harmonic IFCs, the dynamical matrix for a given wave vector $\mathbf{k}$ can be calculated by Fourier transformation,

$$D_{\alpha,\beta}\left(bb', \mathbf{q}\right) = \frac{1}{\sqrt{m_b m_{b'}}} \sum_{l'} \Phi_{\alpha\beta}\left(b0, b'l'\right) \cdot e^{\left(i\mathbf{q}\cdot\mathbf{R}_{l'}\right)} \quad (2.35)$$

Where κ is atomic position of the primitive cell. Cubic IFCs are used to compute the three-phonon scattering matrix elements given by

$$V_3\left(\mathbf{q}s, \mathbf{q}'s', \mathbf{q}''s''\right) = \left(\frac{\hbar}{8N_0\,\omega(\mathbf{q}s)\omega(\mathbf{q}'s')\omega(\mathbf{q}''s'')}\right)^{1/2} \sum_{b}\sum_{b'l'}\sum_{b''l''}\sum_{\alpha,\beta,\gamma} \psi_{\alpha,\beta,\gamma}\left(b0, b'l', b''l''\right) e^{i\mathbf{q}'\cdot\mathbf{R}_{l'}} e^{i\mathbf{q}''\cdot\mathbf{R}_{l''}} \frac{e_b^\alpha(\mathbf{q}s)\, e_{b'}^\beta(\mathbf{q}'s')\, e_{b''}^\gamma(\mathbf{q}''s'')}{\sqrt{M_b M_{b'} M_{b''}}} \quad (2.36)$$

Where N_0 is the total number of mode in the first Brillouin zone, $\hbar$ is the Planck constant divided by 2π , and s denotes different polarizations. Phonon lifetimes due to umklapp and normal three-phonon scattering processes can be calculated using Fermi's golden rule to the cubic Hamiltonian[52,53]

$$\frac{1}{\tau_{\mathbf{q}s}} = \pi \sum_{\mathbf{q}'s'} \sum_{s} \left|V_3(\mathbf{q}s, \mathbf{q}'s', \mathbf{q}''s'')\right|^2 \times \left[2\left(n_{\mathbf{q}'s'} - n_{\mathbf{q}''s''}\right)\delta\left(\omega(\mathbf{q}s) + \omega(\mathbf{q}'s') - \omega(\mathbf{q}''s'')\right) + \left(1 + n_{\mathbf{q}'s'} + n_{\mathbf{q}''s''}\right)\delta\left(\omega(\mathbf{q}s) - \omega(\mathbf{q}'s') - \omega(\mathbf{q}''s'')\right)\right] \tag{2.37}$$

where $n_{\mathbf{q}s}$ is the Bose-Einstein distribution. The conservation of momentum requires $\mathbf{q} + \mathbf{q}' + \mathbf{q}'' = \mathbf{G}$, where $\mathbf{G}$ is the reciprocal lattice vector. For normal process $\mathbf{G} = 0$ while for Umklapp process $\mathbf{G} \neq 0$.

The mass disorder is treated as a perturbation. Therefore, the net scattering rate of a phonon mode is calculated as the sum of scattering rate due to mass disorder and anharmonicity, according to Matthiessen's rule:

$$\frac{1}{\tau_{\mathbf{q}s}} = \frac{1}{\tau_{\mathbf{q}s}^{p-p}} + \frac{1}{\tau_{\mathbf{q}s}^{m}} \tag{2.38}$$

The second term is Tamura harmonic mass disorder scattering rate, which is calculated by using perturbation theory[12],

$$\frac{1}{\tau_{\mathbf{q}s}^{m}} = \frac{\pi}{2N}\omega_{\mathbf{q}s}^2 \sum_{\mathbf{q}'s'} \delta\left(\omega_{\mathbf{q}s} - \omega_{\mathbf{q}'s'}\right) \sum_{\sigma} g_2(\sigma) \left|\mathbf{e}_{\mathbf{q}'s'}^{*}(\sigma) \cdot \mathbf{e}_{\mathbf{q}s}(\sigma)\right|^2 \tag{2.39}$$

where $g_2(\sigma) = \sum_i f_i(\sigma)\left[1 - m_i(\sigma) \big/ m_{i,eff}(\sigma)\right]^2$, $f_i(\sigma)$ and $m_i(\sigma)$ are the atomic concentration and mass of i^{th} isotope of the σ atom. The quantity $m_{i,eff}(\sigma) = \sum_i f_i(\sigma) m_i(\sigma)$, is the weighted average mass of atom σ and $\mathbf{e}$ is its polarization vector.

The size effects can be accounted for by using Matthiessen's rule

$$\frac{1}{\tau_{\mathbf{q}s,eff}} = \frac{1}{\tau_{\mathbf{q}s}} + \frac{1}{\tau_{\mathbf{q}s,b}} \tag{2.40}$$

where the second term is the boundary scattering rate, $\tau_{\mathbf{q}s,b}^{-1} = L \big/ 2\left|\mathbf{v}_{\mathbf{q}s}\right|$. Finally TC can be calculated based on RTA

$$\kappa = \frac{1}{3\Omega N_0} \sum_{\mathbf{q}s} v_{\mathbf{q}s}^2 \tau_{\mathbf{q}s} \hbar \omega_{\mathbf{q}s} \frac{\partial n_{\mathbf{q}s}}{\partial T} \tag{2.41}$$

where $v_{\mathbf{q}s}$ is the group velocity of mode and Ω is the volume of unit cell.

The VCA has been widely applied to many alloys including Si-Ge alloy[13], $PbTe_{(1-x)}Se_x$ [8], $(Bi_{(1-x)}Sb_x)_2Te_3$[15], and $Mg_2Si_xSn_{1-x}$[18], to name a few. However the application of VCA in alloys is questionable from the standpoint of the mode character. The limitation with the usage of the VCA is because it is based on PGM that needs a well-defined wavevector for each phonon in order to calculate the dispersion relation and group velocity. The lack of a clearly defined velocity is critical, because the PGM hinges on the velocity being defined in order to properly describe a mode's contribution to TC.

CHAPTER 3

CLASSIFICATION OF VIBRATIONAL MODES IN DISORDERED SOLIDS

As discussed in Chapter 1, most of our understanding and intuition regarding phonon transport has been derived from studies of homogenous crystalline solids, where the atomic composition and structure are periodic. For this specific class of materials, the solutions to the equations of motions for the atoms (in the harmonic limit) result in plane wave modulated velocity fields for the normal modes of vibration. However, as shown previously, whenever a system lacks periodicity, either compositional or structural, the normal modes of vibration can still be determined (in the harmonic limit), but the solutions take on different characteristics, and many modes may be non-plane wave modulated. For such systems, as we showed in Chapter 1, the normal modes of vibrations can be segregated into three types of modes, propagons, diffusons, and locons. Propagons are delocalized modes with sinusoidally modulated velocity fields that exhibit a rather identifiable wavelength and corresponded to low frequencies vibrations that in concept must occur in the low frequency limit as one must eventually observe sound waves. Diffusons are spatially delocalized modes that do not exhibit sinusoidally modulated velocity fields, but instead appear to exhibit random vibrations similar to the randomized amorphous structure itself. Lastly, locons correspond to localized vibrations that often center on atoms with significant deviations in local coordination than the rest of the structure. Conceptually, one might expect that each of the three classes of modes might contribute to thermal transport in a fundamentally different way. For example, one might expect that propagons can still be treated with the PGM, since they largely resemble the traditional phonon, as they are a sinusoidally modulated vibration (propagating

modes) that can carry energy from one location to another at a speed given by their group velocities[34]. However, it is still not clear how diffusons and locons contribute to thermal transport. Nonetheless, to develop a thermal transport framework that properly accounts for the role a mode's character plays in its contribution to TC, a critical step is to first develop a means of identifying each type of mode in a quantitative/systematic way. In this Chapter, we first review the existing methods for distinguishing propagons, diffusons, and locons. In particular, the participation ratio (PR) and SF methods to identify locons and propagons in a given structure, respectively will be discussed. Then we will present the EPA method, that quantifies the extent to which a mode's character corresponds to a propagating mode, e.g., exhibits plane wave modulation. This new method allows for clear and quantitative distinctions between propagons and diffusons. As will be shown, using EPA, we can automate the classification of modes for any arbitrary material or structure, subject to a single constraint that the atoms must vibrate stably around their respective equilibrium sites. Finally, we will discuss the PQ, which is a quantity that can be used to evaluate whether a mode more shares properties of acoustic vibrations, or optical vibrations.

3.1 Classifying Locons

Methods exist for distinguishing locons from propagons and diffusons by measuring the extent to which a mode is localized. For example, AF[30] introduced the usage of the PR as a means of distinguishing delocalized modes (i.e., propagons and diffusons) from localized modes – namely locons. This approach is straightforward and can be applied to an individual mode by assessing the size of the eigenvectors for different atoms in the mode. Mathematically PR can be defined as[31,33]

$$PR_n = \frac{\left(\sum_i \mathbf{e}_{i,n}{}^2\right)^2}{N\sum_i \mathbf{e}_{i,n}{}^4} \tag{3.1}$$

where $\mathbf{e}_{i,n}$ is the eigenvector of atom i (which runs over all the atoms in the supercell) for mode n, N is the number of atoms in the system. The above definition implies that spatially extended modes have a large value of PR_n, on the order of 1, whereas localized modes have small ratios that can reach a minimum value of $1/N$ for a mode completely localized on a single atom. In concept, locons are modes that involve a small fraction of the system and hence have low PR values. For various structures[23,31,43,47,54], the PR appears to change by more than an order of magnitude, so it seems reasonably acceptable that somewhere in the $10^{-2} - 10^{-3}$ regime, a mode could be referred to as localized, since it would mean that only 0.1-1% of the atoms in the system are participating in such a mode. Here it is important to point out that spectrum of PR values is continuous, and there is in general no strict set of rules that would require any abrupt shift in mode character. Thus, even though any scheme for identifying modes will be somewhat arbitrary, it is no different than the distinctions between photons. For example, the border between visible and infrared (IR) photons is approximate/arbitrary, and it is well acknowledged that the regime of wavelengths between 699-701 nm is approximately the regime where the transition occurs. Thus, one cannot strictly claim that a photon with a wavelength of 701.5 nm is not in the visible spectrum, but rather that it lies near the border between visible and IR light as the exact boundary is arbitrary. Nonetheless, distinguishing photons by terms such as visible, IR, ultra-violet and X-Rays etc. is still quite useful, since each regime has rather unique and distinguishing types of interactions with matter, despite the fact that all photons are simply excitations of the electromagnetic field.

Similarly, it is likely to be quite valuable to distinguish between different types of phonons, since each group may contribute to thermal transport in fundamentally different ways, despite the fact that these phonons exist on a spectrum of spatial delocalization, rather than falling into distinct, obvious categories.

3.2 Classifying Propagons vs. Diffusons

3.2.1 Structure factor method

Distinguishing between propagons and diffusons is challenging, since both are spatially delocalized. One approach is to manually look for the frequency range where the mode character changes, which is usually quite narrow, i.e. < 1 THz. This is also generally regarded as the frequency regime where the relaxation times deviate from the well-known ω^{-2} behavior, termed the Ioffe-Regel cut-off [34]. Larkin and Mcgaughy[34] used this approach to estimate the transition cut-off frequency between propagons and diffusons in amorphous silicon (a-Si) and silica using the mode relaxation times calculated via MD simulations. The problem with this method is that the distinction between propagons and diffusons is described from a collective trend, rather than being defined for an individual mode based solely on in its own characteristics. For example, it is often described by a transition/cut-off frequency, above which the modes are all diffusons and locons and below which the modes are all propagons. This transition frequency and the modes that fall on one side of the cut-off verses the other may shift slightly with temperature, or different trajectories. Therefore, this classification approach can be temperature/trajectory dependent and it is much more robust to have a classification method that relies solely upon information for a single mode obtained from a LD/SCLD calculation.

Calculation of structure factor (SF) of the supercell gamma modes is another approach that has been extensively used in the literature[34] to predict effective dispersion curves of disordered and amorphous materials experimentally and numerically[34,35,55-62]. This approach performs a space and time Fourier transform of the eigenvectors as:

$$S_{L,T}\left(\mathbf{q},\omega\right)=\sum_{\upsilon}E_{L,T}\left(\mathbf{q},\omega\right)\delta\left(\omega-\omega\left(\mathbf{q}=0,\upsilon\right)\right) \tag{3.2}$$

where ω is the frequency, $\mathbf{q}$ is the phonon wavevector and the summation is over all the modes υ at the gamma point . E_L and E_T refer to the longitudinal and transverse polarizations, respectively and are defined as

$$E_L\left(\mathbf{q},\upsilon\right)=\left|\sum_i\left[\mathbf{q}\cdot\mathbf{e}\left(\upsilon,i\right)\right]e^{i\mathbf{q}.\mathbf{r}_i}\right|^2 \tag{3.3}$$

$$E_T\left(\mathbf{q},\upsilon\right)=\left|\sum_i\left[\mathbf{q}\times\mathbf{e}\left(\upsilon,i\right)\right]e^{i\mathbf{q}.\mathbf{r}_i}\right|^2 \tag{3.4}$$

where the summation is over all atoms indexed by i in the domain, $\mathbf{q}$ is a unit vector, $\mathbf{e}\left(\upsilon,i\right)$ is the eigenvector describing the direction of motion of the atom, and $\mathbf{r}_i$ is the equilibrium position of atom i.

Equation (3.2) quantifies the spatial and temporal frequency content of the collective motions of the eigenvectors. If a collective motion exists with a well-defined frequency and wavevector, the distribution of E_L and E_T is a delta function. Therefore, the SF represents the frequency spectrum required to create a wave packet with a well-defined wave vector and polarization[34,35]. For a perfect crystals, the SF peaks are delta functions centered at the vibrational mode frequencies, indicating that the modes are pure plane-waves. With increasing disorder, the SF spreads in width, particularly at high frequencies, which is an indication that the

modes are not pure plane waves. There are three issues with SF method: (i) while the SF gives the frequency spectrum needed to construct a propagating state with pure wave vector $\mathbf{q}$, the individual mode spectra E_L and E_T [Eqs. (3.3) and (3.4)] predict the plane-wave character of each mode [34,35]. It is not generally possible to assign a unique wave vector to individual modes in disordered systems, even at low frequency. The second issue with SF method is that the SF yields different magnitudes for different materials. Therefore, the magnitude of the SF alone cannot distinguish propagons or diffusons on a universal scale and as a result, one must compare the relative magnitudes for different modes in the same structure. Thus, even though it only requires information about one mode to calculate the SF, determining the mode's classification still requires a comparison to other modes. Finally, similar to first technique discussed above, SF allows one to only define a transition frequency between propagons and diffusons. However, as will be shown in section 3.2.4, there is no requirement that the mode character must change abruptly with respect to frequency. In essence, there are almost no strict rules for the mode character, other than the fact that in the low frequency limit, one will likely always observe the existence of sound waves – which are propagons – for large systems (e.g., not small individual molecules). Thus, one cannot rule out the possibility of finding a system where very low frequency diffusons and locons and/or high frequency propagons exist, despite the fact that in practice one typically observes rather sharp transitions and segregations with respect to frequency. For example, if one were to make a bulk material that consisted of an crystalline matrix with amorphous nanoparticles embedded that are distributed throughout the structure randomly, it might be possible to observe localized modes in each nanoparticle at low frequencies. Thus, it would be particularly useful to develop an approach that can distinguish propagons from diffusons that is general and will measure the extent to which a mode is propagon-like or diffuson-like, on a universal scale that is material agnostic. Such a

method allows us to systematically and quantitatively discern the difference between propagons and diffusons.

In the next section, we present the EPA method that quantifies the extent to which a mode's character corresponds to a propagating mode, e.g., exhibits plane wave modulation[31]. The method uses equilibrium atomic positions and eigenvectors of atoms in each vibrational mode and then calculates the degree of periodicity in the mode's velocity field – termed eigenvector periodicity. It then compares the EP of a mode to another fictitious mode that has pure sinusoidal modulation. In this way the method normalizes the EP so that every mode falls between zero and unity. The extremes of zero and unity then correspond 0% and 100% sinusoidal/propagating velocity field periodicity for a given mode. After developing the mathematical formulation of EPA, we demonstrate its application to several crystalline and amorphous solids, which for the first time allows us to clearly quantify what fraction of the modes in a given structure are propagons as a function of the degree of disorder. The key here is that calculation of the EP for a mode is well-defined for any normal mode of vibration and can be evaluated in its entirety for a single mode, without any reference or relative scaling to the values of other modes.

3.2.2 Eigenvector Periodicity Analysis

Starting with a harmonic or anharmonic LD calculation (e.g., at the gamma point, since wave vectors are not well-defined for non-periodic systems and the objective here is to remain general); the eigenvectors (e.g., the velocity field) is calculated for all atoms in a supercell. For N atoms that can move in 3 dimensions, one then obtains all 3N solutions to the equations of motion at one time, each of which consists of a list of eigenvectors that describe the direction and

magnitude of each atom's motion (referred to herein as its velocity field) and a frequency for each of the 3N solutions/normal modes.

We then seek to calculate the degree of spatial periodicity for the eigenvectors of each mode. Here, in essence, we are defining the key characteristic that makes a mode a propagon as motions of the atoms that repeat spatially, in some way. This trait is not observed for diffusons, as diffusons seem to exhibit almost random velocity fields, with no clear preferred direction or periodicity, which is indicative of the underlying structure or composition that is disordered/non-symmetric. Towards measuring the degree of spatial periodicity, we note that what periodicity implies, is that two atoms separated by some distance in a particular direction will have eigenvectors pointing in the same or opposite directions, with similar magnitudes. For such pairs of atoms the inner product of their eigenvectors $\mathbf{e}_i \cdot \mathbf{e}_j$ will be a larger number than a pair of atoms that have randomly pointed vectors. This distinction then becomes the basis of distinguishing propagons from diffusons.

By comparing the inner product of the eigenvectors for a pair of atoms to the corresponding value that would have been obtained if the eigenvectors followed a periodic function oriented along a particular direction denoted by $q = 2\pi/\lambda$, where λ is the wavelength/period of spatial repetition, one can then assess the extent to which the functions match. This matching can be determined by simply taking the product of the two functions integrated over the entire super cell, via

$$\Psi_n(\mathbf{q}) = \sum_i \sum_{j \geq i} \left| \left[A_{ij,n} \right] \cdot \left[B_{ij,n} \right] \right| = \left| \sum_i \sum_{j \geq i} \left[\mathbf{e}_{i,n} \cdot \mathbf{e}_{j,n} \right] \left[f(\mathbf{q} \cdot \mathbf{r}_i + \phi) f(\mathbf{q} \cdot \mathbf{r}_j + \phi) \right] \right| \tag{3.5}$$

where the function f represents the periodic function chosen for comparison. Here, any spatially oscillatory function such as, $\sin(\mathbf{q} \cdot \mathbf{r})$, $\cos(\mathbf{q} \cdot \mathbf{r})$, or $\exp(i\mathbf{q} \cdot \mathbf{r})$ can be used for f and each will yield the same final answer when properly normalized. The first product in brackets $\mathbf{e}_{i,n} \cdot \mathbf{e}_{j,n}$ measures whether the two atoms have the same direction and magnitude. If this is true for many pairs then the sum of the products will be a large number. The second product in brackets $f(\mathbf{q} \cdot \mathbf{r}_i + \phi) f(\mathbf{q} \cdot \mathbf{r}_j + \phi)$ yields the corresponding value that would be obtained if the velocity field corresponded to a periodic function with wavelength L, phase ϕ and direction $\mathbf{q}$. The summation over all pairs then yields the equivalent of a spatial integral, which only becomes large when the values in each set of brackets match for many pairs of atoms. As a result, the function $\Psi_n(\mathbf{q})$ becomes large if the mode velocity field resembles that of the periodic function, and it provides a direct and quantitative measure of the degree of resemblance. The problem is then that one does not know for a given propagon, a priori, what direction and what wavelength will best resemble its motion. Thus, one can simply search over a wide range of values for $\mathbf{q}$ and phase ϕ, to determine which values maximize $\Psi_n(\mathbf{q})$. In the ensuing description, the prime superscript and n subscript will be used to denote the values of $\mathbf{q}$ and ϕ that maximize Ψ_n, for mode n.

The next issue then becomes the criterion used to determine the search space for $\mathbf{q}$ and ϕ. To minimize computational expense one would prefer to minimize the search space as much as

possible. Therefore, for crystalline solids (i.e., alloys), the $\mathbf{q}$-space can be defined using reciprocal lattice vectors of the primitive cell. For strongly structurally disordered systems, such as an amorphous solid, since the wave vector cannot be defined, the search space for $\mathbf{q}$ can be based on the ($R_{\max}$) and minimum ($R_{\min}$) distance between any two atoms in the super cell i.e., $\mathbf{q}_{\min} = 2\pi/R_{\max}$, $\mathbf{q}_{\max} = 2\pi/R_{\min}$. The spacing between adjacent points on the three-dimensional $\mathbf{q}$ point grid can then be calculated based on the maximum possible wavelength that can occur in that supercell, namely $\Delta\mathbf{q} = \mathbf{q}_{\min}$. In addition, since the underlying function is periodic one need only search through phase factors between $\left[0, \pi/2\right]$.

The next issue becomes the normalization, since we specifically seek to define a value that measures the degree of EP, which should be 100% for a perfectly periodic propagating mode and likely near zero for a non-propagating mode such as a diffuson. The normalization can then be done by comparing the value of Ψ_n for the actual mode, with Ψ_n for a fictitious mode that is based on the value of $\mathbf{q}'$ and ϕ' that maximized Ψ_n for the mode in question. Thus, the appropriate fictitious mode for comparison is one that is oriented along the $\mathbf{q}'$ vector with phase ϕ'. To do so, we construct a fictitious mode and assign a displacement vector proportional to $f(\mathbf{q}' \cdot \mathbf{r}_i + \phi')$ for every atom i as follows,

$$\mathbf{d}_i\left(\mathbf{r}_{i_0}\right) = \frac{\mathbf{e}_{i,n}}{\left|\mathbf{e}_{i,n}\right|} f(\mathbf{q}' \cdot \mathbf{r}_{io} + \phi') \tag{3.6}$$

where the subscript index o denotes the equilibrium position and $\mathbf{d}_i$, $\mathbf{q}'$ and ϕ' are the displacement vector of atom i in the fictitious mode, wave vector and phase angle corresponding

to maximum value of Ψ_n, respectively. Therefore, the polarization vector of each atom in the fictitious mode used for comparison can be written as,

$$\mathbf{s}_{i,n} = \frac{\mathbf{d}_i\left(\vec{\mathbf{r}}_{io}\right)}{\sqrt{\sum_i \mathbf{d}_i\left(\vec{\mathbf{r}}_{io}\right)\cdot\mathbf{d}_i^{\,*}\left(\vec{\mathbf{r}}_{io}\right)}} \tag{3.7}$$

where $\sqrt{\sum_i \mathbf{d}_i\left(\vec{\mathbf{r}}_{io}\right)\cdot\mathbf{d}_i^{\,*}\left(\vec{\mathbf{r}}_{io}\right)}$ is the normalization factor for the eigenvectors, $\mathbf{s}_{i,n}$ is the eigenvector of the fictitious mode, and the superscript $*$ indicates the complex conjugate. Therefore, the normalized Ψ_n can be calculated as

$$\gamma_n = \frac{\left|\sum_i \sum_{j\geq i}\left[\mathbf{e}_{i,n}\cdot\mathbf{e}_{j,n}\right]\left[\, f\left(\mathbf{q}'\cdot\vec{\mathbf{r}}_i+\phi'\right) f\left(\mathbf{q}'\cdot\vec{\mathbf{r}}_j+\phi'\right)\right]\right|}{\left|\sum_i \sum_{j\geq i}\left[\mathbf{s}_{i,n}\cdot\mathbf{s}_{j,n}\right]\left[\, f\left(\mathbf{q}'\cdot\vec{\mathbf{r}}_{io}+\phi'\right) f\left(\mathbf{q}'\cdot\vec{\mathbf{r}}_{jo}+\phi'\right)\right]\right|} \tag{3.8}$$

The γ_n is called eigenvector periodicity parameter (EPP) and its value represents the degree of EP on a normalized scale from zero to unity. For a mode with 100% propagating character $\gamma_n = 1$, while modes with γ_n values far from unity correspond to either localized or de-localized but non-propagating modes. By introducing the normalization factor, a propagon is not only be identified by a plane-wave that most closely matches its velocity field, but it quantifies the extent to which the mode actually resembles a plane-wave on a universally normalized scale. In this way, a single mode in any material can be assessed and compared to a single mode in any other system on equal footing. It is very important to note here that based on the analysis of an amorphous and defected

structures studied in this thesis[31], the transition between propagons and diffusons occurred round 0.2. This value is not derived or based on anything other than visual inspection, but nonetheless could be considered as a universal value that they claimed could be interpreted or used across all materials/systems (i.e., it is not an adjustable parameter).

3.2.3 Computational cost

The computational time required to calculate γ_n for a given vibrational mode in the system depends on the number of atoms in the supercell, N_{atoms}, and the resolution of both the wave vector (N_q) and phase (N_ϕ) in the search space used to evaluate Ψ_n function. Here, N_q and N_ϕ are the number of discrete wave vectors and phases in the search space. For a given mode, ${N_{atoms}}^2 {N_q}^3 N_\phi$ evaluations of Ψ_n are required to search the entire search space. This is because the search should be conducted for all q_x, q_y, q_z and ϕ points in the phase and wave vector space, in addition to evaluation of Ψ_n for each i, j pair, i.e. the double summation in Eq. (3.5). Therefore, for a given vibrational mode there are 6 "*for loops*" in the code for evaluation of Ψ_n at all the points in the search space. For example, for a crystalline silicon ($a = 0.538 nm$) with 5,000 atoms in the super cell, i.e., $N_{atoms} = 5000$, the minimum and maximum distance between two atoms can be used to calculate the maximum and minimum wave vector in the structure, i.e., $\mathbf{q}_{\max} \sim 26.97 nm^{-1}$ and $\mathbf{q}_{\min} \sim 1.08 nm^{-1}$. Therefore, the total number of $\mathbf{q}$-points in the $\mathbf{q}$-space is $N_k = \mathbf{q}_{\max} / \mathbf{q}_{\min} \sim 24$. Assuming 6 discrete values for the phase space, i.e., $N_\phi = 6$, the total number of Ψ_n evaluation will be ${N_{atoms}}^2 {N_q}^3 N_\phi \sim 2.3 \times 10^{12}$. Such a large number of Ψ_n evaluations limits the study of

systems with more than ~10,000 atoms in the super cell (as might be required for a nanostructure such as a thin film). However, such a calculation is trivially parallelizable on multi-core architectures over the number of discrete wave vectors and phases in the search space. Nonetheless, it can still be computationally expensive to do the calculations for all the vibrational modes in the system. Therefore, to further reduce the computational cost, one can break the calculations into many separate calculations where each is responsible for doing the analysis on a couple of modes. For instance, for a system with N atoms, rather than calculating the γ_n of all $3N$ from a single job, up to 3N parallel jobs corresponding the total number of vibrational modes in the system can be run to obtain the γ_n of all the modes in the supercell.

Finally, in performing calculations for γ_n, it is important to ensure that the resolution of the $\mathbf{q}$-point grid is sufficiently high. This can make it challenging to evaluate γ_n for large systems due to significant increase in computational cost, but it can have a significant effect, particularly for propagating modes with high values of γ_n as shown in Figures. 3.1 and 3.2. Typically, propagating modes are strongly sensitive to the $\mathbf{q}$-space density while non-propagating modes are not and can consequently be calculated using a coarser $\mathbf{q}$-space grid. This is due to the fact that non-propagating modes are not well represented by any periodic function and thus their values of γ_n converge quickly with increasing $\mathbf{q}$-point resolution, while propagating modes are described by a single unique $\mathbf{q}$ vector, that may not exactly lie on the $[\mathbf{q}_{\min}, \mathbf{q}_{\max}]$based grid. Therefore, in order to decrease the computational cost, one can use the baseline $\mathbf{q}$-point density based on $[\mathbf{q}_{\min}, \mathbf{q}_{\max}]$ and for modes with low values of γ_n, while for modes with $\gamma_n \geq 0.25$, an

increasingly finer grid can be used until convergence. Furthermore, one can center the refinement on the $\mathbf{q}'$ of each iteration thereby reducing the size of the search space and making the procedure efficient. As seen in Figure 3.1 and 3.2, there is a discernible $\mathbf{q}$-space density dependence for resolutions smaller than $9\times9\times9$ for c-Si, while less $\mathbf{q}$-space resolution is needed for the diffusons and locons in a-Si. It is also important to note that the phase ϕ has a significant effect on the value of γ_n for the modes with high values of γ_n, while locons and diffusons are quite insensitive to phase offsets. To decrease the computational cost associate with ϕ, one can use the baseline ϕ of $\left[0,\pi/2\right]$ for non-propagating modes ($\gamma_n \leq 0.25$), and for modes with higher values, an increasingly finer grid can be used until convergence. Furthermore, to further reduce the size of the search space –and ultimately the computational cost – it is suggested that the refinement be conducted around ϕ'.

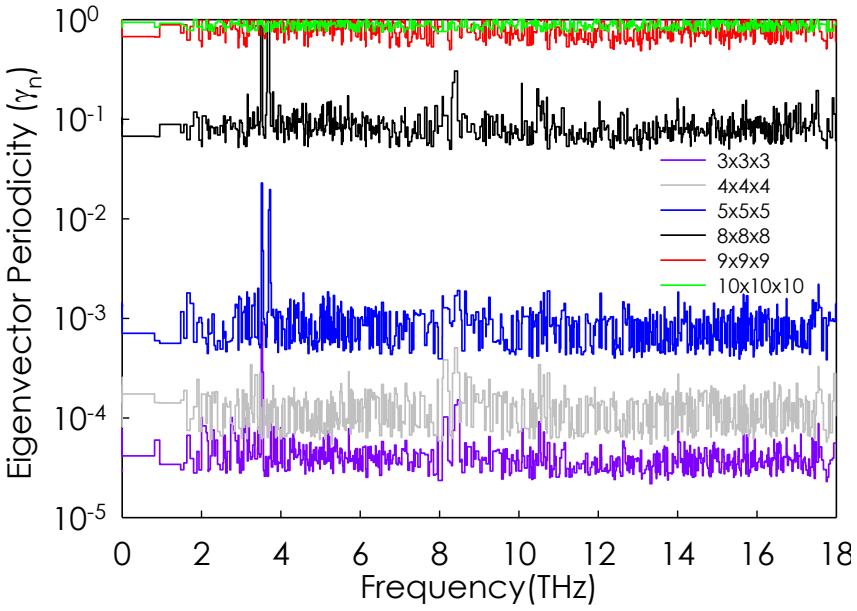

Figure 3.1. The effect of reciprocal space resolution on the determination of EP in c-Si with 512 atoms. All vibrational modes in this system are propagating.

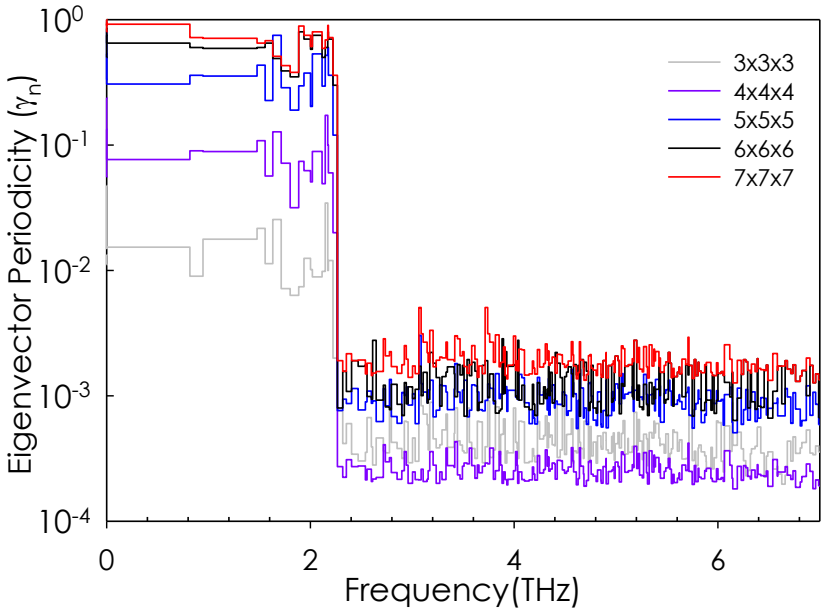

Figure 3.2. The effect of reciprocal space resolution on the determination of EP in a-Si with 512 atoms. Only low frequency vibrational modes, i.e., <2.2 THz are propagating.

3.2.4 Application of eigenvector periodicity analysis to crystalline and amorphous solids

We now examine the vibrational modes in crystalline and amorphous silicon and germanium as two example test cases. First, we calculate the γ_n for crystalline (denoted by the "c-" prefix) and amorphous (denoted by the "a-" prefix) silicon and germanium supercells with 216 atoms and compare the results to visual, qualitative inspection to confirm that the method correctly distinguishes individual eigenmodes. Second, we consider larger systems of a-Si and a-Ge to study size effects and examine convergence in the infinite system size limit.

The frequencies and eigenvectors were computed using harmonic LD calculations in the General Utility Lattice Program (GULP)[63] employing the Tersoff potential (Si[64], Ge[65]). For crystalline silicon (c-Si) and germanium (c-Ge), we used 216 atom supercells and the lattice constants were 5.431 A˚ and 5.658 A˚, respectively. The amorphous structures have between 216

and 4100 atoms, with densities of 2.33 g/cm^3 and 5.32 g/cm^3 for a-Si and a-Ge, respectively. The amorphous structures were generated using the melt and quench method as discussed in the report by Larkin and McGaughey[34]. In order to avoid structural metastability, the initial structures were annealed at 1000 K for 10 ns (Reference[34]) using the Large-scale Atomic/Molecular Massively Parallel Simulator (LAMMPS)[66] and subsequent energy relaxation performed in GULP[63].

Figures 3.3 and 3.4 illustrate γ_n vs. frequency for c-Si and a-Si, and c-Ge and a-Ge, respectively. It can be seen that in crystalline systems, all of the vibrational modes are periodic ($\gamma_n = 1$) and therefore correspond to propagons, as would be expected. However, in the amorphous materials, only some of the low frequency modes have a large value of γ_n, and the majority of the modes have less than 10% eigenvector periodicity. It is also particularly interesting to note that in the a-Si structure, there are several modes with high values of γ_n at frequencies significantly higher than ~1 THz, which would have been deemed the Ioffe–Regel cut-off, which is where the predominant shift in character occurs at 2 THz. This result is particularly interesting and is evidence that even in a typical amorphous structure, the transition between propagon-like and diffusion-like behavior may not occur at a particular frequency. Instead, the new methodology employed here shows that propagons and diffusons can exist at different frequencies with a significant amount of overlap. Figure 3.5 shows illustrations of the eigenvectors associated with several example propagons, diffusons, and locons in the a-Si studied, as identified in Figure 3.3. In the top, middle, and bottom panels, the three propagons, labeled P_1, P_2, and P_3, three diffusons, labeled D_1, D_2 and D_3, and the three locons, labeled L_1, L_2 and L_3, were identified by their respective γ_n in Figure. 3.3. The propagating modes (P_1, P_2, and P_3) from the top panel

have some plane-wave-like character. These modes are representative of modes with large values of γ_n, where modes with $\gamma_n \geq 0.2$ show similar features to that shown in top panel. The high frequency modes (L_1, L_2 and L_3) corresponding to bottom panel are highly localized. The diffusons (D_1, D_2 and D_3) are neither plane-wave-like nor localized and appear to correspond to values of $\gamma_n < 0.2$.

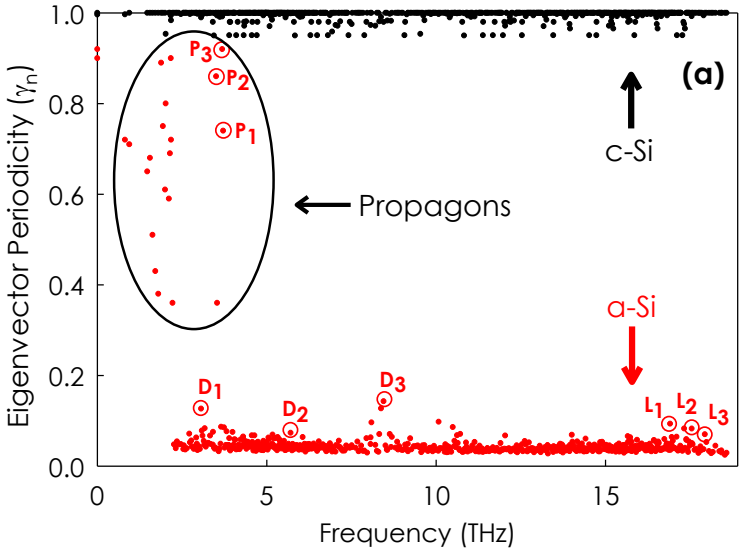

Figure 3.3. EPP for crystalline and amorphous silicon (c-Si, a-Si)

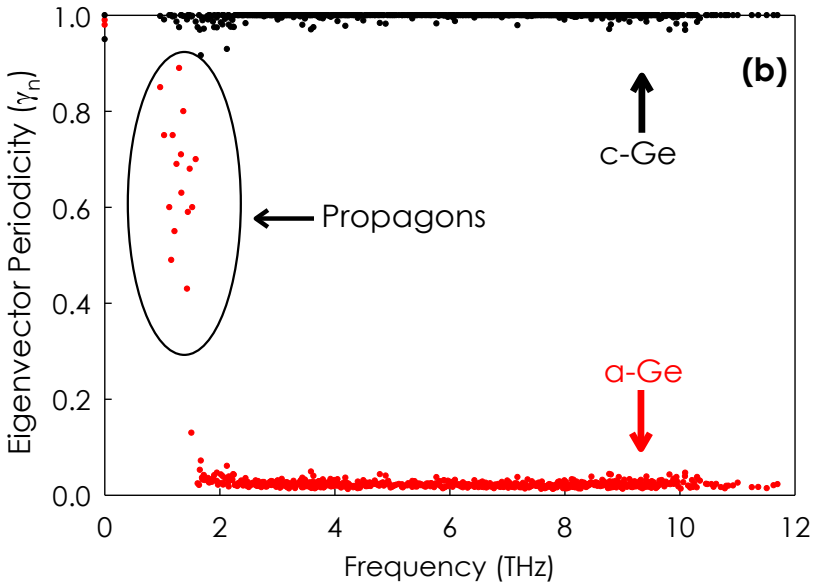

Figure 3.4. EPP for crystalline and amorphous germanium (c-Ge, a-Ge)

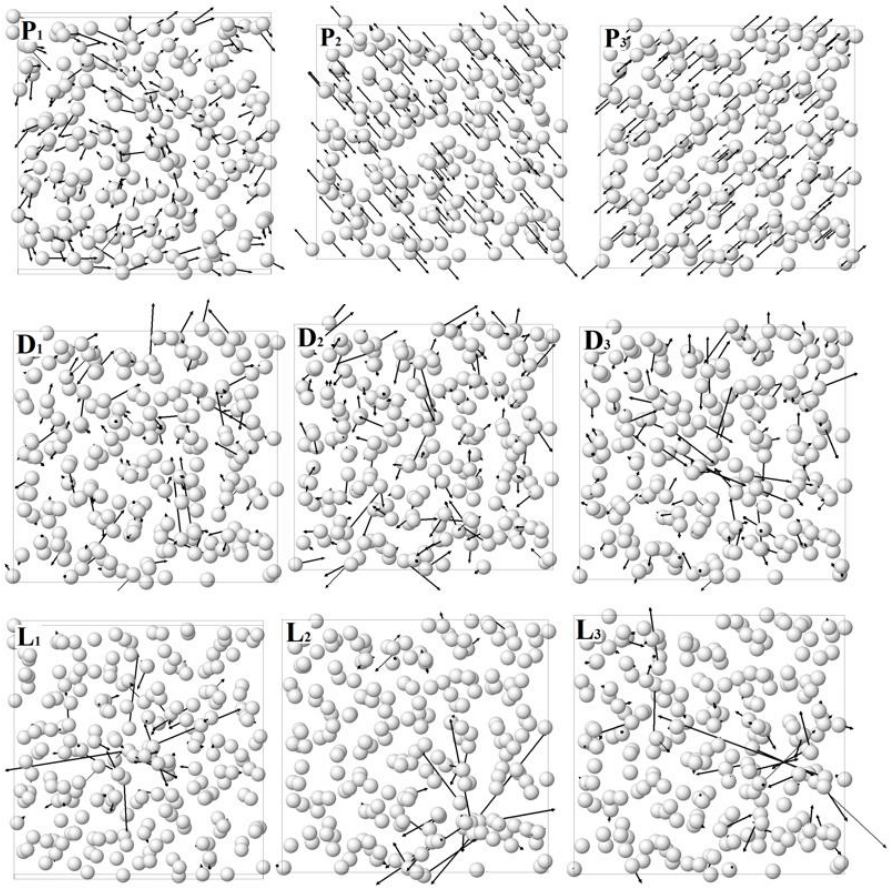

Figure 3.5. Illustration of the velocity field for example normal modes in a-Si System as identified by their value of γ_n in Figure. 3.3.

The PR and γ_n for large structures of a-Si and a-Ge, each consisting of 4096 atoms, are shown in Figures. 3.6-3.7. It can be seen that the PR drops sharply at both the low and high ends of the frequency spectrum. In the high-phonon frequency regime, the modes involve a considerably reduced number of atoms corresponding to locons. This feature is independent of the sample size, suggesting that truly localized states exist in this regime. Such localized vibrational states have also been observed in grain-boundary structures, a-Ge, a-Si, etc. The drop at the low end of the frequency spectrum, however, is due to the presence of resonant or localized modes[31]. Resonant modes are not truly localized, because they are an artifact of the finite size of the supercell and decrease in number as the size of the system increases.

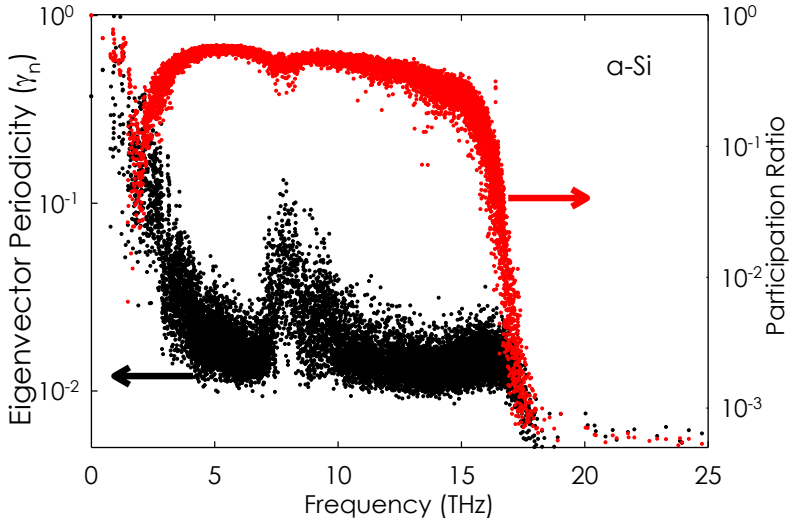

Figure 3.6. EPP and PR for a-Si

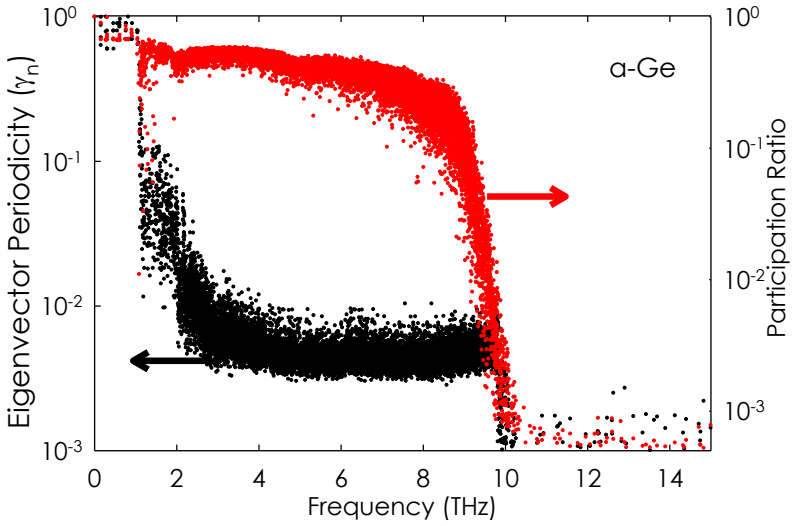

Figure 3.7. EPP and PR for a-Ge

It is important to note that with the EPA, we can now use a universal scale for judging whether a mode is a propagon or diffuson. In reality, just as the cut-off between different types of photons (visible vs. IR) is somewhat arbitrary, one cannot define a single value cut-off for γ_n that will determine whether a mode is a propagon or diffuson. However, with this now physically meaningful normalization embedded in the definition of γ_n, one can define a regime on the absolute scale between zero and unity where the transition between the two occurs, albeit heuristically.

3.2.5 Eigenvector periodicity analysis vs. structure factor method

In this section, we compare SF and EPA. As discussed in section (3.2.1), the SF measures the spatial and temporal frequency content of the collective motions of the eigenvectors. Therefore, the SF provides a different perspective from EPA, which focus on the characteristics of single eigenvectors. Recently Moon *et al[35]* calculated the dynamic SF for a-Si at 0K and 300K. They noted that if propagating waves existed, despite the atomic disorder, the dynamic SF should exhibit a clear peak, which would identify a phonon band, indicating a clear dispersion relation.

Conversely, if propagating waves are not supported, the spread in SF values would appear diffuse without an apparent dispersion relation. In their work, they showed that despite the atomic disorder, a clear dispersion exists up to frequency as high as ~10 THz for longitudinal vibrations and ~5THz for transverse vibrations. They then argued that propagating vibrational modes clearly comprise a substantial portion of phonon density of states. Furthermore, using the Ioffe-Regel criterion, they showed that the crossover frequencies from propagons to diffusons are consistent with the observed sudden broadening in the SF. They also calculated the density of states for the propagating vibrational modes with a Debye model and identified that ~24% of all phonons are propagons. This observation conflicts with the prediction based on EPA in Figure 3.6 as well as prior conclusions that propagons have frequencies less than 2-3 THz in a-Si[31].

To assess the accuracy of the SF prediction, we first visually inspect at random some of the vibrational modes in 2-10 THz region. Figures 3.8-3.10 show the mode shape for some randomly selected modes up to ~10.6 THz. It can be seen that the low frequency vibrational modes, i.e., <2.2 THz are propagating while the eigenvectors for modes with frequencies greater than 2.2 THz are random indicating they are diffusons. This is in agreement with EPA prediction in Figure 3.6 but contradict with SF prediction by Moon *et al[35]*. Delving deeper into the characteristics of the vibrational modes and the discrepancy between the EPA and SF results, we plot γ_n versus absolute value of wave vector ($|\mathbf{q}|$) as we check the values of different components of wave vector (q_x, q_y, q_z) and phases (ϕ) in the search space. To do this, we first divide the density of states between 0-10 THz into 10 bins (width of each bin is 1 THz), calculate the γ_n for 10 randomly selected mode in each frequency bin, then average the γ_n values in each bin. Figure 3.11 shows

the average γ_n vs absolute value of wave vector, i.e., $|\mathbf{q}| = \sqrt{q_x^{\,2} + q_y^{\,2} + q_z^{\,2}}$ for the phase value ϕ' that maximize the Ψ_n function. Each curve in the figure shows the frequency around which that bin is centered. As can be seen in the low frequency (<2THz) region of spectrum where all the modes are propagating ($\gamma_n \geq 0.4$), there is a clear peak with a large value which is consistent with the SF method prediction. According to SF, for modes with a plane wave character, i.e., a well-defined wave vector, the SF peaks are delta functions centered at the vibrational mode frequencies. However, for high frequency bins (>2THz), although there exist peaks at a certain wave vector, the values are significantly smaller ($\gamma_n \leq 0.2$) than the ones observed in low frequency phonons (<2THz), i.e, $\gamma_n \geq 0.4$. Due to the existence of these peaks, the SF method, based on the Moon et al. interpretation, these modes are considered propagating. However, as seen, these modes have a <20% similarity to a pure 100% plane wave mode. This finding suggests that the magnitude of the SF alone cannot distinguish propagons or diffusons on a universal scale and as a result, one must compare the relative magnitudes for different modes in the same structure. For EPA on the other hand, due to the use of a normalization embedded in the definition of γ_n, one can assess the degree of periodicity of a given mode without additional information/normalization. The analysis presented in Figure. 3.11 clearly show why the normalization factor is critical to discern between propagons and diffusons. The normalization used in EPA allows one to compare modes in any material, all on a single scale from zero to one.

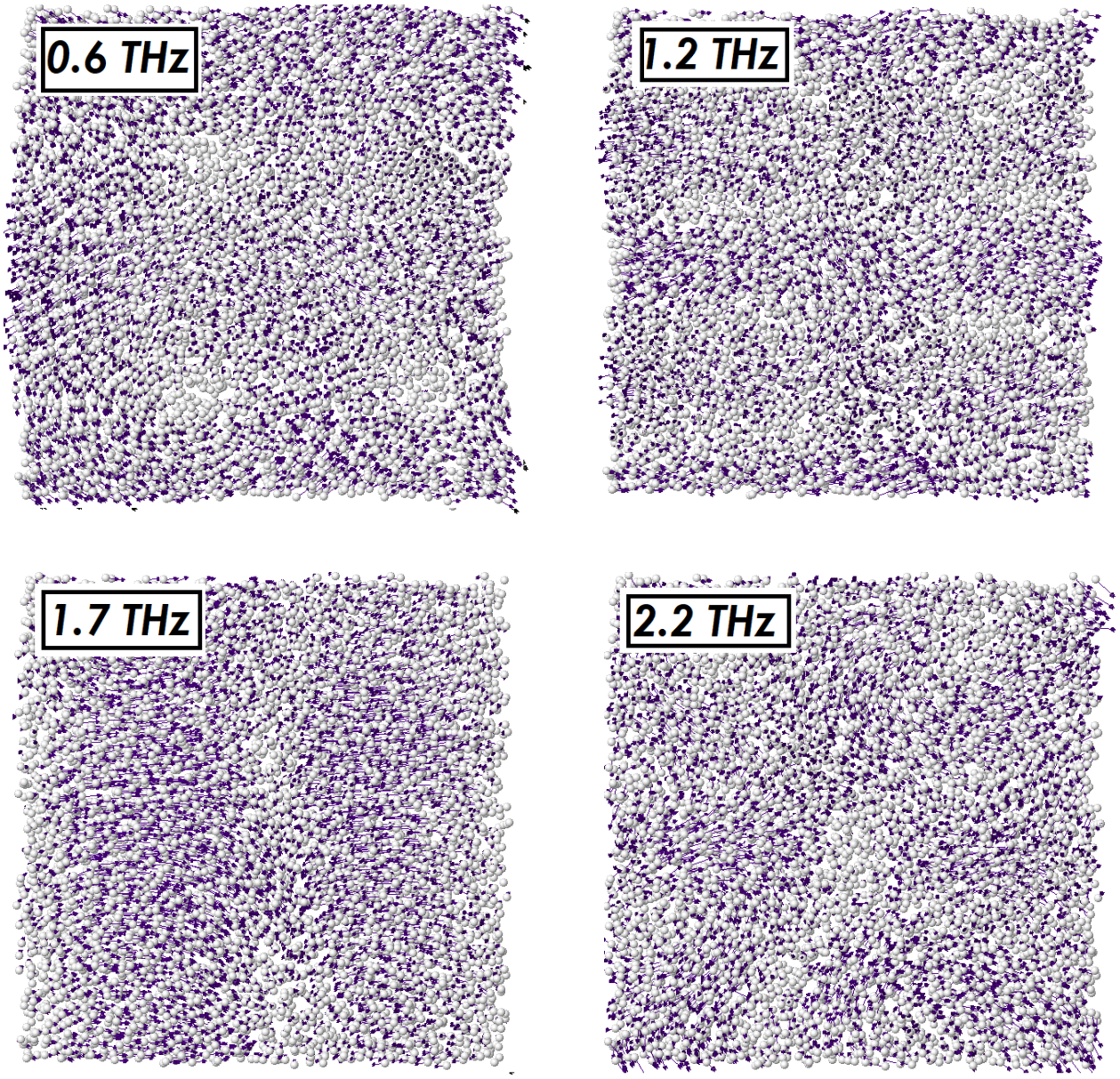

Figure 3.8. Eigenvectors of 4 randomly selected propagating modes between 0.6-2.2 THz. The arrows show eigenvector magnitude and direction

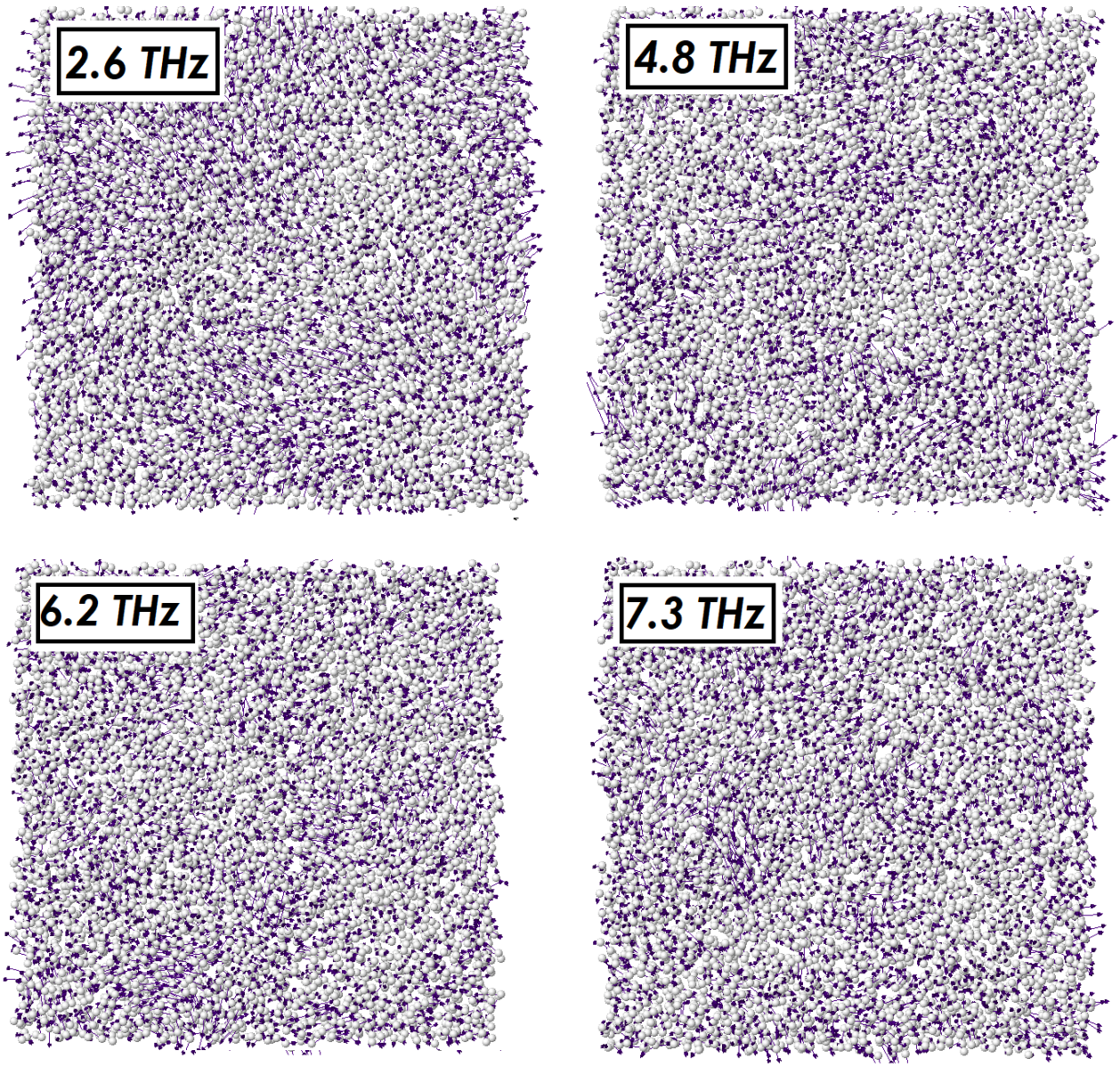

Figure 3.9. Eigenvectors of 4 randomly selected diffusons between 2.6-7.3 THz. The arrows show eigenvector magnitude and direction

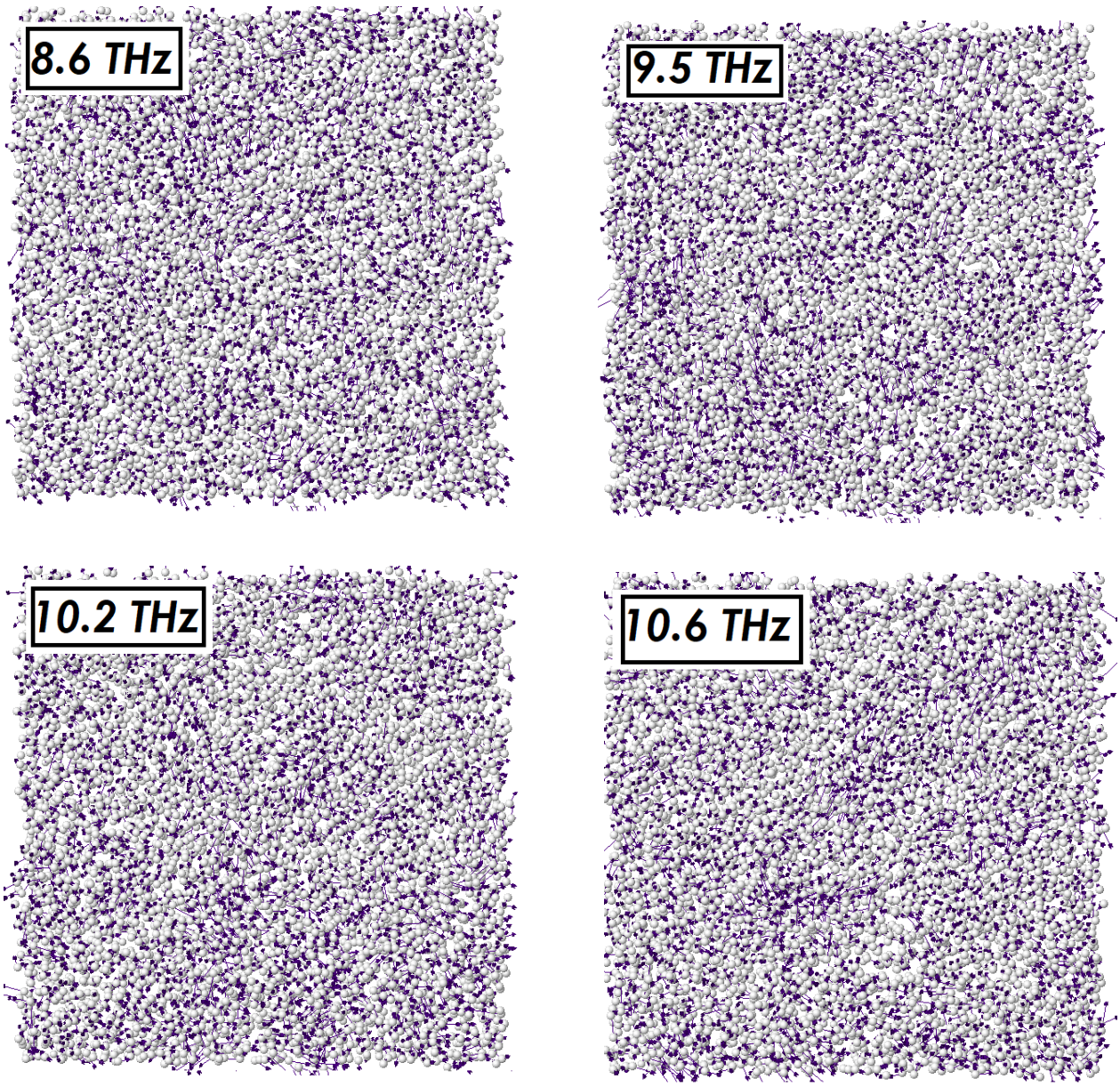

Figure 3.10. Eigenvectors of 4 randomly selected localized modes between 8.6-10.6 THz. The arrows show eigenvector magnitude and direction

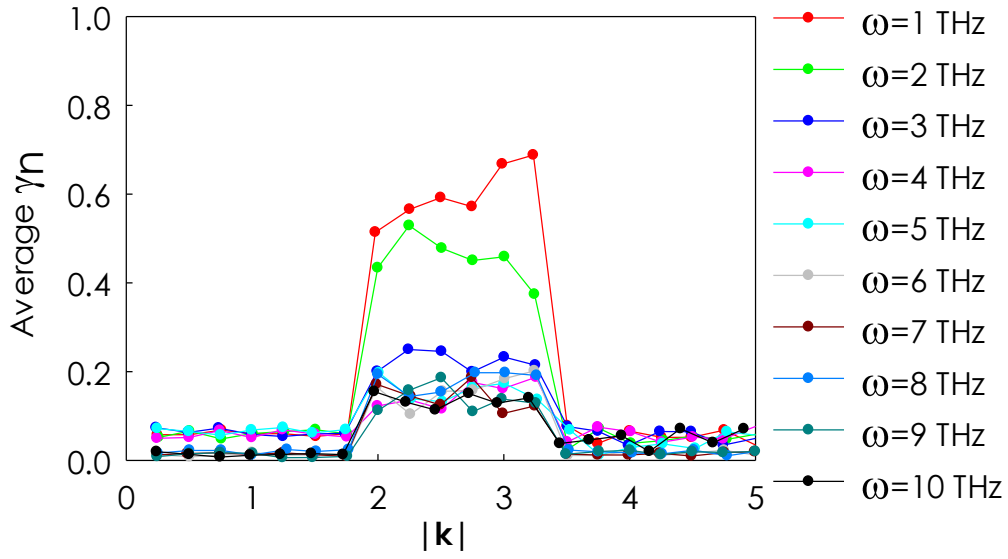

Figure 3.11. Average EPP as a function of absolute value of wave vector for a phase value that maximize the Ψ_n function

3.3 Acoustic vs. Optical Classifications

As discussed in Chapter 1, most of the phonons/modes in disordered materials have a different character, thus they may contribute to heat conduction in a fundamentally different way than described by the PGM. For the modes in crystals, which have a sinusoidal character, one can separate modes into two primary categories, namely acoustic and optical modes. However, for the modes in disordered materials, such designations may no longer rigorously apply. In this section we review the phase quotient (PQ) formula[30,43], a quantity originally proposed by Allen and Feldman [30], that can be used to evaluate whether a mode more shares a distinguishing property of acoustic vibrations manifested as a positive PQ, or a distinguishing property of an optical vibrations manifested as negative PQ.

3.3.1 Phase Quotient

Before introducing the PQ, it is important to clearly define what is meant by acoustic vs. optical. In crystalline materials, one characteristic of acoustic phonons is that they represent in-phase movements of atoms along with their immediate neighbors. Acoustic phonons also have energies that become vanishingly small in the long wavelength limit, corresponding to sound waves – hence the name acoustic. An important characteristic of optical phonons, on the other hand, is that they correspond to out-of-phase motions between an atom and its nearest neighbors. These out-of-phase vibrations in polar materials generate electric fields, which correspondingly can couple to the electromagnetic field, hence the name optical. They also have a minimum frequency of vibration that does not decay to zero as the wavelength tends to infinity. It is important to note that although these are important and distinguishing features of acoustic and optical phonons in crystals, they are not the only distinguishing features. One could presumably incorporate into their definition other attributes, but here we have simply focused on the specific attributes associated with the way in which atoms move as they participate in such modes. Therefore, in moving towards a more general definition, what would have been termed acoustic or optical vibrations in a crystal are more generally characterized by collective vibrations, whereby the atoms and their nearest neighbors (in the case of an amorphous material, these would be the atoms associated with the first peak in the radial distribution function) tend to move in either the same or opposing directions. By invoking this basic concept, in this thesis we shift our focus away from the terminology of acoustic and optical, to that of the value of the PQ[43]. The PQ of a mode was introduced by AF[30] and it directly measures the extent to which an atom and it nearest neighbors move in the same or opposing directions,

$$PQ_n = \frac{\sum_m \mathbf{e}_{i,n} \cdot \mathbf{e}_{j,n}}{\sum_m \left| \mathbf{e}_{i,n} \cdot \mathbf{e}_{j,n} \right|} \tag{3.9}$$

where the summation is done over all first-neighbor bonds in the system. Atoms i and j constitute the m^{th} bond, $\mathbf{e}_i$ is the eigenvector of atom i, and n is the mode number. In concept, when the PQ of a mode is positive, it means that the atoms move more so in the same direction as their neighbors, as opposed to the opposite direction, which would give rise to a negative PQ. The PQ is normalized such that a static displacement, where all atoms move in the same direction, i.e., a translational mode corresponding to bulk motion of the entire material, gives rise to PQ = 1. Conversely, a PQ = -1 corresponds to every atom moving in the opposite direction of its neighbors. In these extremes, one can draw correspondence to the more widely used terms “acoustic” and “optical”. At intermediate values, in between -1 and 1, the correspondence to the acoustic and optical terminology is no longer rigorous, but it is still useful to note that modes with positive PQ are arguably more “acoustic-like” than “optical-like”, and modes with negative PQ are arguably more “optical-like” than “acoustic-like”. Near PQ = 0, one cannot necessarily distinguish the difference between acoustic and optical like modes with this methodology. For example, consider modes at the Brillouin zone boundary in a crystal. Modes defined traditionally as both acoustic and optical in this region of q-space will exhibit PQ values near or equal to zero. In the analysis and discussion presented in next chapter, it is from this perspective that, we proceed, using PQ as a descriptor.

3.3.2 Application of phase quotient to pure homogenous crystalline systems

It is instructive to inspect the PQ of pure homogenous crystalline solids and compare the acoustic/optical features with the ones can be obtained from the dispersion curve. Figure 3.12 shows the PQ for crystalline InAs and GaAs systems verses frequency. As expected for both systems, the PQ starts from 1 at the low-frequency region of the spectrum and ends at -1 for high frequency phonons. For InAs, the majority of the phonons below the lower edge of the phonon band gap (~5.2THz) have a PQ >0, while the majority of phonons above the upper edge of bandgap (~5.8THz) are optical with PQ <0. These results are in good agreement with *ab initio* phonon dispersion calculations of Zhou *et al*[67] which predicts a similar transition frequency between acoustic and optical modes. For GaAs, there is no phonon band gap, and therefore we observe a mixture of optical and acoustic phonons around 6-8 THz as the transition from acoustic to optical occurs around this point, which is in agreement with the *ab initio* phonon dispersion calculations of Sternik *et al.*[68].

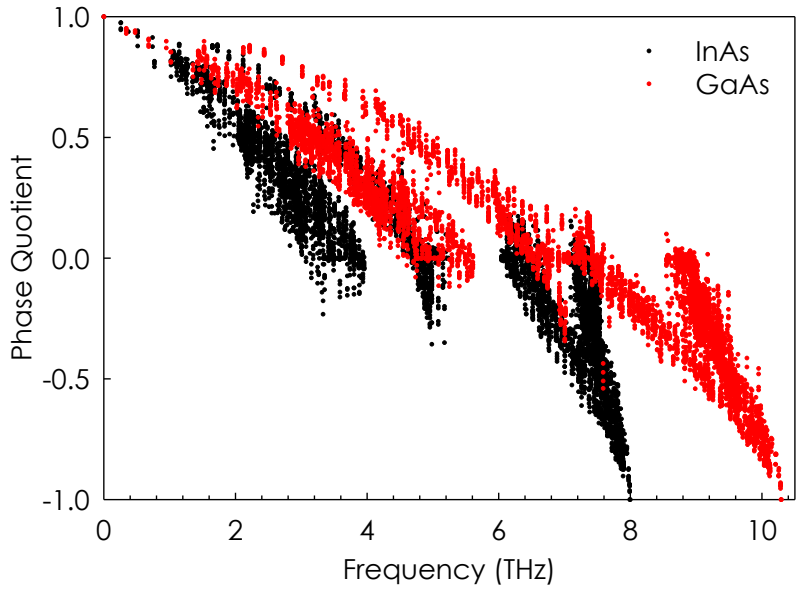

Figure 3.12. PQ verses phonon frequency for InAs and GaAs.

In conclusion, in this chapter, we have introduced a new method, EPA, for classifying normal modes of vibrations; the method is general and based on individual mode character. Previous classification methods have been restricted to SF based methods and qualitative sorting of the vibrational modes according to their frequencies, which is not be accurate in many instances. However, with the introduction of "eigenvector periodicity", one can classify the propagating vibrational modes based on their mode character, which is more general and provides a universal scale that can allow for comparisons between different materials. As opposed to the SF method, which considers many modes collectively, EPA assess the degree of periodicity of individual modes. Thus, this new method is currently the only method that can be used to study individual modes in the system. The EP parameter (EPP) introduced in this chapter measure the extent to which a mode is propagon like or diffuson like, on a universal scale (between 0 and 1) that is material agnostic. The extremes of zero and unity correspond 0% and 100% sinusoidal/propagating velocity field periodicity for a given mode. It is important to note that the calculation of the EPP for a mode is well-defined for any normal mode of vibration and can be evaluated in its entirety for a single mode, without any reference or relative scaling to the values of other modes. We also showed that there no requirement that the mode character must change abruptly with respect to frequency. By studying the trend of EPP versus frequency for different structures, it was observed that there is no sharp cutoff frequency between propagons and diffusons, suggesting there is no strict set of rules that would require any abrupt shift in mode character. Finally, we also discussed the reason for discrepancy between EPA and the SF method used by Moon *et al*[35] for distinguishing propagating modes in a-Si. Finally, we introduced the PQ formula that can be used to study the acoustic/optical character of vibrational of modes in disordered solids.

CHAPTER 4

NEW INSIGHTS INTO THERMAL TRANSPORT IN RANDOM ALLOYS

In Chapter 1, we discussed the fact that for the majority of vibrational modes in random alloys, due to lack of a well-defined phonon group velocity, the application of the PGM/VCA is highly questionable. However, because of the absence of a suitable alternative theory, the PGM/VCA has been used extensively during the last 50 years to study thermal transport in various random alloys [3,11,13-21,23,50,51,69]. This is because the PGM/VCA is the sole theoretical framework to have ever been introduced to study thermal transport in alloys[11]. In Chapter 2, we reviewed the formulation of the newly developed correlation-based theory of phonons, i.e., GKMA, and showed that it does not have the problems associated with the PGM/VCA. Since GKMA doesn't require a group velocity to calculate the contribution of individual vibrational modes to the TC, it can be used to study disordered systems such as random alloys and amorphous solids. The excellent agreement between experimental data and GKMA results for various disordered materials [23,32,43,45,47,48,54,70] has helped to validate its formulation, lending confidence to its predictive power. To more deeply understand the role of different type of vibrational modes – and in particular, the role of mode character – to heat conduction, it is critical to distinguish between propagons, diffusons, and locons. Toward this end, in Chapter 3, we introduced EPA to calculate the mode character in disordered solids and distinguish between propagating and non-propagating vibrational modes (diffusions and locons). EPA quantifies the extent to which a mode's character corresponds to a propagating mode, e.g., exhibits plane wave modulation. We have studied different systems and showed that EPA is the only method that allows for clear and quantitative distinctions between propagons and diffusons/locons in any

arbitrary material or structure. In the proceeding chapter, we will use EPA and GKMA to answer two fundamental questions raised in Chapter 1: (i) how does vibrational mode character change in random alloys when alloy composition changes? According to the PGM, introducing any type of disorder to a pure homogenous solid only alters the phonon scattering mechanisms in the solid, while the vibrational modes are still the same as the ones exist in the pure homogenous system. However, it is not clear if this assumption is valid. (ii) What is the fundamental reason for the failure of the PGM in random alloys? More specifically, what fundamental information is missing in the PGM when it comes to predicting the TC of random alloys? Answering these questions will refine our understanding of how phonons behave in random alloys, which ultimately might lead to the ability to manipulate phononic contributions to the TC.

4.1 Determining if the scattering paradigm is invalid

As previously discussed, in infinitely large, pure, homogeneous crystalline solids, the vibrations experienced by an atom are a superposition of oscillations by some or all atoms at a single frequency, which are often termed normal modes of vibration[23]. In such systems, one can solve the equations of motion in the harmonic limit and find that all solutions correspond to plane wave modulated vibrations, which is a result of the structural periodicity. If one adds together solutions with similar wave vectors, one then obtains a wave packet that propagates energy at the group velocity ($d\omega/d\mathbf{q}$) and resembles a moving particle. According to the PGM, these vibrational modes can be treated as quasi-particles that travel and scatter with each other, similar to a gas of molecules. In alloys, the theory of phonon transport is based on the VCA, which utilizes the same scattering-based physical picture to describe the interaction of phonons. The VCA treats the presence of dissimilar elements in an alloy lattice as though they act as scattering centers for the phonon gas. In other words, in random alloys, an additional scattering mechanism – namely

compositional impurity/defect scattering – is superimposed to the intrinsic phonon-phonon scattering to account for the effect on heat transport of the alloying atoms. This impurity scattering term is what qualitatively causes the VCA to correctly predict the typical U-shaped curve observed for TC vs. composition in most alloys. However, as discussed in Chapter 1, there are instances where the VCA fails both qualitatively and quantitatively [19-23]. In the following sections, we will discuss the fundamental reason for the failures of the PGM/VCA in random alloys. In particular, we will show the scattering picture is not appropriate to describe the transport in random alloys, because the vibrational modes in alloys are fundamentally different from the modes that exist in pure homogenous crystalline solids. We will examine in-depth the behaviors of phonons in InGaAs random alloys as a representative example, because its compositional disorder reveals a rather fundamental issue with the way phonons have been conceptualized, namely considering them to be plane waves/quasi-particles that propagate and scatter.

4.1.1 The role of disorder on mode character

The fundamental problem with applying the PGM/VCA to an alloy is the presumption that all of the phonons/modes correspond to plane waves, thereby justifying invocation of expressions for TC that are based on the PGM. In reality, when one adds a dissimilar atom or a defect/impurity to a previously pure homogenous crystal, one breaks the symmetry/periodicity that limits solutions to the equations of motion to plane waves. As a result, one obtains solutions with a very different character than a plane wave-modulated distribution of atom displacement/velocities (see Figures. 4.1 and 4.2). Here, we used the EPA introduced in Chapter 3 to analyze the modes in an $In_{1-x}Ga_xAs$ random alloy. Interestingly, the eigenvectors (e.g., the displacement/velocity fields[31]) for the normal modes in a crystalline random alloy fall into the same three categories identified by AF for amorphous materials, i.e., propagons, diffusons and locons[30]. It is important to note that the

existence of non-propagating vibrational modes in crystalline random alloys had previously been theorized by AF, but the data in Figure. 4.1 is the first evidence to confirm AF's claim[30]. Figure 4.2 shows the calculation of the fraction of modes that are propagons in $In_{1-x}Ga_xAs$ as a function of In content. As expected for endpoints solids, i.e., InAs and GaAs, all the vibrational modes have a propagating character, but alloying either composition even slightly, the majority of vibrational modes change their propagating character and they become either diffusons or locons. Based on the data in Figures. 4.1 and 4.2 , one might expect that an expression for alloy TC that is based on the PGM might exhibit significant errors in its description of TC vs. temperature for alloys in the 15-85% composition range, because in this regime, less than 2% of the modes are propagons. Again, this is because the PGM is built on the assumption that all modes propagate; thus when situations occur where this is not true, one would expect PGM based theories/models to breakdown, e.g., for alloys in the 15-85% composition range.

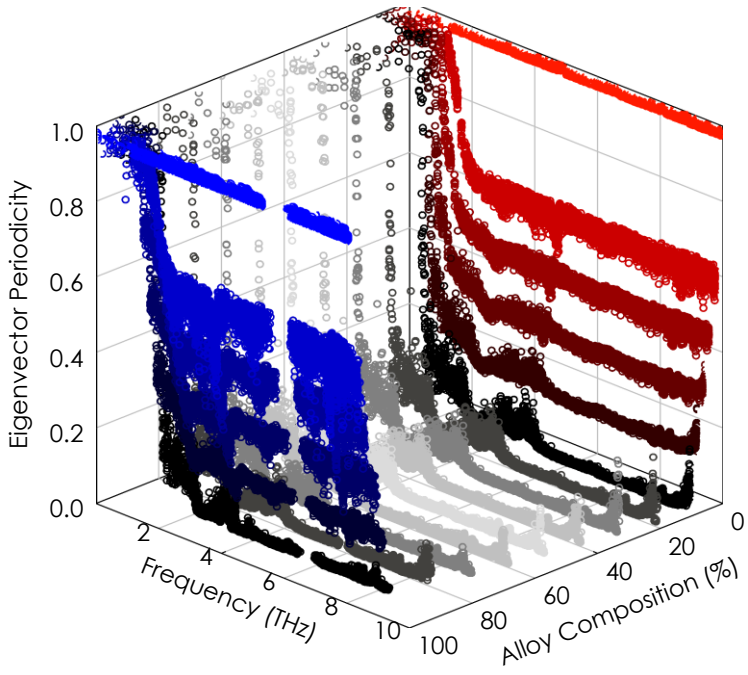

Figure 4.1. EPP for $In_xGa_{1-x}As$, as a function of alloy composition

It is also remarkable that even in the dilute limit, for impurity concentrations between 0.1-2%, most of the modes in what would generally be considered a rather pure crystal are far from being pure plane waves. Figures 4.1 and 4.2 show examples of how the mode character evolves in this regime, and it is clear that such low impurity concentration result in a majority of vibrational modes losing ~40% of their propagating character (the maximum EPP for > 2THz phonons is ~60%). This realization is insightful, because given that the momentum of phonons ($\hbar\mathbf{q}$) is derived from the assumption that phonons are plane waves, this warrants a significant rethinking of how phonons in non-pure crystals interact with other quantum particles such as electrons, photons, and neutrons. It should also be emphasized here that the results in Figure. 4.1 and 4.2 suggest that "pure" for phonons implies impurity concentrations less than 0.1-1%, yet many materials used in industrial applications are only 97-99% pure.

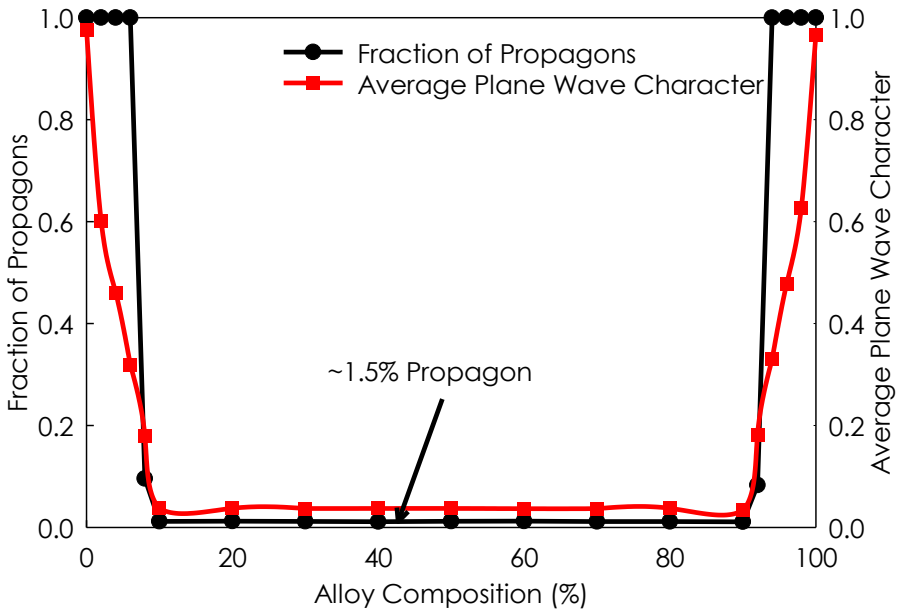

Figure 4.2. Average EPP and fraction of propagating modes vs. In composition

To see how the mode character changes when EPP decreases, the eigenvectors of six randomly selected vibrational modes with different values of γ_n are shown in Figure 4.3. Such visual inspection of modes is insightful, because it shows very clearly what aspects of a mode's propagating character are first lost and how the transition from propagon to diffuson occurs. The panels on the left show the eigenvectors along the length of the computational domain while the panels on the rights show the eigenvectors viewed from the cross section of the computational domain. It can be seen that for $\gamma_n = 1$, the eigenvectors correspond to plane wave modulated vibrations (i.e., propagating waves). In this case, the wavelength can be clearly recognized as the distance over which the wave's shape repeats. By decreasing the EPP, the vibration of atoms becomes more random and the modes tend to become non-propagating. For example, when $\gamma_n = 0.6$, one can clearly see more random vibrations in the cross section of computational domain compared to the mode with $\gamma_n = 0.8$. However, in both cases, along the length of the computational domain, periodicity is still evident. For $\gamma_n = 0.4$, the eigenvector seems to be completely random when viewed from the cross section, and one might consider this mode as diffuson. However, this mode can still be considered a propagons, because the transition between propagon and diffuson occur at $\gamma_n = 0.2$, as discussed in Chapter 3. For $\gamma_n = 0.2$, the vibrational directions are fully random and the mode is a diffuson, hence one cannot define an effective wave vector for this type of vibration. For $In_{0.53}Ga_{0.47}As$, as shown in figure 4.2, the majority of vibrational modes are diffusons. As will be shown in the next section, these modes contribute significantly to TC at room temperature, and their contributions to TC increase with increasing temperature, a phenomenon that cannot be explained by PGM. Finally, the two bottom panels show an example of a localized mode with $\gamma_n = 0.05$. Locons are only a small fraction of vibrational modes in $In_{0.53}Ga_{0.47}As$ system

and do not contribute to TC of this system significantly, as will be seen in the following section. In conclusion, we have shown how vibrational mode character changes with a changing alloy composition. By increasing the disorder in random alloys, the EPP decreases, and consequently the mode character from propagating vibrational modes to non-propagating diffusons.

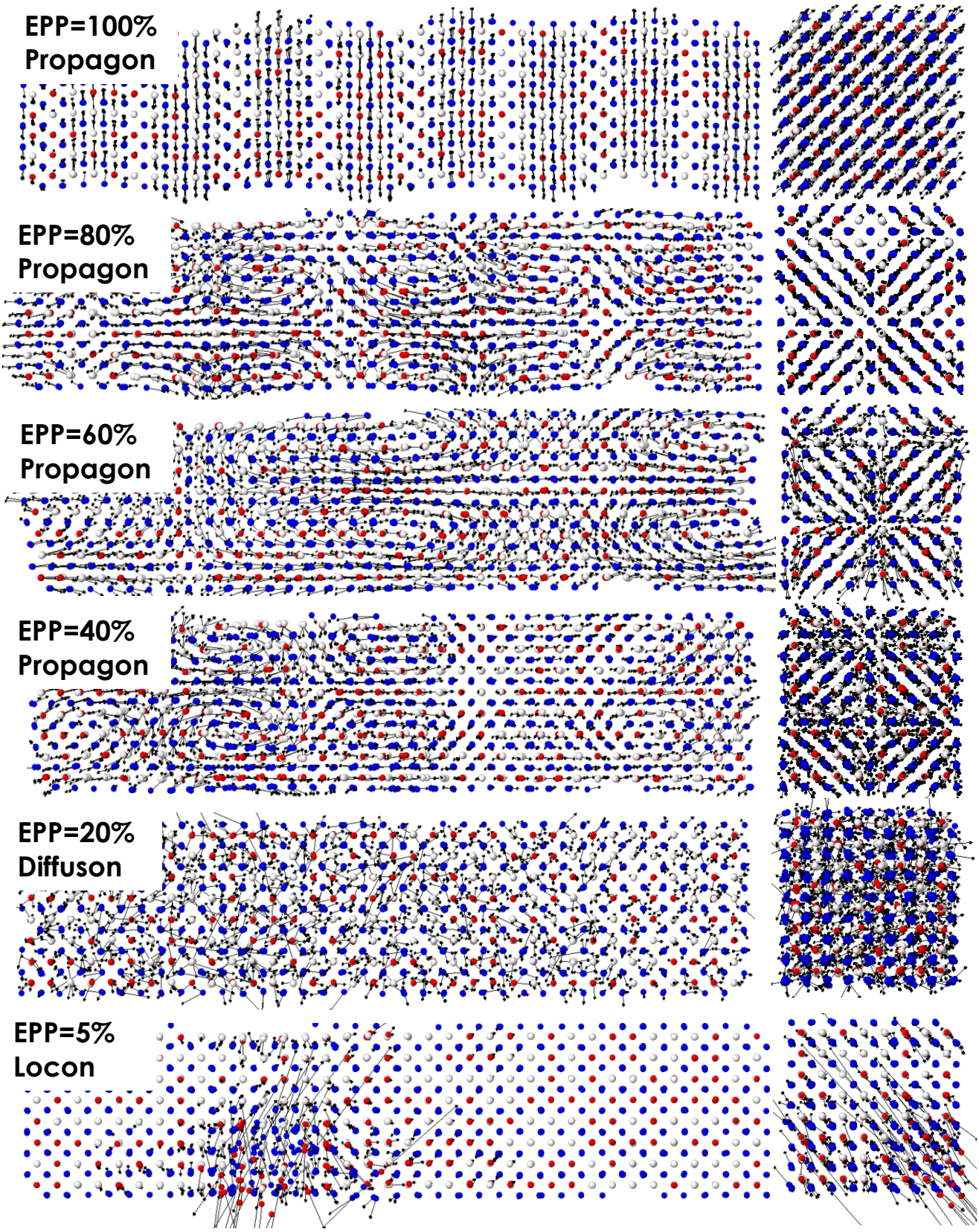

Figure 4.3. The effect of EPP on modes in $In_{0.53}Ga_{0.47}As$

Finally, to qualitatively determine the correlation between γ_n and TC versus alloy composition, we calculated the TC of $In_xGa_{1-x}As$ alloys at different compositions and room temperature. Figure 4.4 shows TC as a function of alloy composition at room temperature, calculated using the GK method. The error bars are the standard deviation of the results from independent simulation ensembles at a given In composition. It is important to note that at 300K, quantum effects play a minimal role, thus GK can calculate accurate values of TC without applying quantum corrections. As seen in Figure 4.4, the predictions yield good agreement with experimental data for the alloy TC at all compositions. Notably, the TC is found to drop sharply after only a small amount of alloying. In the composition range 15 %< x< 85% the alloy TC becomes nearly independent of composition, before again increasing when the composition approach to 100%, i.e, InAs. It is important to note that according to the PGM/VCA, this U-shape trend of TC versus composition is due to phonon-impurity scattering. The validity of this physical explanation is suspect, because at high alloy concentrations, i.e., ~50%, almost every other atom in the system is effectively an impurity. Consequently, it is not clear whether phonons in this system would still have a propagating character. However, the results presented in Figure. 4.4 suggests that the reason the alloy TC drops quickly within the first 10% may be associated with the loss of propagating character, as opposed to impurity scattering; such an explanation is a fundamental shift in how TC in disordered materials is conceptualized.

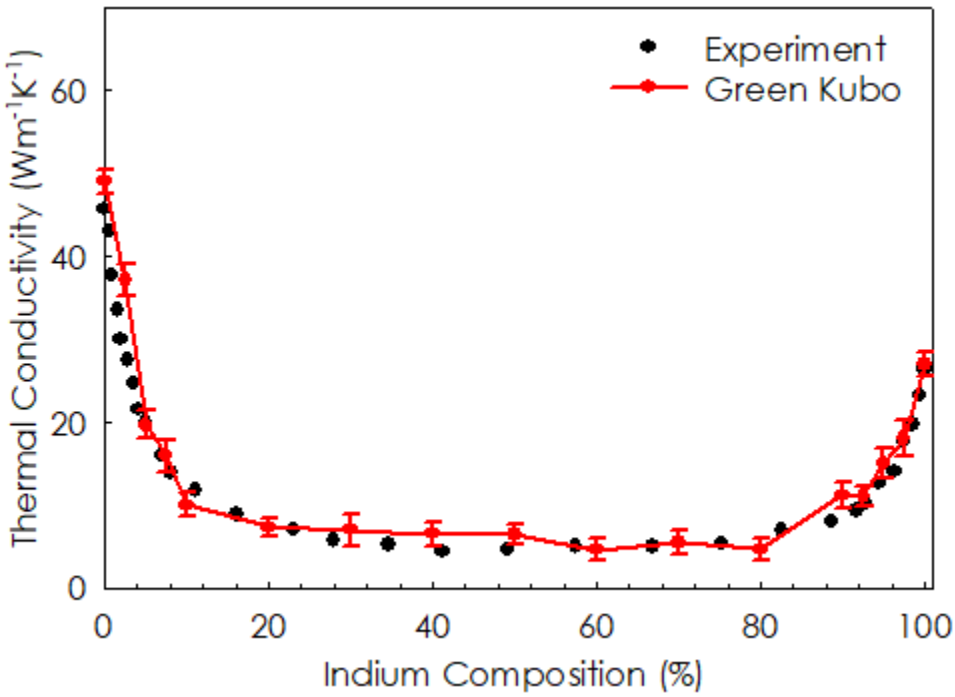

Figure 4.4. TC of $In_xGa_{1-x}As$ vs. Indium composition at 300K calculated using GK-MD

4.1.2 Mode character: The key information missing in the Virtual Crystal Approximations

The results presented in Section 4.2 suggest that the conventional theory and understanding of phonons in random alloys should be revisited, because the critical assumption that all phonons/normal modes resemble plane waves with well-defined group velocities is no longer valid when disorder is introduced, and symmetry is consequently broken. As seen by increasing the alloy concentration, the vibrational mode character changes, and the majority of vibrational modes become non-propagating, i.e., diffusons and locons. Therefore, one can hypothesize that the fundamental reason for failure of PGM/VCA is the absence of knowledge of mode character in its framework. To test this hypothesis, in this section, we study the random alloy $In_{0.53}Ga_{0.47}As$ a test case. Since the majority of vibrational modes in this system are non-propagating (see Figure. 4.2). It is important to note that the PGM/VCA theory cannot be used to calculate the TC contribution

of non-propagating modes, i.e., diffusons and locons because one cannot define their group velocities. Therefore, one must use an alternative method to describe their TC contributions. As discussed in Chapter 2, GKMA is a powerful method that can directly assess a mode's contribution to TC without any invocation of the PGM, as one needs only to utilize the mode level contributions to each atom's velocity to calculate mode's contribution to heat flux and consequently TC. In this sense, the key feature of the GKMA method is that it describes phonon transport in terms of correlation, rather than scattering, which is a major shift in perspective from the current understanding. Therefore, in the proceeding sections, we use GKMA to calculate the TCs and test the above hypothesis about the lack of mode character in the PGM/VCA framework. In particular, two case studies are conducted. The first case study examines whether non-propagating modes exhibit size effects. Diffusons and locons are non-propagating modes, hence we hypothesize that they do not exhibit size effects, as they cannot propagate. By comparing the TC of thin film samples with predictions based on GKMA (in which size effects are only applied to propagating modes), we will show that this hypothesis is valid, hence diffusons exist in random alloys and contribute to TC. This serves as evidence that not only do non-propagating modes exist in alloys, but they significantly affect the material's TC, hence the critical assumption of plane-wave vibrational modes in the PGM/VCA is incorrect. The second case study examines the relationship between phonon relaxation time and mode TC for non-propagating vibrational modes. If the PGM/VCA is applicable to non-propagating vibrational modes in random alloys, their relaxation times should be proportional to the mode TC. Using GKMA and NMA, we will compute mode relaxation time and mode TC and show that there is no simple proportional relationship between them. This serves as a second indicator that the PGM/VCA is not suitable to describe the alloy TC, and we need an entirely new paradigm to understand alloy TC.

4.1.2.1 Size effects on thermal conductivity of non-propagating modes

To illustrate the importance of considering mode character, we first modeled a $In_{1-x}Ga_xAs$ system using both the VCA and GKMA. We then determined the TC as a function of composition at room temperature, after which we studied the TC of the $In_{0.53}Ga_{0.47}As$ alloy vs. temperature for several film thicknesses. To model the atomic interactions and calculate the interatomic forces we used an EIP, namely the Abell-Tersoff potential[71], which was optimized using *ab initio* data. The accuracy of the Abell-Tersoff potential[71] was verified first by its predictions of the TC vs. temperature for the InAs and GaAs separately using the BTE[51]. The harmonic and anharmonic IFCs are first calculated using direct displacement method[53] . Then, using Fermi's golden rule[53] the anharmonic phonon lifetimes are calculated. Finally, the total lattice TC is determined under the RTA[51,53] by summing up the modal contributions. For the harmonic IFCs calculation, we used small magnitude displacements (0.005 Å) to suppress the anharmonic contributions, while for anharmonic IFCs, larger displacements (0.02 Å) are used to increase the accuracy of sampling and reduce the error in anharmonic IFCs. We then used a cubic supercell of a $2\times2\times2$ conventional unit cell, which consists of 64 atoms in total to compute the IFCs. To calculate the TC, a $30\times30\times30$ $\mathbf{k}$ -point mesh within the first Brillouin zone was used to ensure convergence. We have confirmed that the TC is converged with respect to grid size when a $30\times30\times30$ grid is used. For further details, readers are directed to Reference[51,53]. Figure 4.5 shows the calculated lattice TC of InAs and GaAs, and the values are compared against available *ab initio* and experimental data [72-76]; for both compounds, the calculated TC agrees reasonably well with previous data. The small discrepancies between the present work and experimental results might come from defect scattering and impurities in the experimental sample, which results in lower thermal conductivities compared to theoretical predictions. Higher order phonon scattering, which is not

included in this calculation, might be another reason for such discrepancy, especially at higher temperatures. The good agreement between the theoretical predication and experimental data demonstrate the accuracy of our approach and the validity of the RTA, and the data support our following discussion.

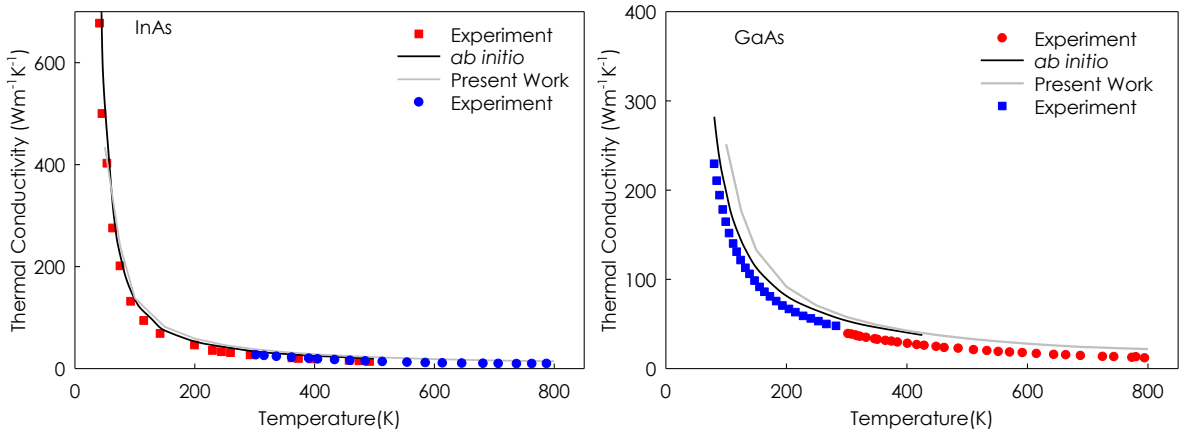

Figure 4.5. Temperature dependent TC of InAs and GaAs as predicted by the empirical potential used in this thesis. Data is compared to *ab initio* results from Li and Mingo[73] (for InAs) and Lue *et al*[74] (for GaAs) and to experimental data[72,75,76].

To calculate the TC of alloys using the VCA, the disordered crystal is replaced with an ordered one with a compositionally weighted lattice constant, IFCs, and atomic masses. The mass disorder and anharmonicity are both treated as a perturbations, as discussed in Chapter 2. The room temperature bulk TC of $In_{0.53}Ga_{0.47}As$ using an EIP is 8.07 W m^{-1} K^{-1}, while the prediction based on first principles calculations[77] is 8.28 W m^{-1} K^{-1}. This agreement between the TC predicted using EIP and first principle calculations further indicates that the EIP accurately describes the interatomic forces for the alloy sufficiently well for the purposes herein. Finally, we also employed a second method for calculating the TC of the alloy using the VCA, whereby fitting parameters

were used to describe phonon-phonon and phonon-alloy impurity relaxation times originally developed by Wang and Mingo[50]. A comparison of the TC of $In_xGa_{1-x}As$ calculated using the VCA with an EIP (VCA-1), VCA using fitting parameters (VCA-2), and MD simulations using the GK method as a function of In composition is shown in Figure 4.6. It can be seen that there is good agreement between all methods at room temperature over the full range of In concentrations. It can be seen that the TC drops sharply after only a small amount of alloying – such a result is expected and can be interpreted via the VCA as being due to strong scattering of phonons even in the dilute alloy limit. Unsurprisingly, the results predict that in the composition range of 0.2-0.8 the alloy TC becomes nearly independent of composition, which agrees both qualitatively and quantitatively with experimental data.

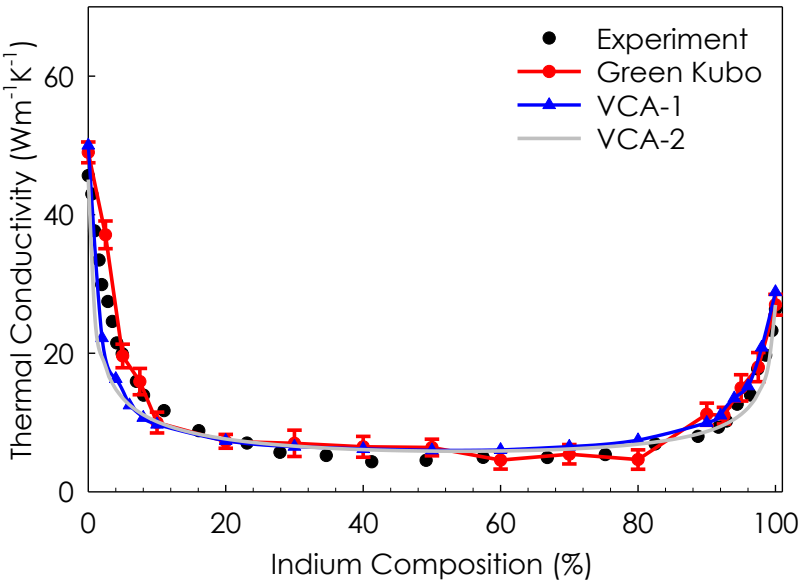

Figure 4.6. TC of $In_xGa_{1-x}As$ vs. In composition at 300K calculated using different methods.

Figure 4.6 shows that good agreement with experiments can be obtained for the TC vs. composition for $In_{1-x}Ga_xAs$ at 300K, when using both the VCA and GK method. However, some differences between the two approaches show up in the predictions of TC vs. temperature. One

reason temperature reveals some discrepancy between the two methods is because phonon contributions to TC are proportional to individual phonon heat capacity. Quantum mechanically, the heat capacity of phonons is strongly temperature dependent and decays to zero at "high" temperatures. The quantum mechanical suppression of specific heat is frequency dependent – at low temperatures, only low frequency modes are excited, in accordance with Bose-Einstein statistics, while high frequency modes are only activated at higher temperatures. As a result, temperature serves as a broadband filter for mode level contributions to TC. Consequently, at low temperatures, one can single out the contributions of low frequency modes, while at higher temperatures, higher frequency mode contributions are also included. Thus, one can probe the non-specific heat related TC contributions for each method by comparing TC vs. temperature, because the specific heat of each model is identical – leaving the major distinction as each model's description of the phonon-phonon interactions. Figure 4.7 shows the TC calculated by each methodology, compared to experimental data [69,78] for a thick 1.6 micron film, which are likely the bulk values. The results show that the VCA values are in the correct range, but the trends with respect to temperature differ somewhat from the experimental data.

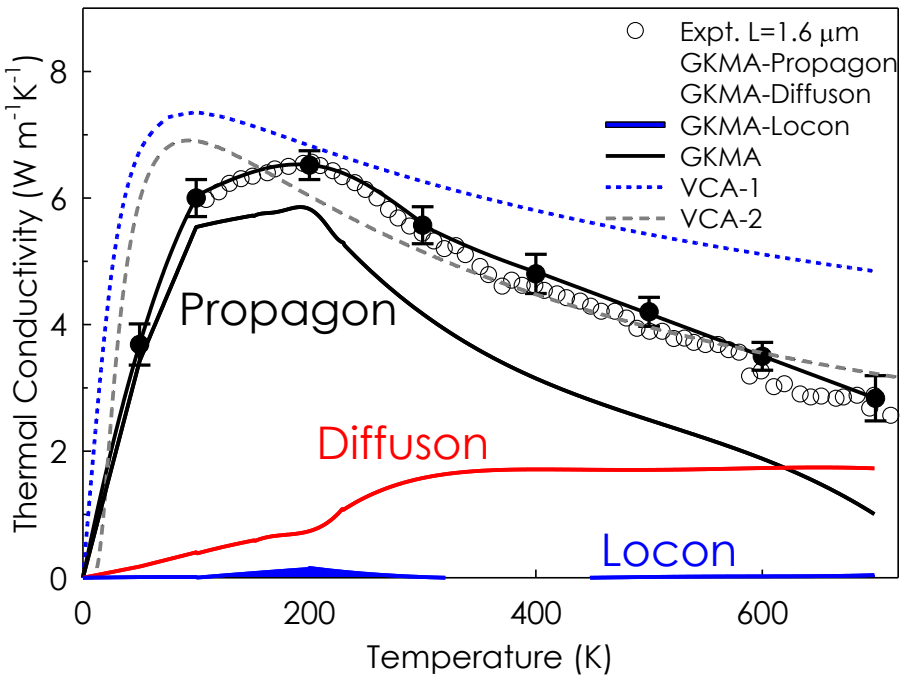

Figure 4.7. TC of $In_{0.53}Ga_{0.47}As$. Temperature dependent TC of $In_{0.53}Ga_{0.47}As$ film [69,78] and the corresponding theoretical predictions using the VCA and GKMA. The error bars were determined based on the standard deviation of GK results. Each labeled curve highlights the respective contributions associated with propagons, diffusons and locons, according to the GKMA and EP methodologies.

Although there are some appreciable differences between the two methodologies, the VCA predictions of total TC are not drastically different from the experimental data, which might in turn lead one to assume that for this specific system at least, the physical picture described by the VCA is still valid. Furthermore, it might seem as though considering the mode character shift illustrated in Figures. 4.1 and 4.2, is unnecessary. However, if this is true, the VCA should still provide the correct guiding intuition and predictions for cases beyond the bulk crystalline behavior; we are specifically interested in investigating a case that will highlight the difference between the two physical pictures (i.e., the PGM/VCA scattering paradigm vs. GKMA mode character and

correlation). In this respect, we note that a fundamental difference between the modes of an infinite pure homogenous crystal (e.g., plane waves) – which are similar to propagons – and the predominant modes (by number) in the alloy – namely diffusons – is that the diffusons cannot be associated with a well-defined group velocity. This then rigorously prevents them from being associated with a corresponding MFP, and because the addition of multiple diffuson velocity fields presumably does not yield a traveling wave packet, it is intuitive to expect that diffusons should not exhibit significant classical size effects[1]. A classical size effect is a well-known phenomenon that is well explained by the PGM and is one of the most valuable pieces of intuition it provides. According to the PGM, TC is proportional to the average distance a phonon can travel before it scatters (i.e., its MFP). Therefore, as one shrinks the size of a material, the propagation of phonons becomes constrained by the material's boundaries, where a phonon must scatter/reflected. As a result, the reduced size of a material eventually limits some phonon's MFP and consequently reduces TC in a predictable way[1,2,79]. Diffusons and locons, however, do not propagate; thus it is intuitive that they should not experience such size effects and their contributions to TC should be unaffected by reduced dimensions. It is important to also emphasize that locons have an associated length scale which can be quantified by a localization length[30], but diffusons do not, since they are delocalized. Although AF[30] proposed a length scale ($l^2\omega$) associated with the mode diffusivity ($D_i(\omega)$), to our knowledge this definition has never been shown to be a useful quantity.

Nonetheless, from this progression of logic, we compared the predictions of both methods (GKMA and VCA) to the TCs of much thinner films of $In_{0.53}Ga_{0.47}As$ (280 nm and 120 nm thick) whereby, according to the revised intuition, we hypothesized that the propagons would most certainly experience classical size effects, but the diffusons and locons should not. The details

associated with the experimental fabrication and measurements are described in Reference[23]. The VCA predictions were generated using the same methods used for the results shown in Figure. 4.7, and boundary scattering was applied to all the modes in the VCA using Mathissen's rule with the diffuse limit $L/2v$ boundary scattering RTA [1,53,79,80]. It should be noted that boundary scattering was also applied to the results in Figure. 4.7, however, because the film thickness was large (1.6 micron) it essentially had no effect on the TC results. Thus the only change between the predictions in Figure. 4.7 and Figure. 4.8 was a change in the value of L, which was changed to the smaller film thicknesses for the results in Figure. 4.8. Based on our revised understanding for GKMA, size effects were applied to the propagons only, and not the diffusons or locons. The propagon relaxation times were calculated using the standard NMA technique proposed by McGaughey and Kaviany[81], and the propagon contributions determined from GKMA were then scaled down according to the decreased relaxation times the propagons would experience in the thinner films, i.e.,

$$\kappa_{propagons} = \sum_{i \geq \gamma_{n,cut}}^{1} \kappa_{GKMA} \frac{\tau_{i,eff}}{\tau_i} \tag{4.1}$$

In the above equation $\gamma_{n,cut}$ is the minimum EPP of non-propagating modes, namely 0.2. Above $\gamma_n = 0.2$, vibrational modes behave like a plane wave vibrational mode and we assume their contributions to depend on MFP, as prescribed by the PGM. Here, τ_i is the net phonon-phonon and phonon-defect relaxation time calculated using NMA in MD and $\tau_{i,eff}$ is the effective net relaxation time after superimposing the effect of boundary scattering. This approach was used to avoid the excessively large computational expense associated with simulating the entire thickness

of the film with free boundaries. Furthermore, the fact that an application of this basic intuition/understanding can allow us to avoid the large computational expense associated with simulating the entire film is precisely why it is so valuable to test and confirm the intuition is correct in the first place. Our predictions were then compared to TC measurements determined by time domain thermoreflectance measurements of single crystalline $In_{0.53}Ga_{0.47}As$ thin film samples that were grown on single crystalline InP substrates via metal-organic chemical vapor deposition, as discussed in the supplementary materials of Reference[23].

The results in Figure. 4.8 show that the GKMA approach exhibits remarkable agreement with the experimental data and most notably, it properly captures the correct trends and magnitude of TC for each film. The VCA, on the other hand, provides a much poorer description, as the added phenomenon of size effects exacerbates its key shortcoming. Of particular concern is the fact that both applications of the VCA (e.g., VCA-1 and VCA-2) incorrectly predict a lower temperature peak of ~50-100K, while only the GKMA method correctly predicts that the peak occurs slightly above 200K.

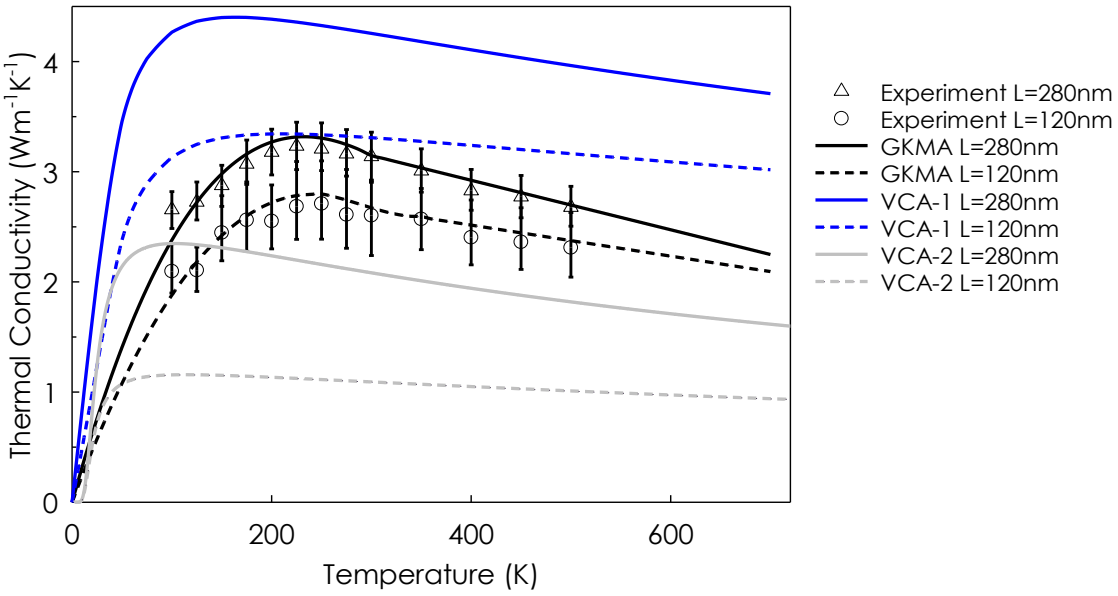

Figure 4.8. Temperature dependent TC of $In_{0.53}Ga_{0.47}As$ for different thin film thicknesses, and the corresponding theoretical predictions using VCA and GKMA. The error bars were determined based on the standard deviation of GK results.

It is also interesting to note that even if one discards the arguably more rigorous implementation of the VCA (e.g., VCA-1) in favor of the approach utilized more frequently before the advent of first principles methods (VCA-2, namely using fitting parameters), one still cannot properly predict the size effects observed in the thin films. When fitting parameters are used, it is interesting that the thicker 1.6 micron film TC and the overall shape of the TC accumulations (see Figure 4.9) more closely match those predicted by GKMA over the entire temperature range. However, because the PGM/VCA implicitly assumes that all of the modes are plane wave-like in nature and should therefore experience size effects, the fitted version significantly under-predicts the TC of the films (i.e., error > 2x for the 120 nm at 300K). Nonetheless, by more properly accounting for the fact that the majority of the modes are diffusons, which should not experience significant size effects, the GKMA predictions agree well with the measurements.

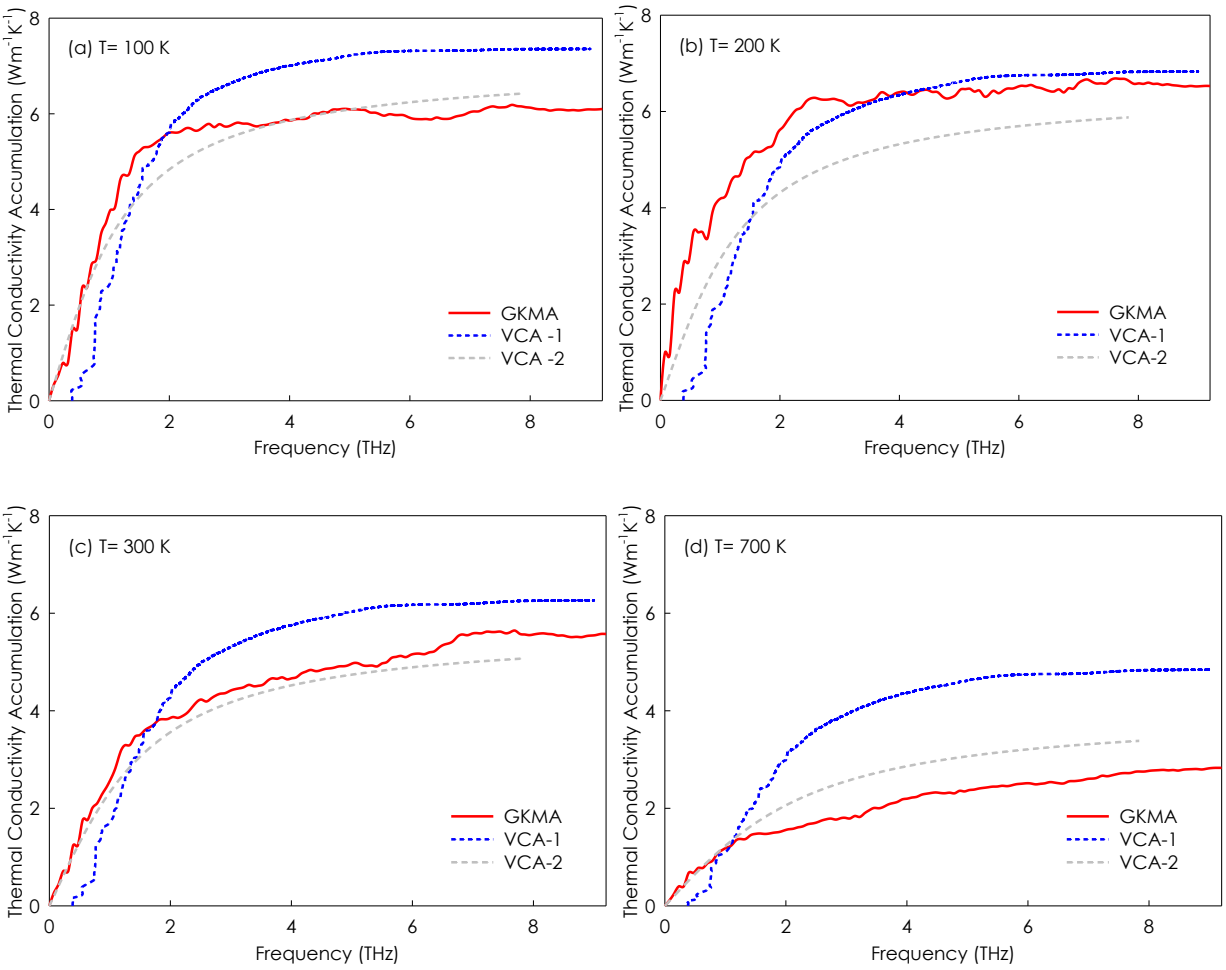

Figure 4.9. TC accumulation of 1.6 micron thin film $In_{0.53}Ga_{0.47}As$ using the VCA with fitting parameters, VCA with an empirical potential, and GKMA.

In conclusion, the results show that consistent with their character, diffusons do not experience significant size effects at the 100 nm length scales probed in this thesis, and as a result, the TC of thin films differs significantly from VCA predictions, even when fitting parameters are employed. Thus, the theory of alloy TC and the concept of phonons more generally should be reconsidered to account for changes in mode character vs. disorder.

4.1.2.2 Relaxation time can become an invalid descriptor

From the PGM perspective, TC depends on individual mode phonon group velocities, heat capacities, and relaxation times. Considering the fact that the TC of solids spans about 5 orders of magnitude (0.1-10,000 W $m^{-1}K^{-1}$), it is instructive to inspect which of these three parameters is primarily responsible for the range of thermal conductivities observed in nature. For example, group velocities scale with the speed of sound and are usually in the range of 1,000-10,000 m/s. Furthermore, the phonon heat capacities are essentially determined by the phonon density of states and are independent of temperature at high temperatures. Therefore, the PGM claims that the relaxation times are the primary descriptors for explaining thermal transport in different materials. Additionally, in a given class of materials, the temperature dependence of relaxation time mainly determine the temperature dependent TC. Utilizing the fact that the relaxation times are predominantly responsible for the temperature dependence of TC above cryogenic temperatures, one can devise a scheme by which to assess the validity of the PGM.

The validity of the PGM/VCA becomes questionable for random alloys, due to the inability to define the phonon velocities for non-propagating vibrational modes, which are expected to be a large fraction of phonons in random alloys. Here it is important to note that structural and compositional periodicities are an inherent requirement for rigorously defining the group velocity for phonons, since they require that one defines the phonon wave vectors, and consequently phonon dispersion curves. Therefore in a random alloys, where there is no compositional periodicity, it is useful to assess whether or not one can still utilize the PGM framework to calculate the TC. If for example, one can still rationalize the behavior of random alloys with the PGM/VCA, then one can potentially define an effective MFP for non-propagating vibrational modes apply the same methods used for pure homogenous crystalline solids. However, if after such an assessment

one determines that the PGM is inapplicable, then one must then proceed to consider alternative physical descriptions of the heat flow.

To determine whether one can rationalize the PGM for random alloys, one can compare the temperature dependent trends of TC and relaxation time in non-propagating modes. To this end, we calculated individual mode relaxation times of $In_{0.53}Ga_{0.47}As$ at 300K and 700K using NMA[81]. In the NMA approach, the atomic trajectories generated by MD simulations are used to calculate the relaxation times. The normal modes amplitudes $S(\mathbf{k},\upsilon)$ can be expressed as a sum over the positions of the atoms in the system[81]

$$S_i(\mathbf{k},\upsilon) = N^{-1/2}\sum_j M_j^{1/2}\exp(-i\mathbf{k}.\mathbf{r}_{j,o})\mathbf{e}_i^*(\mathbf{k},\upsilon).(\mathbf{r}_j(t)-\mathbf{r}_{j0}) \qquad (4.2)$$

where $\mathbf{e}_i(\mathbf{k},\upsilon)$ is the eigenvector, υ is mode polarization, M_j is mass of atom j, $\mathbf{k}$ is wave vector, N is total number of atoms in the system, and $\mathbf{r}_{j,o}$ and $\mathbf{r}_j(t)$ are the equilibrium lattice position vector and the atom's position vector, respectively.

Under the harmonic approximation, the total energy of each mode is given by[81]

$$E_i(t) = E_{i,P} + E_{i,K} = \frac{\omega_i^2 S_i S_i^*}{2} + \frac{\dot{S}_i \dot{S}_i^*}{2} \qquad (4.3)$$

where $*$ denotes complex conjugate and ω_i is the frequency of the normal mode. The first term in Eq.4.3 corresponds to potential energy ($E_{j,P}$) and the second term to the kinetic energy ($E_{j,K}$). The vibrational mode relaxation time can be calculated by calculating the decay of the autocorrelation of each mode's total energy via[81,82]

$$\tau_i = \frac{\int_0^{\infty} \left\langle E_i(t) E_i(0) \right\rangle dt}{\left\langle E_i^2(0) \right\rangle} \tag{4.4}$$

In the present work the eigenvectors are calculated using GULP[63] at the gamma point. It is important to note that the relaxation time calculated using this method measures the net phonon-phonon scattering rate and does not distinguish between umklapp and normal processes or interactions with the alloying element(s). This is due to the explicit inclusion of the alloying elements and comprehensive inclusion of temperature dependent anharmonicity expressed within the atomic trajectory.

Figure 4.10 shows the relaxation times of non-propagating modes versus EPP in $In_{0.53}Ga_{0.47}As$ at T=300K and T=700 K. It can be seen that as temperature increases, relaxation times decreases. According to the PGM, lower relaxation times at higher temperatures are primarily due to higher phonon-phonon scattering at higher temperatures. To understand the correlation between the relaxation time of non-propagating modes and their contribution to the TC, we used GKMA to calculate the TC of $In_{0.53}Ga_{0.47}As$ at 300K and 700K. As shown in the previous section, GKMA yields excellent agreement with experimental results of TC of $In_{0.53}Ga_{0.47}As$. Therefore, GKMA can be regarded as a meaningful step towards improved insight and assessment of the validity of the PGM. However, one can argue that even though GKMA provides a fundamentally different physical picture of thermal transport (i.e., based on correlation and not scattering[32]), one could potentially still view the problem from a PGM perspective via some correction to the MFP. Here, we investigate this question and show that the behavior in random alloys is distinctly different from what can be predicted by the PGM/VCA, thus the

PGM/VCA is a fundamentally problematic way of viewing phonon transport in random alloys, since one cannot rationalize the use of a MFP based explanation.

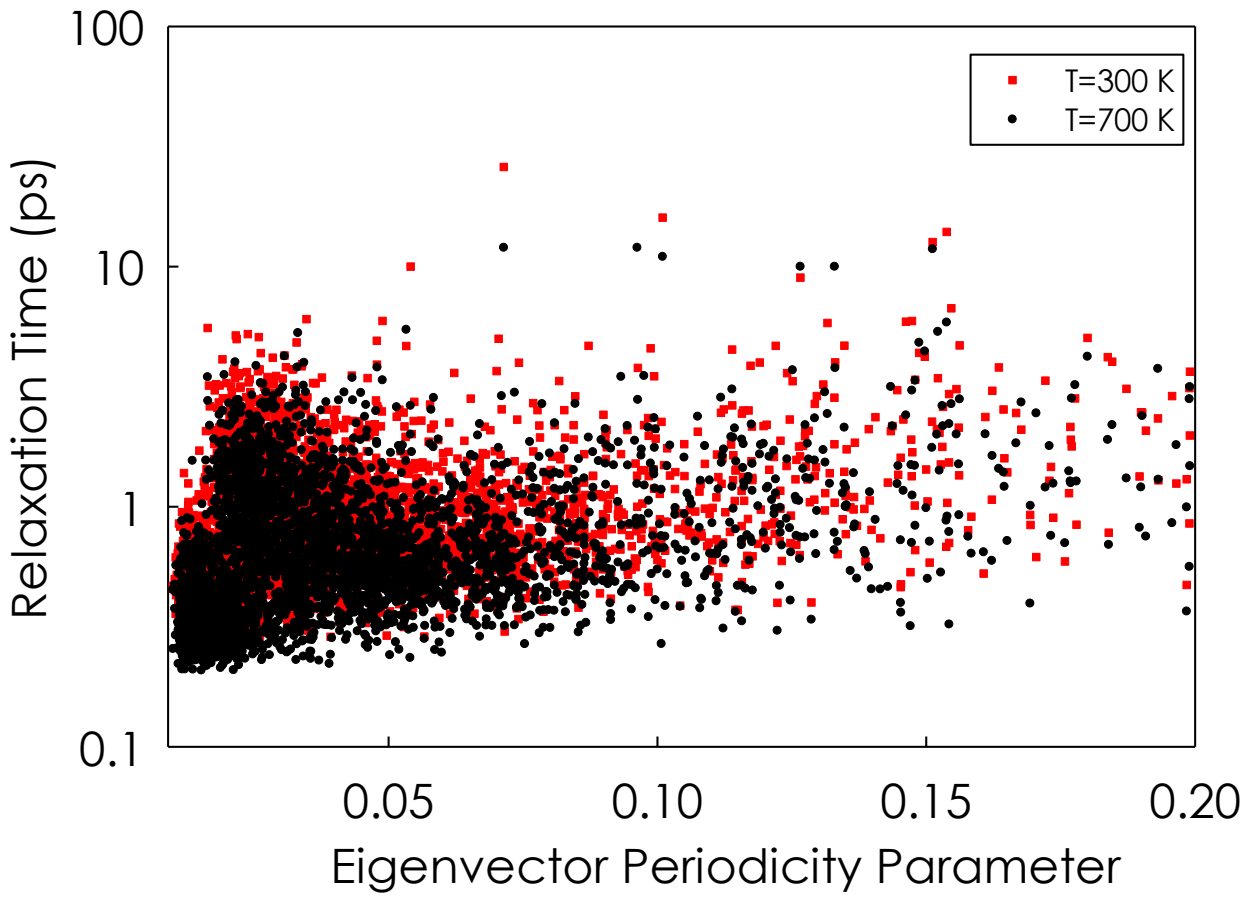

Figure 4.10. Relaxation time of non-propagating modes ($\gamma_n < 0.2$) in $In_{0.53}Ga_{0.47}As$ at 300K and 700K using NMA

In Figure 4.11, TC accumulation with respect to the EPP is shown at 300 K and 700K. For $In_{0.53}Ga_{0.47}As$, at these temperatures, all the vibrational modes are excited and therefore have an identical heat capacity of k_B/V. As a result, the accumulation curves for 300K and 700 K do not reflect the temperature dependence of heat capacity. After dividing by the constant heat capacity k_B/V for every mode, one can think of the accumulation as a thermal diffusivity accumulation,

where $D = v^2\tau$. If one were to then try and rationalize the results in terms of the PGM, one would expect that the corresponding thermal diffusivity contributions must follow the same temperature dependence as the relaxation times determined from MD. As seen, at both 300 K and 700K, the TC accumulations are identical while the relaxation times (Figure 4.10) decreases by 30% on average. In particular, it can be seen that at T=300K the cumulative contribution of phonons up to $\gamma_n \approx 0.05$ is lower than cumulative contribution of phonons at T=700K. This is in contrast with the trend of relaxation times shown in Figure 4.10. Therefore, the relaxation time trend required for consistency with the PGM is not observed. This shows that the standard PGM/VCA model for the modes in random alloys does not offer a good description of the actual behavior.

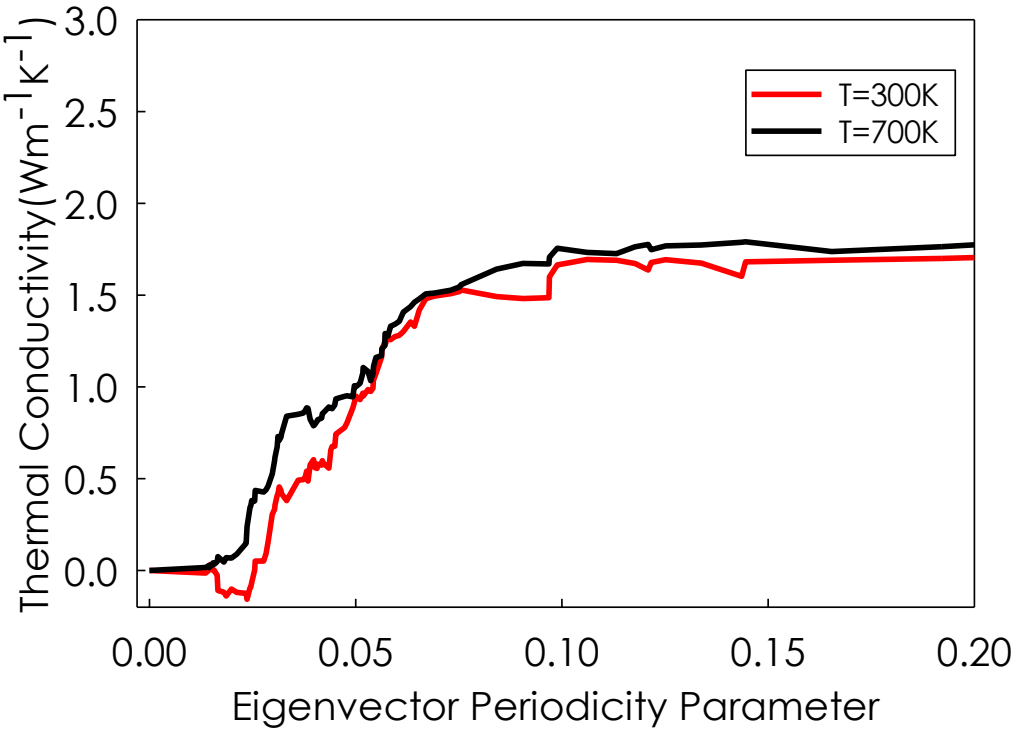

Figure 4.11. TC accumulation of non-propagating vibrational modes in $In_{0.53}Ga_{0.47}As$ as a function of EPP at 300K and 700K.

In conclusion, in this chapter, we answered the third question raised in Chapter 1 regarding the validity of PGM/VCA in predicting the TC of random alloys. Using InGaAs as a test case, we have systematically proved that missing information in the PGM/VCA is knowledge of the vibrational mode character. In general, in random alloys, the majority of vibrational modes in can be non-propagating, thereby one cannot define group velocity for them and consequently PGM/VCA fails to predict their contribution to the TC. We also showed that the relaxation time is not a valid descriptor for non-propagating vibrational modes in random alloys.

CHAPTER 5

THE IMPORTANCE OF NEGATIVE PHASE QUOTIENT PHONONS

It is generally understood that in bulk crystalline materials, the contributions associated with optical phonons to TC are small, due their low group velocity and short relaxation times. For example, in bulk Si, the contribution of optical phonons at room temperature is ~5% [36,83,84]. However, in nanostructures where there are significant size effects for acoustic modes, optical mode contributions can become more significant [85-87]. Furthermore, optical phonons are still important in bulk materials, because they provide an important means of scattering for acoustic phonons and therefore are responsible for a significant decrease in TC, since if they were non-existent, conceptually the TC would be higher.

As shown in the previous chapters, due to the lack of periodicity in structurally/compositionally disordered materials, the majority of vibrational modes are non-propagating (i.e., diffusons and locons)[23,31,43], so one cannot clearly define the phonon dispersion and group velocity. Therefore, one may not be able to extend insights about optical phonons in pure, homogeneous crystalline materials to disordered solids. Furthermore, as we discussed in Chapter 3, for disordered solids, one can use PQ to evaluate whether a mode shares more distinguishing properties with acoustic vibrations (PQ>0) or optical vibrations (PQ<0). The key question then becomes: Do negative PQ modes in structurally/compositionally disordered systems contribute significantly to heat conduction? Understanding the contributions to TC from PQ>0 and PQ<0 phonons is important, because once the dominant phonon types and their transport mechanism is understood, the means by which their contributions can be manipulated might then be explored. In this section, in an attempt to determine to what extent the PQ>0 and PQ<0 phonons

in disordered systems contribute to the TC, we study several example materials, i.e., a-SiO_2, amorphous carbon (a-C), and random crystalline $In_{0.53}Ga_{0.47}As$ alloy.

5.1 Phase quotient in disordered systems

In this section, we first use PQ formula introduced in Chapter 3 to calculate the PQ of vibrational modes in a-SiO_2, a-C, and random $In_{0.53}Ga_{0.47}As$ alloy, and then use GKMA to calculate the modal thermal conductivities. The interatomic interactions between atoms in $In_{0.53}Ga_{0.47}As$ and a-SiO_2 systems are described by Tersoff potential[71,88] while the interactions in a-C system are described by modified Tersoff potential[89] that has been tested to accurately reproduce the mechanical properties of diamond-like carbon and hydrogenated diamond-like carbon. The GKMA details for In0.53Ga0.47As alloys is discussed in Chapter 4. Therefore, in this section, we briefly discuss the details for calculation of the TC of the a-SiO2 and a-C. To generate a-SiO_2 and a-C structures, we used the melt-quench method[90]. The detailed procedures for generating the amorphous structures have been described elsewhere [45,48]. For a-SiO_2, after quenching, the structure was annealed at 1100 K for 10 ns to avoid the meta-stability reported by Larkin *et al.*[34]. For a-C, in order to offer the fairest comparison with the experimental results, we used a DLC structure with a density of 3.0 g/cm^3, which is identical to the DLC measured in the associated experiments[91]. This is important, because the TC of a-C is known to depend strongly on the density, which ultimately determines the sp^2 /sp^3 bonding ratio (i.e., graphite/diamond like bonding). After quenching the structures to the desired density, we then relaxed the structures using a constant number of atoms, volume, and temperature for 1 ns and then simulated the structure in the microcanonical ensemble for 5 ns (a-C) and 2 ns (a-SiO_2), which is when the modal contributions to the heat flux are calculated. Simulations were run with 0.25 fs

(a-C) and 0.1 fs (a-SiO_2), time-steps and the total heat flux and mode heat flux are calculated every 5 fs to reduce the computational time. All MD simulations were conducted using LAMMPS package[66] and the eigen modes were determined from LD calculations using GULP[63]. It is worth mentioning for each material excellent agreement with experimental data has been achieved elsewhere [23,45,47,48], using the methods employed here. Thus, we proceed with confidence that the elucidated modal contributions are correct and therefore the insights derived from the following analysis are physically meaningful.

Figure 5.1 shows the participation ratio and PQ for $In_{0.53}Ga_{0.47}As$, a-C and a-SiO_2. It can be seen that for a-C and $In_{0.53}Ga_{0.47}As$ the transition between diffusons and locons occurs around 65THz and 9 THz, respectively. However, in a-SiO_2 the transition occurs around 25THz and 35THz, as there exist two regions that have localized modes, from 25 to 30THz and above 35THz. Given the low PR of vibrational modes in these regions, one can classify both of these groups of modes as locons, which are spatially localized and typically only involve a small group of atoms in the vibration[31]. The sharp drop in PR for a-SiO_2 around 25THz is interesting because in crystalline SiO_2, at approximately the same point in the spectrum[92,93], the TA branch ends and the density of states has a local minimum. Therefore, 25THz marks an interesting point in the spectrum where non-propagating vibrational modes change their character from acoustic-like to optical-like phonons, in both the crystalline and amorphous phases of SiO_2. It is interesting to note that the cross-over frequency regime for the PQ remains largely unchanged despite the dramatic difference in structure and mode character. Finally, it is worth mentioning that for carbon materials, such as diamond, graphene, and a-C, at low and intermediate temperatures ($T<300$ K) the heat capacity is far below the Dulong–Petit limit, which indicates that most of the localized

vibrational modes are not excited. As a result, the contribution of localized modes, i.e, phonons with frequency greater than 65THz to the TC is negligible at these temperatures.

The general trends for PQ in a-SiO_2, a-C and the $In_{0.53}Ga_{0.47}As$ random alloy are similar (see Figure. 5.1). It is interesting to see an example case, where PQ does not traverse fully from PQ = 1 to PQ = -1. In concept, one might have expected there to always be some intrinsic balance between the number of modes with positive PQ and negative PQ, but the results of the SCLD calculations show that the net summed PQ is not always near zero, as it was for the crystalline materials InAs and GaAs studied in Chapter 3. However, one would also expect that a crystalline material with a basis larger than two, would have more optical branches/modes than acoustic, and thus, it might not be expected that there is any general balance in PQ for crystalline materials. Nonetheless, it is interesting to note the differences in the net PQ for each material, as shown in Table 1. In Table 1, the sum of positive and negative PQs for a-C, a-SiO_2, and random $In_{0.53}Ga_{0.47}As$ alloy are -465, -374, and 59, respectively, which is an order of magnitude larger than the sum of PQs for InAs and GaAs, which are -5.13 and -2.21 respectively.

Table 5.1. The sum of PQ for all modes in each system studied

Sum of PQ	**Random $In_{0.53}Ga_{0.47}As$**	**a-C**	**a-SiO_2**	**Crystalline InAs**	**Crystalline GaAs**
Positive PQ	1135.41	2817.39	2049.06	1041.17	1101.02
Negative PQ	-1076.21	-3283.06	-2424.06	-1046.30	1103.3
Net PQ	59.22	-465.66	-374.9	-5.13	-2.21

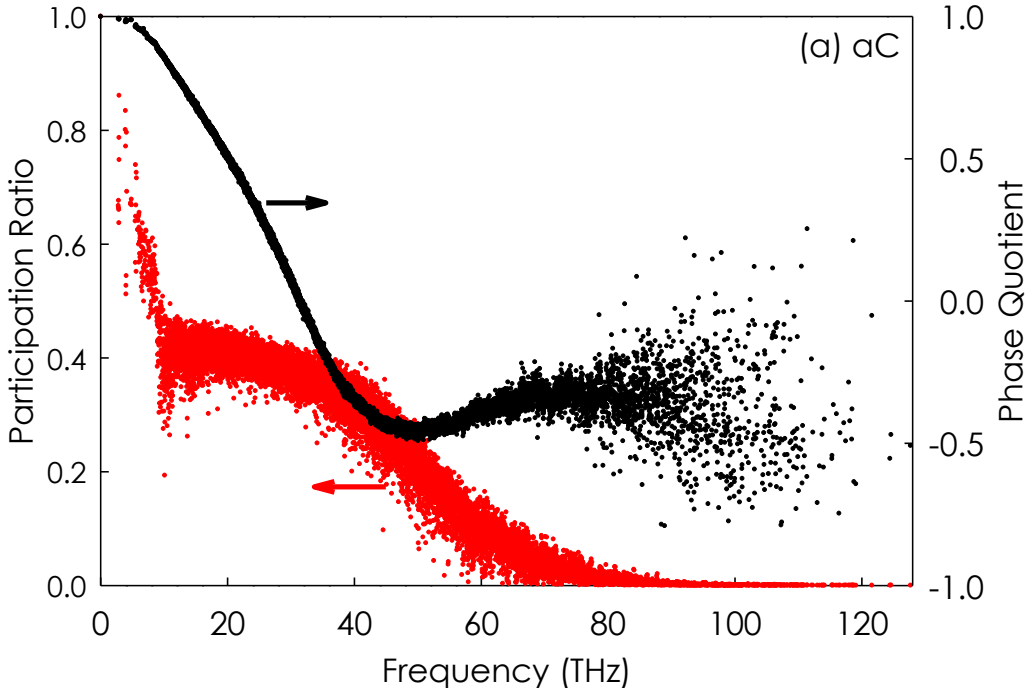
(a) aC
Participation Ratio
Phase Quotient
Frequency (THz)
1.0
0.8
0.6
0.4
0.2
0.0
0.5
-0.5
-1.0
0
20
40
60
80
100
120

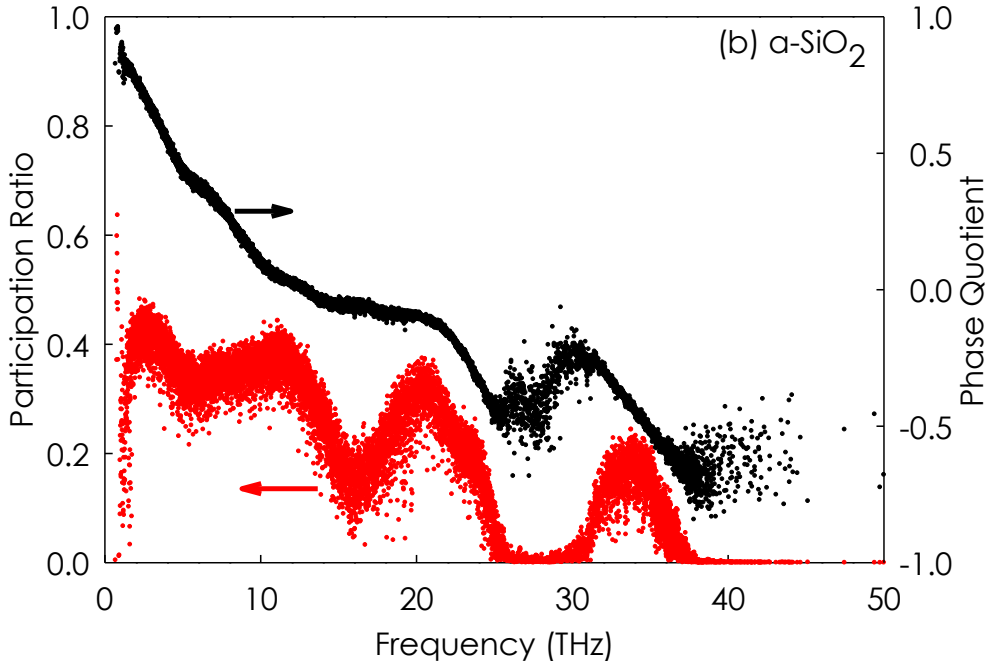
(b) a-SiO2
Participation Ratio
Phase Quotient
Frequency (THz)
1.0
0.8
0.6
0.4
0.2
0.0
0.5
-0.5
-1.0
0
10
20
30
40
50

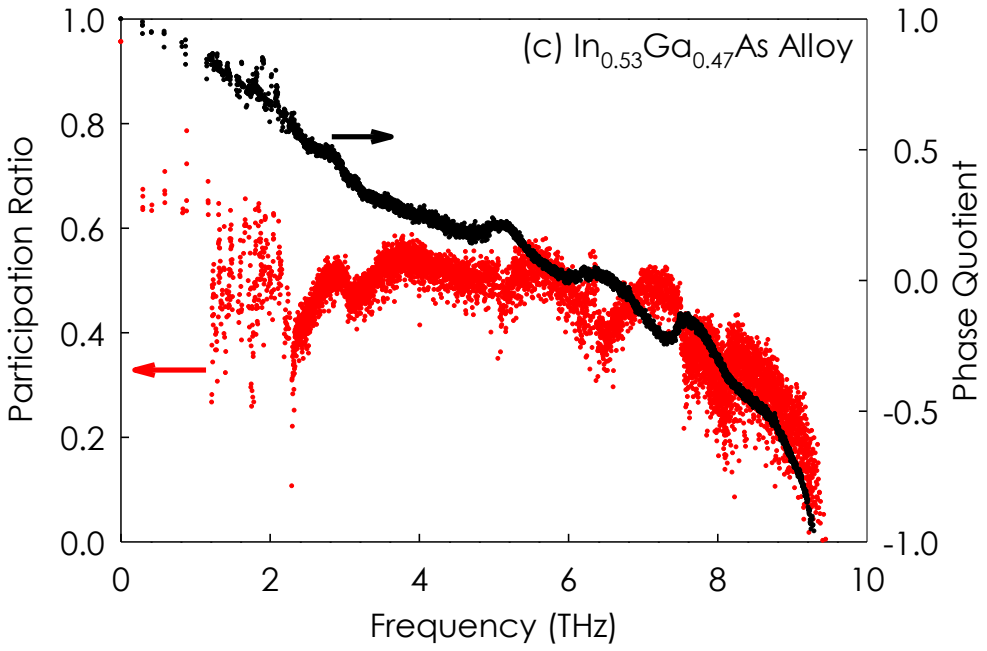

Figure 5.1. Participation ratio and PQ for a-C, a-SiO_2, and $In_{0.53}Ga_{0.47}As$ alloy

5.2 The contribution of negative phase quotient phonons on thermal conductivity

To study the contribution of modes with negative PQ to the heat conduction, we then computed the modal contributions to the TC. Here, we segregated the modes according to their PQ to directly quantify the contributions of modes with positive/negative PQ on TC. Figure 5.2 shows the TC accumulation and DOS as a function of PQ at different temperatures for a-C, a-SiO_2 and $In_{0.53}Ga_{0.47}As$. The color-shaded regions in the DOS plots represent the quantum specific heat contributions at different temperatures. Since the classical volumetric specific heat is constant, the area under the black line (i.e., not the black area) is proportional to the specific heat in the Dulong-Petit limit. It can be seen that for $In_{0.53}Ga_{0.47}As$, at low temperatures ($T < 200K$) the contribution of modes with PQ<0 is negligible, because they are not excited in this temperature range. However, when temperature increases the high frequency/negative PQ modes become excited and they

contribute to the TC. For example, phonons with negative PQ contribute 13% and 6% to the TC of $In_{0.53}Ga_{0.47}As$ at 700K and 300K, respectively.

As seen in a-SiO_2 at T < 400K, the slope changes in the TC contributions when PQ is near zero. This increase is due to the increase in contributions from modes with positive PQ. Based on what is known for crystals, negative PQ modes might have been expected to have low to negligible contribution to the TC, yet in a-SiO_2 they become dominating contributors to the TC at high temperatures once they are excited. It can also be seen that by increasing temperature, the contributions of modes with negative PQ increases, for example at 1200K, 800K and 400 K, they contribute to 53%, 47% and 44% to the total TC, respectively in a-SiO_2. Furthermore, the modes in a-SiO_2 with PQ > 0.83 have almost negligible contribution to the TC due to their low density of states. Another interesting distinction from pure crystals is that the positive PQ contributions do not seem to be correspondingly reduced by the fact that the negative PQ contributions increase with temperature. From a fundamental perspective, the physics associated with this feature is one way of explaining why the TC of disordered materials often increases with temperature.

Finally, for a-C as seen at low temperatures (<100K), only positive PQ phonons contribute to the TC while at 1000K negative PQ modes are responsible of 40% of TC. To the best of our knowledge, this is in stark contrast to any other material previously analyzed. The sharp increase in TC of a-C at T=1000K at PQ around -0.3 is mainly due to the high DOS in this region. The results for TC vs. PQ for a-C, a-SiO_2 and $In_{0.53}Ga_{0.47}As$ suggest that phonons with negative PQ can have major contributions in structurally disordered systems, especially at high temperatures, but they don't seem to have significant contributions in $In_{0.53}Ga_{0.47}As$.

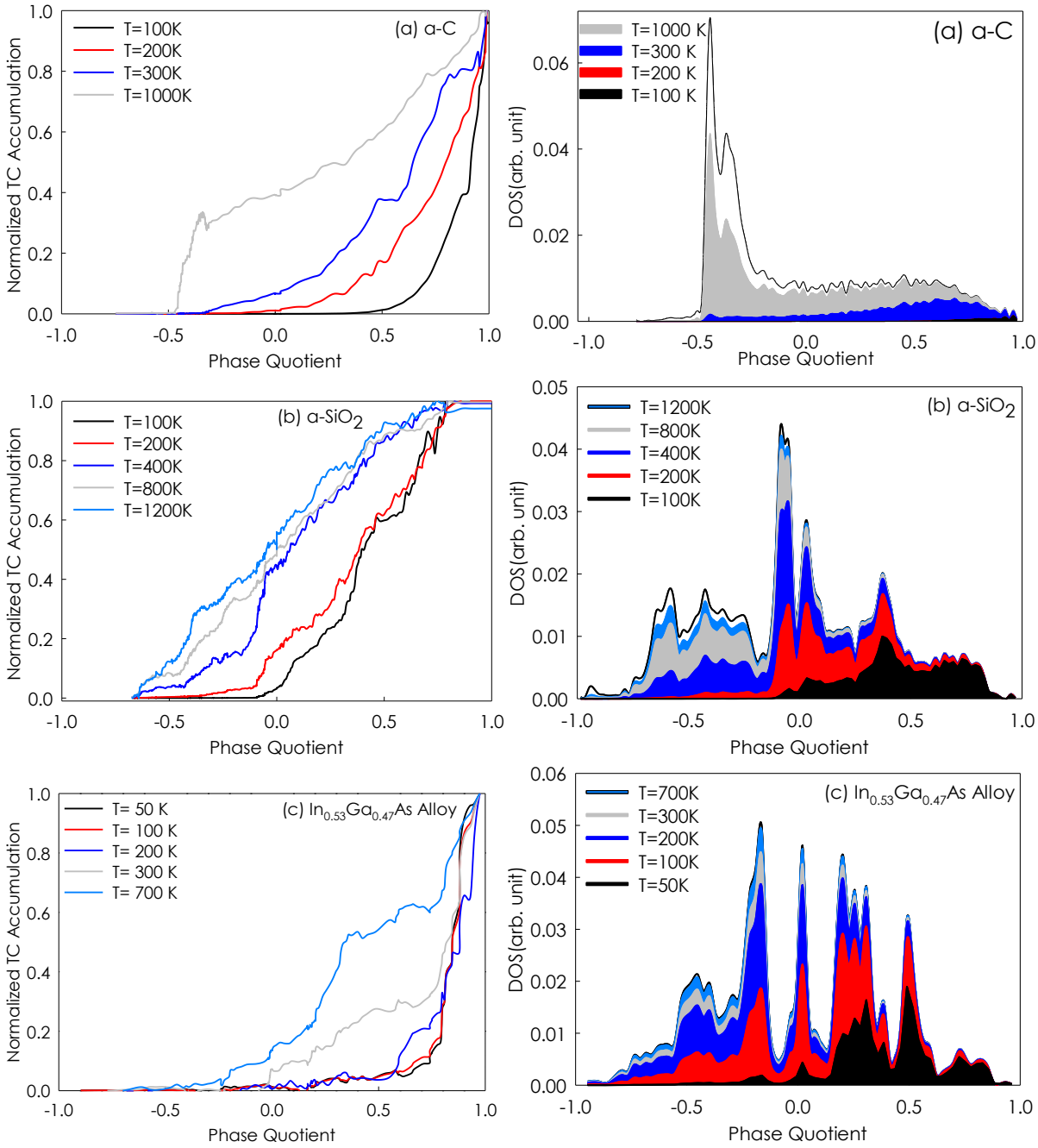

Figure 5.2. TC accumulation and density of states verses PQ for a-C, a-SiO_2, and $In_{0.53}Ga_{0.47}As$ alloy

Figure 5.3 shows the ratio of the percentage of TC ($k(\%)$) to the percentage of heat capacity ($C_p(\%)$) associated with positive and negative PQ phonons. This ratio, represented by α , essentially measures how much each sub category of modes is contributing, on a per unit heat

capacity basis. This quantity is in many ways similar to the mode diffusivity introduced by AF[30]. However, here we are representing it on a normalized basis to allow for easy comparison between the different materials, which have very different total diffusivities and thermal conductivities. The reason this quantity (α) is useful, is because it allows us to assess to what extent are the TC contributions are purely limited by the specific heat, vs. the actual interactions with other modes, which in concept are associated with everything else in the TC other than the heat capacity. The results show that modes with negative PQ at 1200K in a-SiO_2 have the highest contribution to TC on this per unit heat capacity like basis (e.g., here 40X higher than the positive PQ values for α). Interestingly, for this system, at almost all temperatures the α for negative PQ modes is higher compared to positive PQ modes, while for the other systems the positive PQ modes consistently have higher contributions than negative PQ at all temperatures.

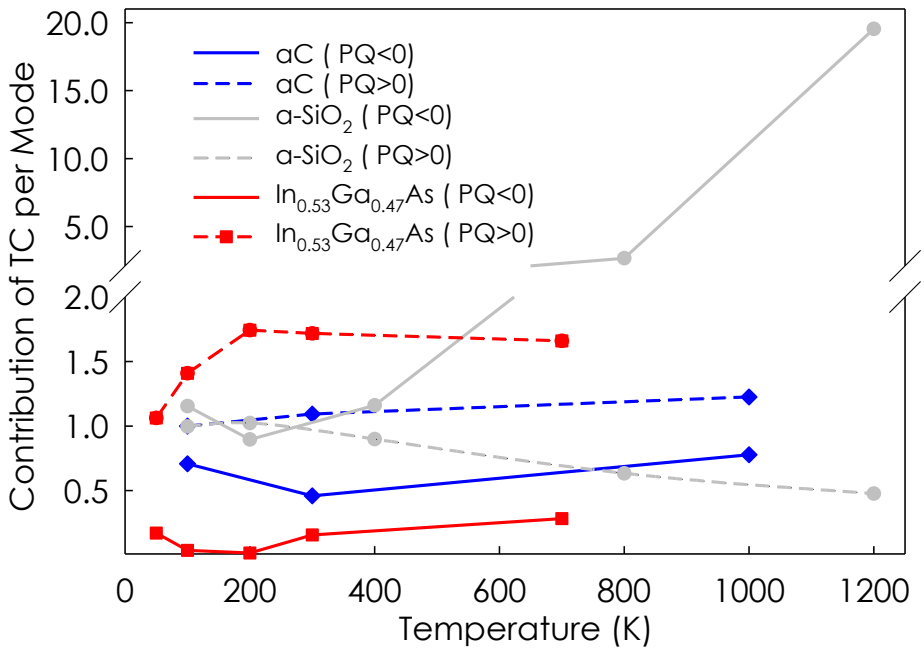

Figure 5.3. The ratio of the percentage of TC to percentage of heat capacity associated with positive and negative PQ.

In conclusion, in this chapter, we have studied the contributions of phonons with negative PQ on the TC of $In_{0.53}Ga_{0.47}As$, a-SiO_2, a-C. We showed that phonons with negative PQ comprise

up to 40%, 53% and 13% of the total TC in a-C, a-SiO_2, and $In_{0.53}Ga_{0.47}As$ at 1000K, 1200K, and 700K, respectively, despite what one might expect based on optical modes in crystals, where their contributions are usually small/negligible. This finding brings to light the importance of contributions from phonons with negative PQ to heat conduction in disordered solids. Although a-SiO_2, a-C and $In_{0.53}Ga_{0.47}As$ are taken as the model materials, one might expect that similar behaviors will arise in many other materials. Furthermore, we found that in general the trend of PQ verses frequency for every material can be different. Some materials exhibit clear trends in PQ with increasing frequency, moving from 1 to -1, but others less so. In theory, as one approaches the zero-frequency limit for a solid with a homogenous density, one should observe sound waves, so one would expect to see PQ start at unity and smoothly translate away from it at least initially. But the rest of the behavior could in theory vary quite a lot. Thus, based on the results herein, we believe PQ is an interesting and important descriptor for phonons that should be examined in future studies to determine the extent to which important quantities (e.g. relaxation times), trends or mechanisms may depend on this sub-classification ($PQ>0$, $PQ<0$) of modes.

CHAPTER 6

CONCLUSIONS AND FUTURE DIRECTIONS

6.1 Conclusions

Current understanding of phonons treats them as plane waves/quasi-particles of atomic vibrations that propagate and scatter. The problem is that conceptually, when any level of disorder is introduced, whether compositional or structural, the character of vibrational modes in solids changes, yet nearly all theoretical treatments continue to assume phonons are still waves. For example, the phonon contributions to alloy TC rely on this assumption and are most often computed from the VCA. Good agreement is obtained in some cases, but there are many instances where it fails—both quantitatively and qualitatively. In this dissertation, we showed that the conventional theory and understanding of phonons requires revision, because the critical assumption that all phonons/normal modes resemble plane waves with well-defined group velocities is no longer valid when disorder is introduced. We showed that the character of phonons changes dramatically within the first few percent of impurity concentration, beyond which phonons more closely resemble the modes found in amorphous materials. We then utilized a different theory that can treat modes with any character and experimentally confirm its new insights.

In Chapter 2, we reviewed the mathematical formalism and implementation of GKMA, the newly developed correlation-based theory of phonon transport in disordered solids. We also briefly described the PGM/VCA, the existing scattering-based theory of phonon transport in random alloys, and discussed the difference between correlation and scattering paradigms.

In Chapter 3, we reviewed the existing methods for distinguishing different type of vibrational modes in disordered solids, i.e., propagons, diffusons, and locons. We first discussed issues with the SF method, the most widely used method for distinguishing between propagating and non-propagating modes. We showed that the SF method is unable to measure the extent to which a mode is propagon-like or diffuson-like on a universal scale, hence it is not material agnostic. To solve this issue, we introduced a new approach, EPA, which can quantify the extent to which an individual mode's character exhibits plane wave modulation. As we showed, using EPA one can classify the vibrational modes in any arbitrary material/structure on a universal scale of 0 to 1. Afterwards, we investigated whether the transition between propagons and diffusons in a disordered solid is sharp. By applying EPA to different crystalline and amorphous solids, we showed that there is no requirement that the mode character must change abruptly with respect to frequency. Finally, we briefly reviewed the physical meaning and mathematical formulation of PQ, a quantity that can be used to evaluate whether a mode shares properties more so with acoustic or optical vibrations.

In Chapter 4, we applied EPA and GKMA to answer two fundamental questions raised in Chapter 1: (i) how does vibrational mode character change when alloy composition increases and (ii) what is the fundamental reason for the failure of the PGM in random alloys? By calculating the EPP for a crystalline $In_{1-x}Ga_xAs$ as an example random alloy, we showed that the majority of vibrational modes become non-propagating when disorder introduced to the system, which suggests that the conventional theory and understanding of phonons in random alloys requires revision. We then devised two test cases to examine the validity of the PGM/VCA in a random alloy and test the hypothesis that the key fundamental information missing in the VCA is knowledge of the mode character. We first hypothesized that non-propagating do not exhibit size

effects in random alloys and proved this hypothesis experimentally. The excellent agreement between the experimental values of TC and the GKMA results for thin films suggest that the non-propagating modes exist in alloys, hence the fundamental assumption of plane-wave vibrational modes in the PGM/VCA is not right. We then conducted an analysis to see if the relationship between relaxation time and TC for non-propagating vibrational modes is consistent with the PGM/VCA. Our analysis showed that in $In_{1-x}Ga_xAs$, there is no simple proportional relationship between the relaxation time and TC of non-propagating modes, which is additional evidence that the PGM/VCA is not suitable to describe the alloy TC.

In Chapter 5, we answered the last question raised in Chapter 1: Do PQ<0 modes in structurally/compositionally disordered systems contribute significantly to heat conduction? By calculating the PQ of the vibrational modes in several example materials, i.e., a-SiO_2, a-C, and random crystalline $In_{0.53}Ga_{0.47}As$ alloy, we first showed that, the trend of PQ verses frequency for every material can be different, and there are no strict rules for PQ. Then, we calculated the TC of these materials and showed that phonons with PQ<0 contribute up to 40%, 53% and 13% of the total TC in a-C, a-SiO_2, and $In_{0.53}Ga_{0.47}As$ at high temperatures, respectively. This finding brings to light the importance of contributions from phonons with negative PQ to TC in disordered solids.

6.2 Future work

Future work should be dedicated towards understanding the thermal properties of materials with various types of defects such as solids with point defects, dislocations, and grain boundaries. Furthermore, it is expected that even in crystals with strong anharmonicity (phonon MFPs on the order of the lattice spacing), as well as crystalline solids with large number of atoms in the unit cell, the application of PGM becomes questionable[94]. For example, recent first principle

calculations on higher manganese silicide ladder structures[95] and TI_3VSe_4 [96] show that heat may be carried by both phonons and 'hopping' of localized vibrational modes. The investigation of phonon transport in these class of materials are still in its infancy, and further research on these materials is necessary. Another possible direction for the future research is to study the thermal transport in other alloys. In general, there are many unresolved problems in random alloys, some examples are listed below.

As shown in Chapter 4, the TC contributions in $In_{0.53}Ga_{0.47}As$ calculated by GKMA are generally constant for non-propagating modes with respect to temperature, yet the relaxation times decreased in the same temperature range. This suggest that the relaxation times are simply inappropriate descriptors for the modal contributions, which then implies that the PGM may not be an appropriate model for the non-propagating modes in random alloys. Therefore, the question arises is: "what is the correct physical picture for phonon transport through diffusons?" If the PGM is not able to properly describe the behavior of non-propagating modes what model can? Although, GKMA allow us to compute the contributions of different modes to the TC, obtaining their quantitative and qualitative behaviors does not necessarily translate to the conceptualization of a corresponding physical picture. Therefore, the development of a correctly modified or new physical picture can be the focus of future studies. Such physical picture has tremendous value, as it can identify and explain phenomena that might be completely non-intuitive or non-obvious otherwise.

Another important question that should be addressed in the future is: "Do diffusons actually experience size effects?". As shown in Chapter 4, for $In_{0.53}Ga_{0.47}As$, the diffusons don't experience size effects at length scales up to 100 nm. However, it is not clear what happens at smaller length scales. "Is it possible that diffusons do actually experience size effects, just at a much smaller

length scale than the propagons?" Previous works on amorphous solids[97] show that it is possible that diffusons exhibit size effect, albeit at much smaller length scales than were probed in the simulations and experiments presented in this thesis. This raises the next question of "what circumstances are required such that a diffuson will experience a size effect?". Furthermore, if only some diffusons experience size effects at all, why would only some diffusons exhibit this characteristic, while others do not? Another critical question then becomes, "can diffuson MFPs ever greatly exceed 100 nm, and potentially enabling the engineering of high thermal conductivity disordered materials? ". Answering such questions can be the focus of future experimental and numerical studies.

Furthermore, as shown in Chapter 4, locons don't contribute significantly to the thermal conductivity of $In_{0.53}Ga_{0.47}As$. The question arises is: "What is the contribution of locons in other random alloys?" Do they ever contribute significantly to the thermal conductivity? If not, is it possible to design an alloy where the majority of its vibrational modes are localized? Such an alloy might have important applications in development of thermoelectric generators. Although, intuitively, it is difficult to imagine an alloy, where majority of its phonons are localized, there is nothing that theoretically prevents this from happening. Intuitively, the presence of multiple atom types with a high coordination number leads to an increased fraction of locons – particularly when the atoms' masses differ greatly[97]. For example, one could design an alloy with substantial inhomogeneity, i.e., with multiple atom types in combination with lightweight atoms (e.g. hydrogen) dispersed throughout the material. This is because the light atoms, due to their lower mass, would likely be forced to vibrate at much higher frequencies than the surrounding atoms to which they are bonded. Consequently, if the surrounding atoms' solutions to the equations of motion cannot access the frequencies needed for the light atoms, then localized solutions will have

to form around the light atoms. Figure 6.1 shows an example of this through SCLD calculations of a crystalline SiGe alloy. What is clear is that when one starts with Si as the base crystal and adds a heavier atom like Ge, the solutions to the equations of motion change, but since Ge vibrates at the same or lower frequencies than Si, the new/modified modes all continue to fall within the original frequency range of Si. Furthermore, since the new/modified solutions are within the same frequency space as the base crystal/material, they simply induce the creation of diffusons, since a localized solution is not necessary. However, when one starts from Ge as the base crystal and adds Si, the Si atom is lighter and can vibrate at frequencies that exceed that of Ge. As a result, localized solutions are required to describe the Si atom vibrations, and it can also cause the surrounding Ge atoms to vibrate above the maximum frequency in bulk crystalline Ge as well. Therefore, the addition of lighter atoms to a base material as isolated defects or impurities is likely to generate localized modes. Furthermore, by spreading them apart from each other at a distance that is randomized, one could try to optimize by compensating between two conversely competing effects. On the one hand, one should increase the number of light atoms included per unit volume, which would result in smaller distances between them, but should increase the fraction of locons. On the other hand, it will be important to keep the distance between the light atoms large enough so that the locons are unable to merge into an interconnected and therefore delocalized solution, which would then convert them into diffusons. By accounting for these two competing mechanisms, one could likely construct a system with a large and maximized fraction of locons. Thus, there are still several open questions regarding locons, such as: “Is it possible to experimentally prove that locons actually contribute to thermal conductivity, and is it possible that a system exists where they become large or even the dominant contributors?”; “What approaches

can be used to maximize the number of locons?" These questions will be important to answer in future work.

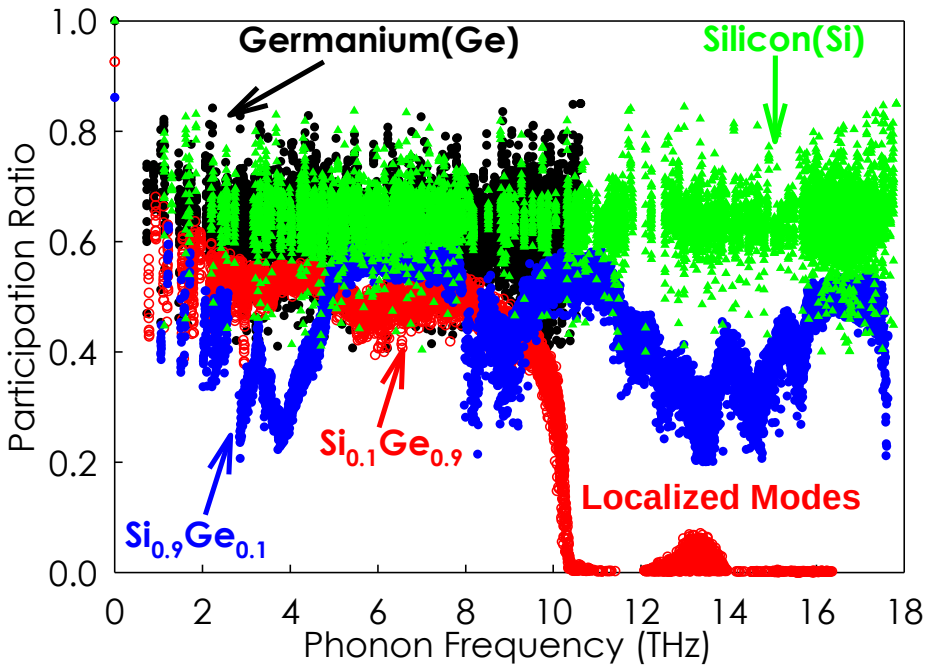

Figure 6.1. PR, showing the degree of localization of phonons. For $Si_{0.1}Ge_{0.9}$, the PR is reduced for high frequency phonons, indicating localization.

Finally, there are several important fundamental questions, which should be undertaken as the subject of future work. For example, "What is the crystal momentum associate with diffusons and locons?" This question is particularly important, because it is likely to impact how such modes will interact with other quantum particles. For propagons, since there is periodicity in the mode's displacement/velocity field, one can conceivably identify a representative wave-vector. However, for diffusons and locons, due to the lack of periodicity it is not clear how one can calculate the mode momentum. Additionally, the notion of the phase quotient is worth further study [132]. In the quest to rethink the physical picture of phonons, new or alternative descriptors that are ideally

well-defined for all phonons regardless of their character are needed. By identifying/developing new descriptors and assessing propgaton, diffuson, and locon contributions with respect to them, it may be possible to identify non-dimensional parameters i.e., groups of descriptors that ultimately predict with high accuracy how strongly a given mode contributes to thermal conductivity.

REFERENCES

[1] G. Chen, *Nanoscale Energy Transport and Conversion: A Parallel Treatment of Electrons, Molecules, Phonons, and Photons* (Oxford University Press, 2005).

[2] J. M. Ziman, *Electrons and Phonons* (Oxford University Press, New York, 2001).

[3] T. Feng and X. Ruan, Journal of Nanomaterials **2014**, 206370, 206370 (2014).

[4] A. J. McGaughey and J. M. Larkin, Annual Review of Heat Transfer **17** (2014).

[5] A. J. McGaughey and M. Kaviany, Advances in heat transfer **39**, 169 (2006).

[6] A. Maradudin and A. Fein, Physical Review **128**, 2589 (1962).

[7] A. Maradudin, A. Fein, and G. Vineyard, physica status solidi (b) **2**, 1479 (1962).

[8] Z. Tian, S. Lee, and G. Chen, Journal of Heat Transfer **135**, 061605 (2013).

[9] L. Lindsay, D. A. Broido, and T. L. Reinecke, Physical Review B **87**, 165201 (2013).

[10] M. T. Dove, *Introduction to Lattice Dynamics* (Cambridge University Press, 1993).

[11] B. Abeles, Physical Review **131**, 1906 (1963).

[12] S.-i. Tamura, Physical Review B **27**, 858 (1983).

[13] J. Garg, N. Bonini, B. Kozinsky, and N. Marzari, Physical Review Letters **106**, 045901 (2011).

[14] J. Shiomi, K. Esfarjani, and G. Chen, Physical Review B **84**, 104302 (2011).

[15] N. A. Katcho, N. Mingo, and D. A. Broido, Physical Review B **85**, 115208 (2012).

[16] M. Takuru, S. Takuma, H. Takuma *et al.*, EPL (Europhysics Letters) **102**, 46002 (2013).

[17] A. Kundu, N. Mingo, D. A. Broido, and D. A. Stewart, Physical Review B **84**, 125426 (2011).

[18] W. Li, L. Lindsay, D. A. Broido *et al.*, Physical Review B **86**, 174307 (2012).

[19] S. Lee, K. Esfarjani, J. Mendoza *et al.*, Physical Review B **89**, 085206 (2014).

[20] W. Liu and A. A. Balandin, Journal of Applied Physics **97**, 073710 (2005).

[21] T. Tong, D. Fu, A. X. Levander *et al.*, Applied Physics Letters **102**, 121906 (2013).

[22] T. Borca-Tasciuc, D. W. Song, J. R. Meyer *et al.*, Journal of Applied Physics **92**, 4994 (2002).

[23] H. R. Seyf, L. Yates, T. L. Bougher *et al.*, npj Computational Materials **3**, 49 (2017).

[24] S.-M. Lee, D. G. Cahill, and R. Venkatasubramanian, Applied physics letters **70**, 2957 (1997).

[25] A. Sztein, J. E. Bowers, S. P. DenBaars, and S. Nakamura, Journal of Applied Physics **112**, 083716 (2012).

[26] A. Sztein, H. Ohta, J. E. Bowers *et al.*, Journal of Applied Physics **110**, 123709 (2011).

[27] B. Pantha, R. Dahal, J. Li *et al.*, Applied Physics Letters **92**, 042112 (2008).

[28] H. Wang, A. D. LaLonde, Y. Pei, and G. J. Snyder, Advanced Functional Materials **23**, 1586 (2013).

[29] T. Tong, D. Fu, A. Levander *et al.*, Applied Physics Letters **102**, 121906 (2013).

[30] P. B. Allen, J. L. Feldman, J. Fabian, and F. Wooten, Philosophical Magazine Part B **79**, 1715 (1999).

[31] H. R. Seyf and A. Henry, Journal of Applied Physics **120**, 025101 (2016).

[32] W. Lv and A. Henry, New Journal of Physics **18**, 013028 (2016).

[33] R. Biswas, A. M. Bouchard, W. A. Kamitakahara *et al.*, Physical Review Letters **60**, 2280 (1988).

[34] J. M. Larkin and A. J. McGaughey, Physical Review B **89**, 144303 (2014).

[35] J. Moon, B. Latour, and A. J. Minnich, Physical Review B **97**, 024201 (2018).

[36] A. S. Henry and G. Chen, Journal of Computational and Theoretical Nanoscience **5**, 141 (2008).

[37] R. J. Hardy, Physical Review **132**, 168 (1963).

[38] J.-P. Hansen and I. R. McDonald, *Theory of simple liquids* (Elsevier, 1990).

[39] W. Lv, Georgia Institute of Technology, 2017.

[40] A. Henry, G. Chen, S. J. Plimpton, and A. Thompson, Physical Review B **82**, 144308 (2010).

[41] S. G. Volz and G. Chen, Physical Review B **61**, 2651 (2000).

[42] A. McGaughey and M. Kaviany, International Journal of Heat and Mass Transfer **47**, 1783 (2004).

[43] H. R. Seyf, W. Lv, A. Rohskopf, and A. Henry, Scientific reports **8**, 2627 (2018).

[44] J. Turney, A. McGaughey, and C. Amon, Physical Review B **79**, 224305 (2009).

[45] W. Lv and A. Henry, Scientific Reports **6**, 35720 (2016).

[46] J. Larkin, J. Turney, A. Massicotte *et al.*, Journal of Computational and Theoretical Nanoscience **11**, 249 (2014).

[47] L. Wei and H. Asegun, Scientific Reports **6**, 35720 (2016).

[48] W. Lv and A. Henry, Applied Physics Letters **108**, 181905 (2016).

[49] W. Lv, R. M. Winters, F. DeAngelis *et al.*, The Journal of Physical Chemistry A **121**, 5586 (2017).

[50] Z. Wang and N. Mingo, Applied Physics Letters **97**, 101903 (2010).

[51] K. Esfarjani, J. Garg, and G. Chen, Annu. Rev. Heat Transf **17**, 9 (2014).

[52] T. Tadano and S. Tsuneyuki, Physical Review B **92**, 054301 (2015).

[53] T. Tadano, Y. Gohda, and S. Tsuneyuki, Journal of Physics: Condensed Matter **26**, 225402 (2014).

[54] W. Lv and A. Henry, Scientific reports **6**, 37675 (2016).

[55] J. M. Larkin and A. J. McGaughey, Journal of Applied Physics **114**, 023507 (2013).

[56] G. Baldi, M. Zanatta, E. Gilioli *et al.*, Physical Review Letters **110**, 185503 (2013).

[57] G. Baldi, V. M. Giordano, G. Monaco, and B. Ruta, Physical Review Letters **104**, 195501 (2010).

[58] G. Baldi, V. M. Giordano, G. Monaco *et al.*, Physical Review B **77**, 214309 (2008).

[59] B. Ruzicka, T. Scopigno, S. Caponi *et al.*, Physical Review B **69**, 100201 (2004).

[60] J. Feldman, Journal of non-crystalline solids **307**, 128 (2002).

[61] J. Horbach, W. Kob, and K. Binder, The European Physical Journal B-Condensed Matter and Complex Systems **19**, 531 (2001).

[62] S. Taraskin and S. Elliott, Philosophical Magazine B **79**, 1747 (1999).

[63] J. D. Gale, Journal of the Chemical Society, Faraday Transactions **93**, 629 (1997).

[64] J. Tersoff, Physical Review B **37**, 6991 (1988).

[65] J. Tersoff, Physical Review B **39**, 5566 (1989).

[66] S. Plimpton, Journal of Computational Physics **117**, 1 (1995).

[67] F. Zhou, A. L. Moore, J. Bolinsson *et al.*, Physical Review B **83**, 205416 (2011).

[68] M. Sternik, P. Jochym, and K. Parlinski, Computational materials science **13**, 232 (1999).

[69] W. Kim, S. L. Singer, A. Majumdar *et al.*, Applied Physics Letters **88**, 242107 (2006).

[70] H. R. Seyf, K. Gordiz, F. DeAngelis, and A. Henry, Journal of Applied Physics **125**, 081101 (2019).

[71] D. Powell, M. A. Migliorato, and A. G. Cullis, Physical Review B **75**, 115202 (2007).

[72] G. Le Guillou and H. J. Albany, Physical Review B **5**, 2301 (1972).

[73] W. Li and N. Mingo, Journal of Applied Physics **114**, 183505 (2013).

[74] T. Luo, J. Garg, J. Shiomi *et al.*, EPL (Europhysics Letters) **101**, 16001 (2013).

[75] A. V. Inyushkin, A. N. Taldenkov, A. Y. Yakubovsky *et al.*, Semiconductor Science and Technology **18**, 685 (2003).

[76] P. D. Maycock, Solid-State Electronics **10**, 161 (1967).

[77] B. Vermeersch, J. Carrete, and N. Mingo, Applied Physics Letters **108**, 193104 (2016).

[78] W. Kim, J. Zide, A. Gossard *et al.*, Physical Review Letters **96**, 045901 (2006).

[79] G. P. Srivastava, *The Physics of Phonons* (CRC Press 1990).

[80] X. Wang and B. Huang, Sci Rep **4**, 6399 (2014).

[81] A. J. H. McGaughey and M. Kaviany, Physical Review B **69**, 094303 (2004).

[82] A. J. Ladd, B. Moran, and W. G. Hoover, Physical Review B **34**, 5058 (1986).

[83] D. P. Sellan, J. Turney, A. J. McGaughey, and C. H. Amon, Journal of Applied Physics **108**, 113524 (2010).

[84] D. A. Broido, M. Malorny, G. Birner *et al.*, Applied Physics Letters **91**, 231922 (2007).

[85] G. Qin, Z. Qin, H. Wang, and M. Hu, Physical Review B **95**, 195416 (2017).

[86] L. Lindsay and Y. Kuang, Physical Review B **95**, 121404 (2017).

[87] Z. Tian, K. Esfarjani, J. Shiomi *et al.*, Applied Physics Letters **99**, 053122 (2011).

[88] S. Munetoh, T. Motooka, K. Moriguchi, and A. Shintani, Computational Materials Science **39**, 334 (2007).

[89] Z. Sha, P. Branicio, Q. Pei *et al.*, Computational Materials Science **67**, 146 (2013).

[90] L. Li, M. Xu, W. Song *et al.*, Applied Surface Science **286**, 287 (2013).

[91] M. Shamsa, W. Liu, A. Balandin *et al.*, Applied Physics Letters **89**, 161921 (2006).

[92] N. Choudhury and S. Chaplot, Physical Review B **73**, 094304 (2006).

[93] S. Ichikawa, J. Suda, T. Sato, and Y. Suzuki, Journal of Raman Spectroscopy **34**, 135 (2003).

[94] L. Lindsay, C. Hua, X. Ruan, and S. Lee, Materials Today Physics **7**, 106 (2018).

[95] X. Chen, A. Weathers, J. Carrete *et al.*, Nature communications **6**, 6723 (2015).

[96] S. Mukhopadhyay, D. S. Parker, B. C. Sales *et al.*, Science **360**, 1455 (2018).

[97] F. DeAngelis, M. G. Muraleedharan, J. Moon *et al.*, Nanoscale and Microscale Thermophysical Engineering, 1 (2018).